Metal Organic Frameworks with catalytically active Metal Nanoparticles

DISSERTATION

zur Erlangung des akademischen Grades eines Doktors der
Naturwissenschaften (Dr. rer. nat.) im Fach Chemie der Fakultät für
Biologie, Chemie und Geowissenschaften der Universität Bayreuth

vorgelegt von

Dipl.-Chem. Georg Paul Justus Hermannsdörfer

geboren am 11. Januar 1985

in Bad Hersfeld - Ludwigsau

Bayreuth, 2013

Die vorliegende Arbeit wurde in der Zeit von 15. September 2009 bis 03. Juli 2013 in Bayreuth am Lehrstuhl Anorganische Chemie II unter Betreuung von Herrn Prof. Dr. Rhett Kempe angefertigt.

Vollständiger Abdruck der von der Fakultät für Biologie, Chemie und Geowissenschaften der Universität Bayreuth genehmigten Dissertation zur Erlangung des akademischen Grades eines Doktors der Naturwissenschaften (Dr. rer. nat.).

Dissertation eingereicht am: 03. Juli 2013

Zulassung durch die Prüfungskommission: 10. Juli 2013

Wissenschaftliches Kolloquium: 22. November 2013

Amtierender Dekan:

Prof. Dr. Rhett Kempe

Prüfungsausschuss:

Prof. Dr. Rhett Kempe   (Erstgutachter)

Prof. Dr. Josef Breu   (Zweitgutachter)

Prof. Dr. Matthias Breuning   (Vorsitz)

Prof. Dr. Stephan Kümmel

This doctoral thesis was prepared at the Department of Inorganic Chemistry ACII at the University of Bayreuth from 15. September 2009 until 03. July 2013 supervised by Prof. Dr. Rhett Kempe.

This is a full reprint of the dissertation submitted to obtain the academic degree of Doctor of Natural Sciences (Dr. rer. nat.) and approved by the Faculty of Biology, Chemistry and Geosciences of the University of Bayreuth.

Date of submission: 03. July 2013

Date of defense (disputation):   22. November 2013

Acting Dean:

Prof. Dr. Rhett Kempe

Doctoral Committee:

Prof. Dr. Rhett Kempe   (1st reviewer)

Prof. Dr. Josef Breu   (2nd reviewer)

Prof. Dr. Matthias Breuning   (Chairman)

Prof. Dr. Stephan Kümmel

„Eine mächtige Flamme entsteht aus einem winzigen Funken."

Dante Alighieri (1265-1321), ital. Dichter

Für meine Eltern, Michaela und Dieter Hermannsdörfer.

Abkürzungsverzeichnis

a.u.	arbitrary units
abs	absolute
Ak	alkyl
Ar	aryl
BET	Brunauer-Emmett-Teller
Cp	cyclopentadienyl
Cp'	methylcyclopentadienyl
conv	conversion
EDX	energy-dispersive X-ray
FFT	fast fourier transform
FTIR	fourier transform infrared
G1	1. generation
GC	gas chromatography
h	hour
HH	abbreviation scheme for reduction conditions: first letter temperature, 2nd letter pressure, H = high, L = low; (e.g. HH1545)
H_2BDC	benzene-1,4-dicarboxylic acid (terephthalic acid)
HRTEM	high resolution transmission electron microscopy
ICP-OES	inductively coupled plasma optical emission spectrometry
IR	infrared
LL	see HH (e.g. LL4842)
M	metal
M	molar (1 mol l^{-1})
Me	methyl
MIL	material of Institute Lavoisier (e.g. MIL-101)
min	minute
ml	milliliter
V	

MD	molecular dynamic
MNP	metal nanoparticle
MOCVD	metal organic chemical vapor deposition
MOF	metal organic framework
mol-%	molar ratio
Ni pwd	nickel powder (Merck)
NP	nanoparticle
P	pressure
PCP	porous coordination polymer
Pd/C	Pd on carbon (5 wt.-percent Pd)
Ph	phenyl
postmod	post modified
Pwd	powder
PXRD	powder X-ray diffraction
RT	room temperature
s	second
sel	selectivity
SEM/REM	scanning electron microscopy
sL	successive loading
t	time
T	temperature
TEM	transmission electron microscopy
THF	tetrahydrofuran
V	volume
VHTP	very high temperature and pressure
vol.-%	volume ratio
wt.-%	weight ratio
XRD	X-ray diffraction

Table of Contents

1   Summary

Content of the present work is the investigation of catalytically relevant metal nanoparticles (MNP) stabilized in porous coordination polymers (PCPs) also called metal-organic frameworks (MOFs). The syntheses of the catalyst family MNP@PCP/MOF as well as the investigation of its catalytic activity are discussed in detail. Furthermore, the MNP@PCP/MOF system is used for the investigation of important catalytic phenomena like dispersion, synergy and leaching.

The synthesis of the metal-organic framework MIL-101 (Cr), which is known from the literature, was performed in a hydrothermal fashion. In this manner high surface area and good phase purity can be achieved in good yield after suitable processing. The cavities of the support (2.9 and 3.4 nm) were infiltrated with volatile metal precursors by means of metal organic chemical vapor deposition (MOCVD). The increased adsorption ability of MIL-101 allows a nearly quantitative loading (> 50 weight percent) and at the same time prevents the undesired desorption of the metal complex. The reduction of the infiltrated metal precursors under hydrogen atmosphere resulted in the formation of MNP, which were restricted in their growth by the cavity walls. The systems were examined with X-ray diffraction, IR spectroscopy, transmission electron microscopy and elemental analysis.

$[(C_5H_5)Pd(C_3H_5)]@MIL-101$
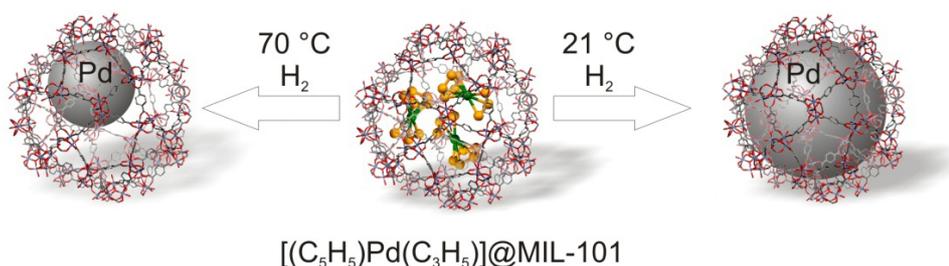
Scheme 1: Schematic presentations of cavity conform (21 °C) and undersized Pd NP (70 °C) within the MIL-101 cavity.

All the time, the critical question about the exact location of the MNP needs to be answered. The desired formation of the MNP within the support (that is the cavities of the MIL-101) is often accompanied by metal deposition at the external surface of the MIL-101 crystallite. Here, the choices of reduction conditions are not only crucial for the location of the metal deposition, but also for the size of the resulting MNP (Scheme 1). While the reduction of the infiltrated Pd precursor $[(\eta^5\text{-}C_5H_5)Pd(\eta^3\text{-}C_3H_5)]$ at low reduction temperatures (21 °C) resulted in the formation of cavity conform MNP (~ 3 nm), raised reduction temperatures (70 °C) led to undersized MNP (~ 2 nm). At temperatures above 220 °C an undesired deposition of metal particles at the external surface of the support was observed.

The Pd@MIL-101 systems were examined concerning their catalytic potential in the reduction of ketones. A selectivity of the systems (cavity conform versus undersized MNP) could be found with regard to the size of the substrate. The entire loading of single cavities limits the accessible metal surface to the area of the cavity windows and thereby reduces possible interactions with sterically demanding substrates. For bigger substrates lower yields are achieved accordingly. Reusability tests (11 x 8 h) did not show a decrease in activity. However, a general agglomeration of particles beyond single cavities was observed for longer reaction times (> 48 h) which was accompanied by a deactivation of the catalyst.

On the basis of the synthesis of undersized MNP we pursued the infiltration of a second metal to generate bimetallic nanoparticle (NP). Originating from the examined Pd@MIL-101 system we chose nickel as the second metal. Here, basically two approaches were possible. The successive loading was compared with the simultaneous loading of the two metal precursors. While the first option led to separated, non-bimetallic NP, the second option resulted in the pursued bimetallic form (Ni/Pd). For nickel rich systems (Ni > 50 wt.-%) the reduction conditions optimized for the Pd@MIL-101 system led to cavity exceeding MNP in the range of 5 – 60 nm, so that an adjustment of the reduction conditions was required. The existence of bimetallic NP is confirmed by molecular dynamic (MD) calculations, X-ray diffraction as well as high resolution transmission electron microscopy and energy dispersive X-ray spectroscopy. In catalytic experiments a significant synergetic effect of the Ni/Pd system could be observed (Scheme 2). The addition of nickel allowed the reduction of aliphatic and cyclic ketones, which have neither been reduced by pure nickel nor by pure palladium to a greater extend. A maximum synergetic effect was found for a ratio of 3:2, which was only observed in the case of an atomic dispersion of both metals. Reusability tests (10 x 5 h) carried out with the bimetallic system confirmed the good stability of the system.
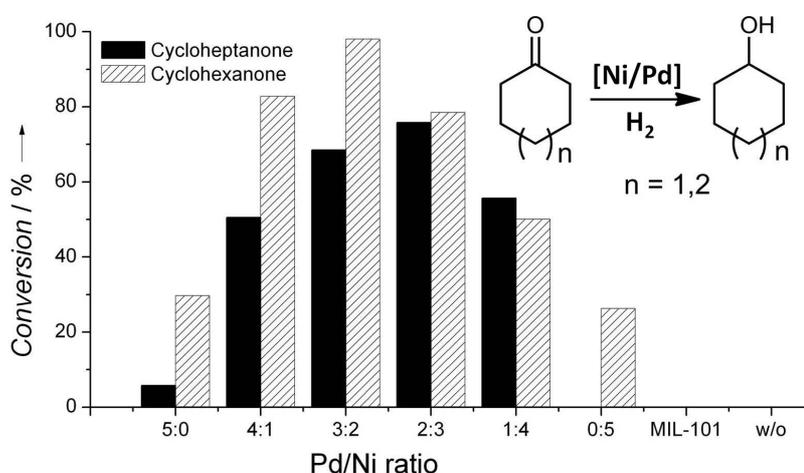
Scheme 2: A maximum in conversion for the reduction of cyclic ketones was achieved for bimetallic Pd_3Ni_2 NP.

Further experiments should provide a more detailed understanding of heterogeneous liquid phase catalysis. The targeted synthesis of MIL-101 crystallites in different sizes and the subsequent loading with Pd NP is the aim of the last chapter. First, the conditions for the size-selective synthesis of the MIL-101 crystallites had to be developed. By varying the concentrations of the educts HF and H_2O, different crystallite size distributions could be realized in the range of 100 nm to 1.5 µm. The by-products obtained could be separated and characterized. The metal loading of the MIL-101 crystallites of different sizes was performed via the already familiar method of MOCVD. A uniform distribution of the MNP (~ 3 nm) in the host material was confirmed by TEM analysis. The hydrogenation of aromatic ketones showed significantly higher yields if smaller Pd-loaded MIL-101 crystallites were used (Scheme 3). Yet, this dependence was only observed if diffusion control was avoided by the suitable choice of solvent and pressure. Further a migration of palladium between different MIL-101 crystallites was observed even at mild conditions. In particular, unloaded MIL-101 crystallites with distinguishable size were added to the catalyst mixture and used as a scavenger for the Pd-loaded MIL-101 crystallites. TEM analysis of the used mixture (50 °C, 66 h) showed Pd NP in the originally unloaded MIL-101 crystallites.
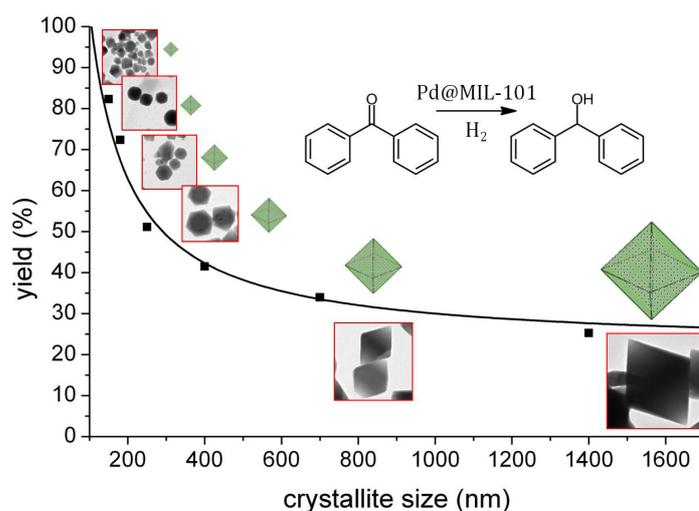

Scheme 3: The MIL-101 crystallite size influences the catalytic activity of the Pd@MIL-101 catalyst system.

Zusammenfassung

Inhalt der vorliegenden Arbeit ist die Untersuchung von katalytisch relevanten Metallnanopartikeln (MNP) stabilisiert in porösen Koordinationspolymeren (PCP), welche auch als metallorganische Netzwerke (MOF) bezeichnet werden. Die Synthese der Katalysatorfamilie MNP@PCP/MOF sowie die Untersuchung ihrer katalytischen Aktivität werden im Detail diskutiert. Desweiteren dient das MNP@PCP/MOF System der Untersuchung katalytisch wichtiger Phänomene wie Dispersion, Synergie und Leaching.

Die literaturbekannte Synthese des Metallorganischen Netzwerkes MIL-101(Cr) erfolgte hydro-thermal. Auf diese Weise können nach geeigneter Aufbereitung in guter Ausbeute eine hohe Oberfläche und gute Phasenreinheit erzielt werden. Die Kavitäten des Trägermaterials (2.9 und 3.4 nm) wurden mittels metallorganisch chemischer Gasphasenabscheidung (MOCVD) mit leicht sublimierbaren Metallpräcursoren infiltriert (Metall-Präcursor@MIL-101). Dabei ermöglicht die hohe Adsorptionsfähigkeit des MIL-101 eine nahezu quantitative Beladung (> 50 Gewichtsprozent) und verhindert gleichzeitig die unerwünschte Desorption des Metallkomplexes. Die Reduktion der infiltrierten Metallpräcursoren unter Wasserstoffatmosphäre führte zur Ausbildung von MNP, welche durch die Kavitätenwände in ihrem Wachstum eingeschränkt wurden (M@MIL-101). Die Systeme wurden mit Röntgen-Pulverdiffraktometrie, IR-Spektroskopie, Transmissionselektronenmikroskopie und Elementaranalyse untersucht.


$[(C_5H_5)Pd(C_3H_5)]@MIL-101$
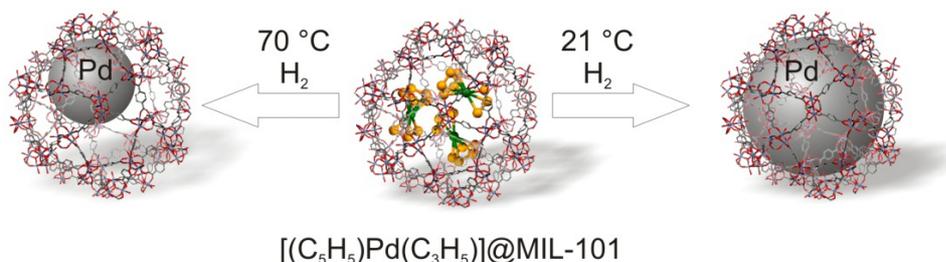
Schema 1: Schematische Darstellung von Kavitäten-konformen (21 °C) und untermaßigen Pd NP (70 °C) in einer MIL-101 Kavität.

Stets bleibt die kritische Frage über den exakten Ort der MNP zu beantworten. Die erwünschte Bildung der MNP innerhalb des Trägermaterials (d.h. in den Kavitäten des MIL-101) wird häufig begleitet von einer Metallabscheidung an der externen Oberfläche der MIL-101 Kristallite. Hierbei ist die Wahl der Reduktionsbedingungen nicht nur entscheidend für den Abscheidungsort, sondern darüber hinaus auch für die Größe der resultierenden MNP (Schema 1). Die Reduktion des infiltrierten Pd-Präcursors $[(\eta^5\text{-}C_5H_5)Pd(\eta^3\text{-}C_3H_5)]$ liefert bei niedrigen Reduktionstemperaturen (21 °C) Kavitäten-konforme MNP (~3 nm), während sich bei erhöhten Reduktionstemperaturen (70 °C) untermaßige Pd NP bilden (~2 nm). Bei Temperaturen über 220 °C kommt es wiederum zur

unerwünschten Abscheidung von Metallpartikeln an der externen Oberfläche des Trägermaterials. Die Pd@MIL-101 Systeme wurden hinsichtlich ihres katalytischen Potentials in der Reduktion von Ketonen untersucht. Dabei konnte eine Selektivität der Systeme (Kavitäten-konforme versus untermäßige MNP) bezüglich der Substratgröße festgestellt werden. Die vollständige Beladung einzelner Kavitäten beschränkt die zugängliche Metalloberfläche auf den Bereich der Kavitäten-fenster und verringert dadurch mögliche Wechselwirkungen mit sterisch anspruchsvollen Substraten. Für große Substrate werden entsprechend niedrigere Ausbeuten erhalten. Wiederver-wendbarkeitstests (11 x 8 h) zeigten keine Abnahme der Aktivität, jedoch wurde bei längeren Reaktionszeiten (> 48 h) eine generelle Agglomeration von Partikeln über einzelne Kavitäten hinaus beobachtet, die mit einer Deaktivierung des Katalysators einherging.

Ausgehend von der Synthese untermäßiger MNP verfolgten wir die Einbringung eines zweiten Metalls zur Generierung bimetallischer Nanopartikel (NP). Auf dem bereits erforschten Pd@MIL-101 System aufbauend wurde Nickel als zweites Metall gewählt. Hier waren grundsätzlich zwei Herangehensweisen möglich. Der sukzessiven Beladung stand die simultane Beladung bzw. Reduktion der zwei Metallpräcursoren gegenüber. Während die erste Variante zu separierten, nicht-bimetallischen NP führte, ergab die zweite Variante die angestrebte bimetallische Form (Ni/Pd). Für nickelreiche Systeme (Ni > 50 %) führten die für das Pd@MIL-101 System optimierten Reduktions-bedingungen zu Kavitäten-überschreitenden MNP im Größenbereich von 5 - 60 nm, so dass eine Anpassung der Reduktionsbedingungen nötig war. Die Existenz bimetallischer NP wird durch Molekulardynamik (MD) Berechnungen, Röntgen-Pulverdiffraktometrie sowie hochauflösende Trans-missionselektronenmikroskopie und energiedispersive Röntgenspektroskopie bestätigt. Bei katalytischen Untersuchungen konnte ein signifikanter synergetischer Effekt des Ni/Pd Systems beobachtet werden.
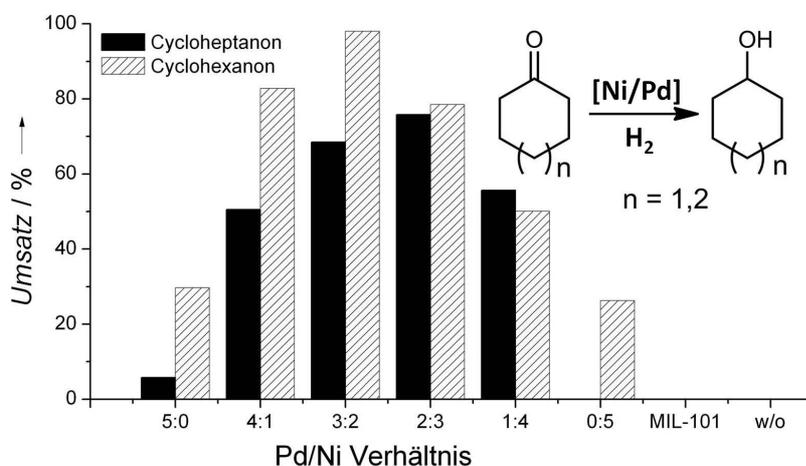
Schema 2: Maximaler Umsatz bei der Reduktion von cyclischen Ketonen wird für bimetallische Pd$_3$Ni$_2$ NP erzielt.

1. Summary

Die Einlagerung von Nickel ermöglichte die erfolgreiche Reduktion aliphatischer und cyclischer Ketone, die weder von reinem Nickel noch von reinem Palladium in größerem Maße reduziert werden. Bei einem Mischungsverhältnis von 3:2 konnte ein maximaler synergetischer Effekt verzeichnet werden (Schema 2), der nur im Falle einer atomaren Dispersion beider Metalle beobachtet wurde. Auch die mit dem bimetallischen System durchgeführten Wiederverwend-barkeitstests (10 x 5 h) bestätigten die gute Stabilität des Systems.

Weitere Untersuchungen sollten ein genaueres Verständnis bezüglich heterogener Flüssigphasen-katalyse liefern. Die gezielte Synthese von MIL-101 Kristalliten unterschiedlicher Größe sowie die anschließende Beladung mit Pd NP ist das Ziel des letzten Kapitels. Dafür mussten zunächst die Bedingungen für eine größenselektive Synthese der MIL-101 Kristallite entwickelt werden. Durch Variation der Eduktkonzentrationen von HF und H_2O konnten unterschiedliche Kristallitgrößen-verteilungen im Bereich von 100 nm bis 1,5 µm realisiert werden. Dabei entstandene Nebenprodukte konnten abgetrennt und charakterisiert werden. Die Beladung der unterschiedlich großen MIL-101 Kristallite erfolgte auf bereits bekanntem Weg über MOCVD. Eine gleichmäßige Verteilung der MNP (3 nm) im Wirtsgitter wurde durch TEM-Untersuchungen bestätigt. Die Hydrierung aromatischer Ketonen zeigte deutlich höhere Ausbeuten bei der Verwendung kleiner, Pd-beladener MIL-101 Kristallite (Schema 3). Diese Abhängigkeit wurde jedoch nur beobachtet, wenn durch die geeignete Wahl von Lösungsmittel und Druck eine Diffusionskontrolle vermieden wurde. Des Weiteren war eine Migration von Palladium zwischen unterschiedlichen MIL-101 Kristalliten bei bereits milden Bedingungen feststellbar. Hierzu wurden unbeladene MIL-101 Kristallite mit unterscheidbarer Größe zum Katalysatorgemisch gegeben und als ‚Fänger' für die Pd-beladenen MIL-101 Kristallite verwendet. TEM Untersuchungen nach der Katalyse (50 °C, 66 h) zeigten Pd NP in den ursprünglich unbeladenen MIL-101 Kristalliten.
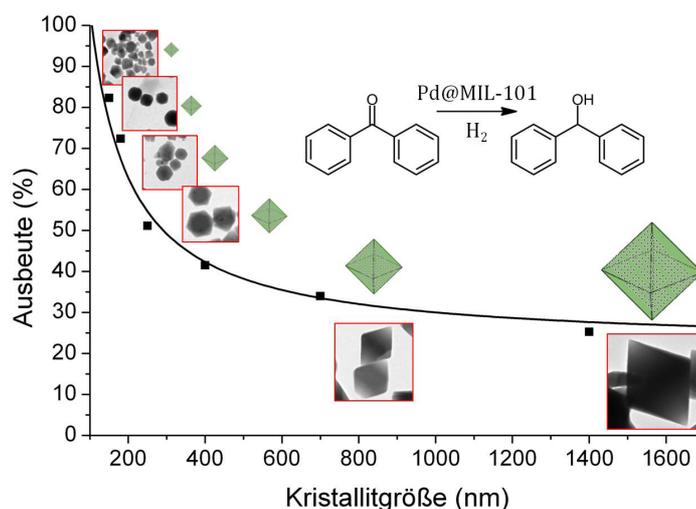
Schema 3: Die Kristallitgröße des Trägers MIL-101 beeinflusst die katalytische Aktivität der Pd@MIL-101 Katalysator Systeme.

2 Introduction

The discovery of porous coordination polymers (PCPs) by Robson *et al.*[1] and the further development of the metal organic frameworks (MOFs) by Yaghi *et al.* [2] enriched the class of porous compounds by a variable, versatile and highly ordered new structure type with extremely high specific surface areas. A multidimensional linkage between inorganic metal centers by multi-functional organic linkers resulted in a highly ordered porous structure. Layers, channels, pores or cavities with a narrow pore size distribution in the range of 1 nm – 4 nm were designed by exchanging the metal centers or the organic linker. This concept allows a variety of possible linkage patterns, pore sizes and geometries. Within 10 years PCPs/MOFs were intensively studied in catalysis, sensing, gas storage and separation.[3] Especially with regards to catalytic applications, PCPs/MOFs are well suited to stabilize very small metal nanoparticles (MNP).

MNP are interesting for many reasons. In general, the ratio of surface area to volume (dispersion) for any material will be described by a function of $B \cdot r^{-1}$, with r being the radius and B a coefficient. The curve is characterized by a step ascent for small r values. Hence, smaller particles in the range of the nanometer scale will have higher dispersions. Based on this increased dispersion, MNP show a different behavior compared to their bulky counterpart. Higher surface tensions affect optical and electrochemical properties, which influences the catalytic behavior concerning activity and/or selectivity of a metal catalyst. Thus, stabilizing MNP by incorporating them within PCPs/MOFs is interesting for three reasons. Firstly, the cavities and windows of the PCPs/MOFs can regulate the particle size and simultaneously guarantee access to the catalytically active sites of the MNP. Secondly, no strongly binding ligands are necessary, as they might influence the accessibility or the chemical and physical properties of the MNP. Furthermore, immobilizing NP in or on a macroscopically visible host structure allows easy separation of liquid reaction mixtures from the catalyst. The reusability of a catalyst with constant activity is one of the great advantages of heterogeneous catalysis.

Different methods like solution infiltration, solid grinding, microwave irradiation, surface grafting, and the metal–organic chemical vapor deposition (MOCVD) method were introduced for the incorporation of MNP in PCPs/MOFs (Scheme 1). Except for solid grinding all methods take advantage of the infiltration of a small dissolved or gaseous metal precursor. Because of the good adsorption behavior of PCP/MOFs, these small precursors are easily trapped within the support (Metal-precursor@PCP/MOF) and can be transformed by various means to the corresponding metal (e.g. by reduction with H_2). The reduced metal atoms will agglomerate, forming MNP, which are now too big to pass the cavity windows or to leave the support (M@PCP/MOF). If two or even more

precursors are infiltrated at the same time (simultaneously), different infiltration and transformation behaviors for each precursor should be taken into consideration. The critical question on the whereabouts of the MNP remains for all methods. Inappropriate conditions during transformation may lead to MNP larger than the cavities or particles localized on the outer surface of the PCP/MOF crystallite. Hence, infiltration and transformation processes need to be carefully adjusted to guarantee a good dispersion of MNP within the cavities of the PCP/MOF system.
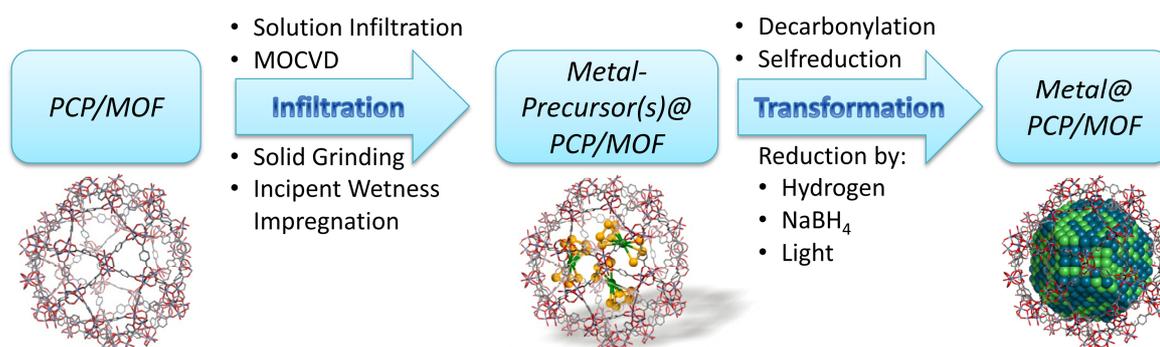
Scheme 1: General procedure for the synthesis of M@PCP/MOF catalysts.

In comparison to other loading methods, MOCVD is of advantage especially in terms of control and high metal loadings as no solvents are needed (> 50 wt.-%).[4] However, special requirements for the precursors have to be considered. Most importantly, the precursor needs to be stable in terms of infiltration via the gas phase yet unstable concerning the transformation of precursor to MNP within the cavities. On the other side, the porous host needs to be stable under conditions such as low vacuum and elevated temperature (150 °C). While air and water stability of the host may not be important for the synthesis procedure, potential applications of the metal loaded PCP/MOF might be more demanding concerning stability (e.g. for oxidation reactions). This way, PCPs/MOFs with different topology, pore size, and pore geometry have been loaded via MOCVD with various metals, each of them with their own favorite way of transformation.

The choice of the host material is also influenced by potential applications, e.g. gas or liquid phase reactions. Several factors like the chemical and physical environment of the cavities play an important role. However, most importantly for the incorporation of MNP within PCPs/MOFs, diffusion phenomena need to be considered. The selective sorption behavior reported for different gases or liquids in separation, storage and catalytic processes is based on size and/or chemical structure of the host and the substrate.[5] For example, bigger substrates are affected more strongly by diffusion problems than smaller gas molecules like CO. Smaller pores/cavities on the other side show different sorption behavior than bigger pores/cavities. This way, catalytic systems can be effectively tuned in terms of selectivity and activity by the right choice of support. Another important

factor concerning sorption behavior is the crystallite size of the support. Cavities, which are situated near the surface of a PCP/MOF crystallite are more readily accessible for substrates and will influence classic applications like gas storage, separation, sensing, and catalysis. As in the case of MNP, an increase in dispersion is observed for smaller MOF/PCP crystallite sizes, leading to a higher concentration of these cavities. Thus, the effective size of the support influences the sorption behavior of PCP/MOF based systems.

Still, a very important drawback of PCPs/MOFs is their instability. Even though problems like the removal of stabilizing solvents, or the instability towards oxygen and water have been solved,[6] thermal stability is still a very important issue. Most of the PCP/MOF systems decompose at temperatures above 250 °C. Even prolonged treatment at 150 °C results in severe decrease in surface area which is equivalent to a destruction of the catalyst. Hence, most moderate reaction conditions are compulsory to ensure a long term stability of the catalyst. Although the thermal stability of PCPs/MOFs limits possible applications at elevated temperature, M@PCP/MOF systems will remain a good model system for the description of 'free' MNP.

This thesis covers the synthesis and characterization of metal-loaded MIL-101 systems and their application as heterogeneous catalysts. We were able to show that cavity conform Pd NP and smaller ones can be generated in the PCP/MOF MIL-101 by altering the reaction conditions. The latter is especially interesting since bimetallic NP might be grown starting from these under-sized particles. However, bimetallic Ni/Pd NP could only be obtained by readjusting the reaction conditions. A pronounced synergetic effect in solution phase catalysis was detected for the bimetallic systems. Furthermore, we were able to show a dependence of the catalytic activity from the size of the M@PCP/MOF crystallite (colloidal size effect) and confirm palladium particle migration from PCP/MOF crystallite to crystallite under very mild reaction conditions.

[1] a) B. F. Hoskins, R. Robson, *J. Am. Chem. Soc.* **1989**, *111*, 5962–5964;

b) B. F. Abrahams, B. F. Hoskins, D. M. Michail, R. Robson, *Nature* **1994**, *369*, 727–729.

[2] H. Li, M. Eddaoudi, M. O'Keeffe, O. M. Yaghi, *Nature* **1999**, *402*, 276–279.

[3] Special Issue Metal Organic Frameworks: *Chem. Rev*. **2012**, *112*, 673– 1268.

[4] a) S. Hermes, M.-K. Schröter, R. Schmid, L. Khodeir, M. Muhler, A. Tissler, R. W. Fischer and R. A. Fischer, *Angew. Chem. Int. Ed*. **2005**, *44*, 6237-6241; b) S. Proch, J. Herrmannsdörfer, R. Kempe, C. Kern, A. Jess, L. Seyfarth, J. Senker, *Chem. Eur. J*. **2008**, *14*, 8204 – 8212.

[5] J.-R. Li, J. Sculley, H.-C. Zhou, *Chem. Rev*. **2012**, *112*, 869–932.

[6] G. Férey, C. Mellot-Draznieks, C. Serre, F. Millange, J. Dutour, S. Surblé, L. Margiolaki, *Science* **2005**, *309*, 2040-2042.

3 Overview of Thesis Results

3.1 Overview and Interconnection of the Publications

This thesis is comprised of three publications, which are presented in chapter 4-6. All three chapters deal with the generation of metal nanoparticles (MNPs) within the porous coordination polymer/metal organic framework (PCP/MOF) MIL-101 and with the catalytic studies of this new catalyst family. The synthesis of the M@MIL-101 catalyst system was accomplished by infiltrating the host MIL-101 with volatile metal precursors via the metal organic chemical vapor deposition (MOCVD) method and the successive reduction of the metal precursors with hydrogen (transformation). The synthesized M@MIL-101 systems were characterized by X-ray diffraction, IR spectroscopy, N_2-physisorption, elemental analysis, and transmission electron microscopy (TEM) and compared on basis of their catalytic activity, selectivity and stability. The influences of the reaction conditions during the infiltration and transformation procedure on the obtained MNPs are described in detail for monometallic (chapter 4) and bimetallic (chapter 5) nanoparticles (NPs). The influences of the host material MIL-101 on the catalytic activity of the M@MIL-101 catalyst system are described in chapter 6. The general approach of this thesis and of the three publications comprised within gives a better understanding of the synthesis and the catalytic activity of the M@PCP/MOF systems.

Previously, our group had been able to infiltrate the porous host structure MOF-177 with the Pt precursor [Me$_3$PtCp′] by the MOCVD method and to generate Pt NPs within the porous host via reduction with hydrogen (Pt@MOF-177)[1]. The Pt loaded system showed an improved sorption and storage capacity for hydrogen and a good activity in the oxidation of alcohols (Figure 1).
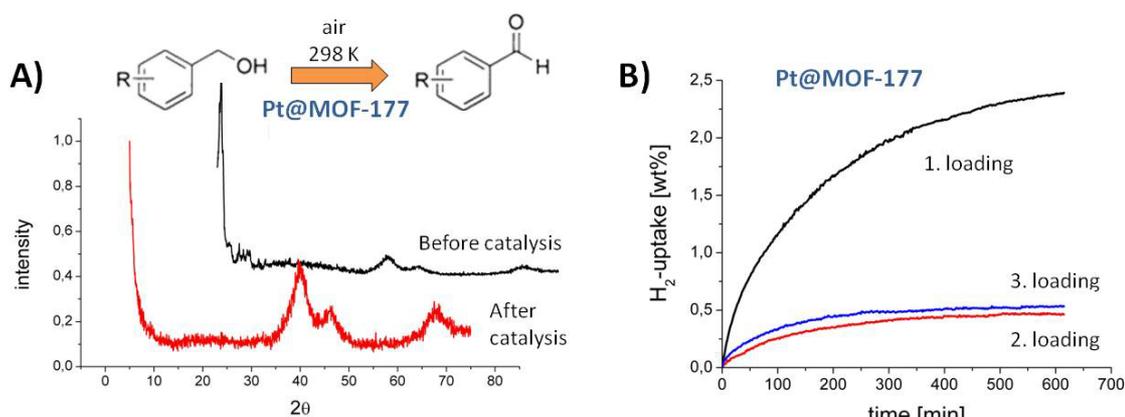

Figure 1: A) Oxidation catalysis with the Pt@MOF-177 catalyst system using air as an oxidant. The catalyst system decomposes during catalysis. B) Hydrogen storage capacity of the hybrid material of three successive loading cycles with hydrogen.[1]

However, fast decomposition of the system was observed due to air and water sensitivity of the host MOF-177. Reusability tests showed a severe drop of activity after the first cycle in the storage of hydrogen and in the oxidation of alcohols. Thus, another PCP/MOF system with better stability and reusability properties had to be found.

Unlike MOF-177, MIL-101[2] is stable in water and air for at least 6 months. Hence, it should be more suitable for the loading and stabilization of MNPs. Although the knowledge of its structure is derived from computational design experimental data (e.g. TEM) seem to confirm these simulations. The structural building unit (SBU) consists of a chromium oxo trimer being connected to six other SBUs via doubly deprotonated terephthalic acid linkers. The resulting tetrahedron is assembled to what have been called "super tetrahedrons" leading to two different cavities with pore dimensions of about 2.9 and 3.4 nm and pore windows of 1.2 and 1.47 - 1.6 nm (Figure 2). These windows are well suited for small metal precursors to enter the cavities of the host. Successive reduction of the trapped metal precursor with hydrogen results in the formation of MNPs whose size is restricted to the cavity dimensions of 3.4 nm. This way, a narrow size distribution of MNPs can be realized. Concerning catalysis, the high surface area and the big cavity windows ensure good accessibility of the MNPs.
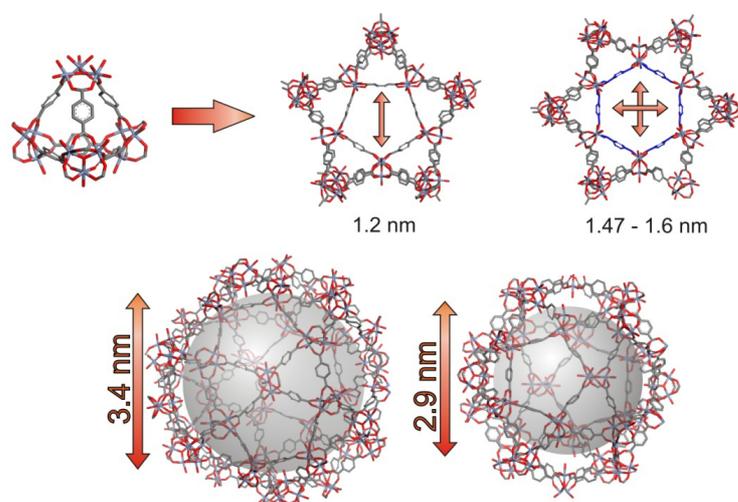

Figure 2: Construction of the pores and the cavities of MIL-101.

In Chapter 4 the synthesis of palladium NPs in the host structure of MIL-101 via the MOCVD method is described in detail. Quantitative loadings higher than 50 wt.-percent were accomplished for the first time with the Pd precursor complex [(C$_5$H$_5$)Pd(C$_3$H$_5$)]. Reduction of the precursor complex with hydrogen has given rise to Pd NPs inside the host MIL-101 (Pd@MIL-101). The reduction conditions, especially temperature, allowed us to control the size of the Pd NPs (Figure 3). Size-conform (size of the Pd NPs correlates with the size of the cavities of the host structure of MIL-101) and undersized Pd

NPs were synthesized. Characterization by X-ray diffraction, IR spectroscopy, N_2-physisorption, elemental analysis, and transmission electron microscopy confirmed the improved stability of the new catalyst system M@MIL-101 after metal loading and after catalysis. Catalytic studies, hydrogenation of ketones, were performed with the Pd@MIL-101 catalysts, and two main aspects were found. These were: 1. Aryl-alkyl ketones are readily reduced however, no conversion is found for alkyl-alkyl ketones. 2. In contrast to the Pd@MIL-101 systems with undersized Pd NPs, higher conversions for smaller substrates and lower conversions for bigger substrates are observed for the systems with size-conform Pd NPs. The complete filling of the cavity space with Pd restricts the accessible metal surface decreasing possible interactions with sterically demanding substrates. Additionally, the improved stability of the host MIL-101 in comparison to MOF-177 was demonstrated by reusability tests with the Pd@MIL-101 catalyst system.
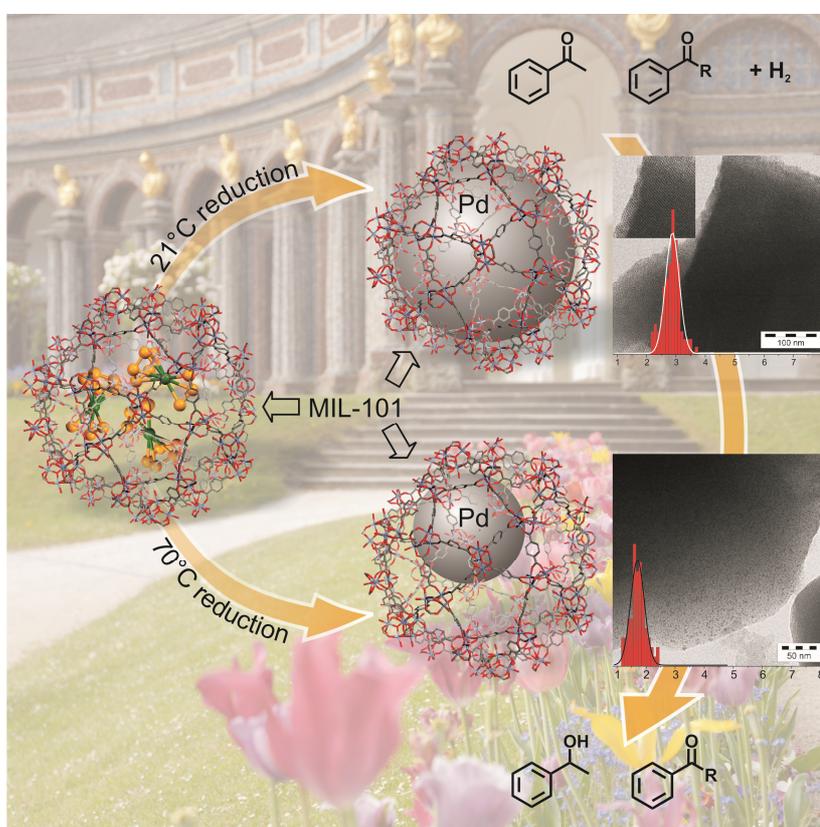
Figure 3: Dependence of the resulting MNP size on the reaction conditions during the reduction of the Pd precursor complex [(C$_5$H$_5$)Pd(C$_3$H$_5$)].[3]

In contrast to the experiments, which were stopped after relatively short reaction times (9 h), experiments after prolonged catalysis (48 h) were marked by a deactivation of the catalyst (Figure 4). This deactivation was accompanied by the formation of bigger agglomerates (24 nm), which consisted of NPs of about 4 nm in size. After 76 h of prolonged catalysis, the agglomerates are merged into single uniform particles with a mean particle size beyond the confinement of the pore

dimensions. However, this deactivation is not derived from the destruction of the host material MIL-101, but is rather based on the instability of the Pd NPs. Furthermore, the deactivation is limited to prolonged reaction times, far after the full conversion of the substrate. Reusability tests after relatively short reaction times (still with 100 % of conversion) showed neither a drop in activity nor an increase in particle size after at least eleven runs. Although the stability of the new catalyst class M@MIL-101 may be limited to short reaction times, its improved stability compared to the MOF-177 based system represents a substantial advance in M@PCP/MOF catalysis.
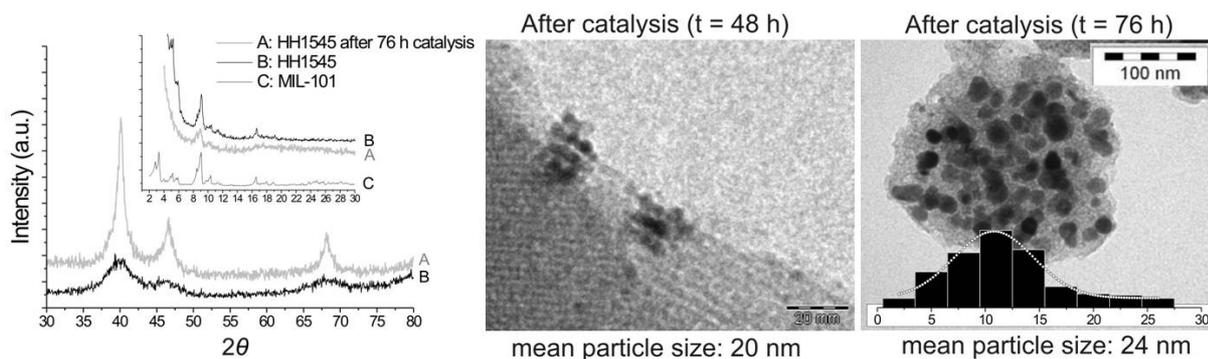
Figure 4: XRD pattern and TEM images of the catalyst system Pd@MIL-101 after prolonged catalysis, reduction of propiophenone. A change in particle size is observed after 48 h and 76 h catalysis time.

In the course of our investigations concerning the synthesis of undersized Pd NPs (chapter 4), efforts were made to introduce a second less noble metal (Ni) within the remaining cavity space to obtain bimetallic NPs (Ni/Pd) (chapter 5). This is interesting for catalytic applications for a few reasons. Firstly, the dilution of costly noble metals by inexpensive metals like nickel is economical. Secondly, bimetallic NP catalysts can show synergistic effects regarding activity and/or selectivity. However, the infiltration of a second metal precursor $[(C_5H_5)_2Ni]$ into the already Pd-loaded MIL-101 systems and the subsequent reduction with hydrogen resulted in the formation of oversized and separated non-bimetallic particles. Only when both metal precursors were infiltrated simultaneously mixed bimetallic NPs were obtained after the reduction with hydrogen. MNPs with different compositions of Ni/Pd were realized by varying the ratio of the two metal precursors. Due to the different stability of the metal precursors, adjustments of the reduction conditions were required to obtain cavity-conform bimetallic Ni/Pd NPs. High resolution transmission electron microscopy and energy-dispersive X-ray analysis performed by Nobuyoshi Miyajima and molecular dynamic calculations done by Rodrigo Albuquerque have confirmed the hypothesis of the formation of bimetallic NPs (Figure 5).

These observations go along with the four main aspects, which were observed in the catalytic studies with the Ni/Pd@MIL-101 system: 1. Alkyl-alkyl ketones as well as cyclic ketones can now easily be reduced with the bimetallic NPs. In contrast to Pt, which is a well-known heterogeneous catalyst for

the hydrogenation of alkyl-alkyl ketones, no such activity has been reported for Ni or Pd before. 2. Maximum activity is found for bimetallic Ni/Pd NPs with a composition of 2:3. 3. The mixture of pure Ni@MIL-101 and pure Pd@MIL-101 in a ratio of 2:3 showed a clearly lower catalytic activity than the corresponding mixed bimetallic catalyst, indicating a synergistic effect which is based on bimetallic particles. 4. The adjustment of the reduction conditions towards bimetallic and cavity conform NPs had a positive influence on the catalytic activity of the catalyst system. Again, the stability of the host MIL-101 was confirmed by reusability tests. No decomposition of the host or a change in particle size was observed under the chosen conditions. The catalyst was reused for at least ten runs without a decrease in conversion, once again demonstrating the improved stability of MIL-101 compared to the MOF-177 based system. In addition, the range of the substrates was successfully extended to alkyl-alkyl ketones, which was not possible for the pure Pd@MIL-101 systems described in chapter 4.
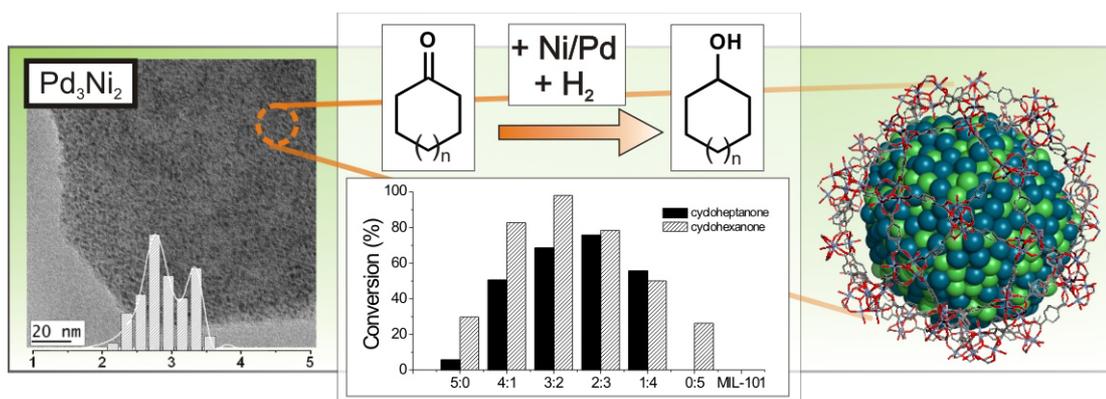
Figure 5: Bimetallic particles are formed within the MIL-101 structure. A maximum in conversion is observed for a Ni/Pd ratio of 2:3.

After detailed experiments concerning the catalytic activity and selectivity in dependence of the size and the composition of the MNPs, further emphasis was put on the influence of the host structure MIL-101 on liquid phase catalysis. As described in chapter 2, the sorption behavior of substrates will be influenced by the crystallite size of the support. The observed effects of this changed behavior on liquid phase catalysis are described in chapter 6. The hydrogenation of aryl-alkyl and aryl-aryl ketones with the well-known catalyst system Pd@MIL-101 is used as an example. The crystallite size of the host MIL-101 can be adjusted via the effective HF concentration during the hydrothermal synthesis. A low concentration of HF results in the formation of small MIL-101 crystallites (100 nm). Extensive washing of the as-synthesized MIL-101 crystallites is crucial to ensure a high surface area and to remove occurring by-products, which were isolated and characterized. Once again the well understood and highly controlled MOCVD method was used to infiltrate the MIL-101 crystallites with the Pd precursor [(C_5H_5)Pd(C_3H_5)]. Reduction of the precursor gave rise to the catalyst system

Pd@MIL-101. The catalytic studies showed a clear dependence of the catalytic activity from the MIL-101 crystallite sizes. This dependence is in good accordance with a theoretical surface:bulk ratio of octahedron shaped MIL-101 (Figure 6). However, careful adjustment of reaction conditions (diffusion control has to be avoided) must be done to observe these effects. Hence, apart from their size and the composition, MNP accessibility seems to be of great importance for catalytic applications.
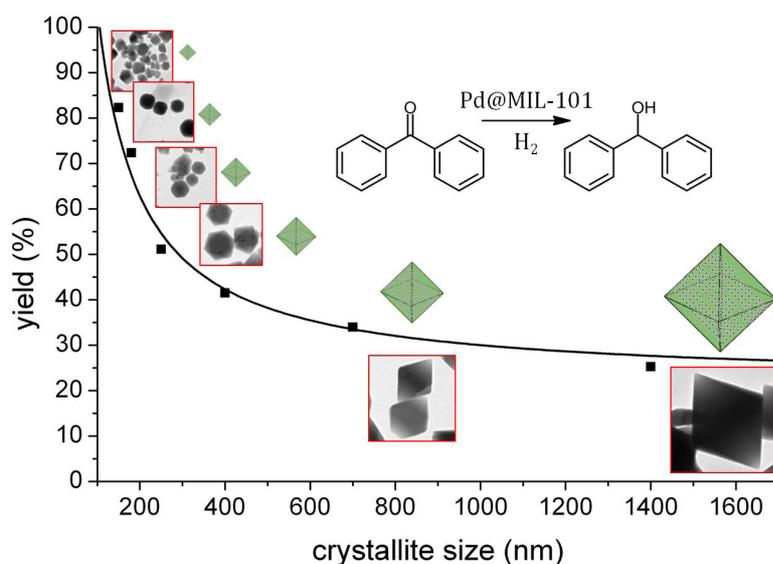

Figure 6: The effect of crystallite size of the support MIL-101 on the hydrogenation of aryl-aryl ketones with the catalyst system Pd@MIL-101.

Furthermore, a Pd NP migration was observed under mild conditions. This effect has already been noted in chapter 4, with the formation of bigger agglomerates of Pd. However, it was not possible to determine the range of the particle migration. By adding small empty MIL-101 crystallites to bigger Pd loaded MIL-101 crystallites (and vice versa), Pd NP migration from crystallite to crystallite was observed for the first time. Not only do Pd atoms and/or particles leave the support but they do also re-enter it. The empty MIL-101 crystallites, with their high surface area, act as scavenger for leached metal species. Reusability tests after short and prolonged reaction times showed neither a drop in activity nor an increase in particle size after several runs. Compared to the higher loaded (45 wt.-%) Pd@MIL-101 systems described in chapter 4, lower metal loadings (16 wt.-%) resulted in a higher remaining surface area of the MIL-101 host ensuring a better recovery of migrated or leached MNP. These observations most definitely will influence future research on M@PCP/MOF catalysis.

In conclusion, the hydrolysis stability of the M@PCP/MOF catalyst system was improved by switching from MOF-177 to a MIL-101 based system. The hydrogenation of alkyl-alkyl, aryl-alkyl and aryl-aryl ketones was researched in detail for the M@MIL-101 catalyst systems. Catalytic effects such as

selectivity, synergism and leaching were discussed in detail. However, long range particle migration still causes a deactivation of the catalyst system during longer reaction times and higher loadings.

[1] S. Proch, J. Herrmannsdörfer, R. Kempe, C. Kern, A. Jess, L. Seyfarth, J. Senker, *Chem. Eur. J.* **2008**, *14*, 8204 – 8212.

[2] G. Férey, C. Mellot-Draznieks, C. Serre, F. Millange, J. Dutour, S. Surblé, L. Margiolaki, *Science* **2005**, *309*, 2040-2042.

[3]   J. Hermannsdörfer, R. Kempe, *Chem. Eur. J.* **2011**, *17*, 7965.

3.2   Individual Contribution to Joint Publications

The results presented in this thesis were obtained in collaboration with others and are published as indicated below. In the following, the contributions of all the co-authors to the different publications are specified. The asterisk denotes the corresponding author.

Chapter 4

This work is published in *Chem. Eur. J.* **2011**, *17*, 8071–8077, with the title

"Selective Palladium-Loaded MIL-101 Catalysts."

Justus Hermannsdörfer, Rhett Kempe*

I synthesized all presented compounds. Furthermore, all analyses were carried out by me and the publication was written by me. Rhett Kempe was involved in scientific discussions, comments and correction of the manuscript.

Chapter 5

This work is published in *Angew. Chem. Int. Ed.* **2012**, *51*, 11473–11477, with the title

"Ni/Pd@MIL-101: Synergistic Catalysis with Cavity-Conform Ni/Pd Nanoparticles."

Justus Hermannsdörfer, Martin Friedrich, Nobuyoshi Miyajima, Rodrigo Q. Albuquerque, Stephan Kümmel, Rhett Kempe*

I synthesized all presented compounds. Furthermore, all analyses and catalyses were carried out by me and the publication was written by me. Martin Friedrich helped with the synthesis, analysis and characterization of the presented compounds in the course of his B. Sc. thesis. Nobuyoshi Miyajima did the HR-TEM analysis. Rodrigo Q. Albuquerque did the molecular dynamic simulations. Stephan Kümmel and Rhett Kempe were involved in scientific discussions, comments and correction of the manuscript.

Chapter 6

This work is published in *Chem. Eur. J.* **2013**, *19*, 13652–13657, with the title

"Colloidal Size Effect and Metal Particle Migration in M@MOF/PCP Catalysis"

Justus Hermannsdörfer, Martin Friedrich, Rhett Kempe*

I synthesized all presented compounds. Furthermore, all analyses and catalysis were carried out by me and the publication was written by me. Martin Friedrich was involved in scientific discussions. Rhett Kempe was involved in scientific discussions, comments and correction of the manuscript.

4   Selective Palladium-Loaded MIL-101 Catalysts

Justus Hermannsdörfer[a], Rhett Kempe*[a]

[a] Lehrstuhl für Anorganische Chemie, Universität Bayreuth, Universitätsstraße 30, 95440 Bayreuth (Germany), Fax: (+49) 921-55-2157, Email: kempe@uni-bayreuth.de

Abstract: Palladium nanoparticles (NPs) of different mean particle size have been synthesized in the host structure of the porous coordination polymer (or metal–organic framework: MOF) MIL-101. The metal–organic chemical vapor deposition method was used to load MIL-101 with the Pd precursor complex $[(\eta^5\text{-}C_5H_5)Pd(\eta^3\text{-}C_3H_5)]$. Loadings higher than 50 wt.% could be accomplished. Reduction of the Pd precursor complex with H_2 gave rise to Pd NPs inside the MIL-101 (Pd@MIL-101). The reduction conditions, especially the temperature, allows us to make size-conform (size of the Pd NPs correlates with the size of the cavities of the host structure of MIL-101) and undersized Pd NPs. The Pd@MIL-101 samples were characterized by X-ray diffraction, IR spectroscopy, Brauner–Emmett–Teller (BET) analysis, elemental analysis, and transmission electron microscopy (TEM). Catalytic studies, hydrogenation of ketones, were performed with selected Pd@MIL-101 catalysts. Activity, selectivity, and recyclability of the catalyst family are discussed.

Abstract in German: Palladium Nanopartikel (NP) unterschiedlicher Partikelgröße wurden in der Wirtstruktur des porösen Koordinationspolymer MIL-101 erzeugt. Die Beladung von MIL-101 mit dem Pd Komplex $[(\eta^5\text{-}C_5H_5)Pd(\eta^3\text{-}C_3H_5)]$ erfolgte über metallorganische chemische Gasphasen-abscheidung. Beladungen mit mehr als 50 Gewichtsprozent konnten dabei erreicht werden. Die Reduktion des Pd Präcursors mit H_2 führte zu Pd NP innerhalb des MIL-101 (Pd@MIL-101). Die Reduktionsbedingungen, im speziellen die Temperatur, erlauben es uns Kavitäten-konforme (Größe der Pd NP entspricht der Kavitätengröße der Wirtsstruktur MIL-101) oder untermäßige Pd NP zu erzeugen. Die Pd@MIL-101 Proben wurden mit Röntgen-Pulverdiffraktometrie, IR Spektroskopie, Brunner-Emmet-Teller (BET) Analyse, Elementaranalyse und Transmissionselektronenmikroskopie (TEM) untersucht. Mit ausgewählten Pd@MIL-101 Katalysatoren wurden katalytische Studien (Hydrierung von Ketonen) durchgeführt. Aktivität, Selektivität sowie Wiederverwendbarkeit der Katalysatorfamilie werden diskutiert.

4.1   Introduction

Porous Coordination Polymers (PCP)[1] or Metal Organic Frameworks (MOF)[2] experienced an enormous development since their discovery. Today, more than a decade later, numerous fields of scientific interest have occurred and advanced significantly.[3] The incorporation of noble metal nanoparticles (= NP) within these porous materials via metal organic chemical vapor deposition (MOCVD) initially developed by Fischer and coworkers are a promising way of developing heterogeneous catalysts.[4] The limiting pore dimensions of the crystalline network display excellent conditions for the generation of small metal NP which surface is not blocked by strongly binding ligands.[5] Furthermore, immobilizing NP in or on a macroscopically visible host structure allows easy separation of liquid reaction mixtures from the catalyst. In this regard several PCP/MOFs have been loaded with metal NP applying different ways of synthesis. Beside solution infiltration techniques,[6],[17] solid grinding,[7] microwave irradiation,[8] and surface grafting,[9] MOCVD displays a potential method for the generation of homogeneously confined metal NP such as Pt, Au, Pd, and Ru. In addition, it allows very high loadings (> 30 wt.-%).[10],[11] Problematic for all methods has been so far the generation of NP within the confined dimensions of the porous system. Many examples explored so far show metal NP beyond the size of the pore diameters which means the energy barriers provided by the host for growth inhibition of particle size are rather low. Very recently the successful incorporation of size conform Au NP has been demonstrated within the hosts ZIF-8 and ZIF-90.[5]
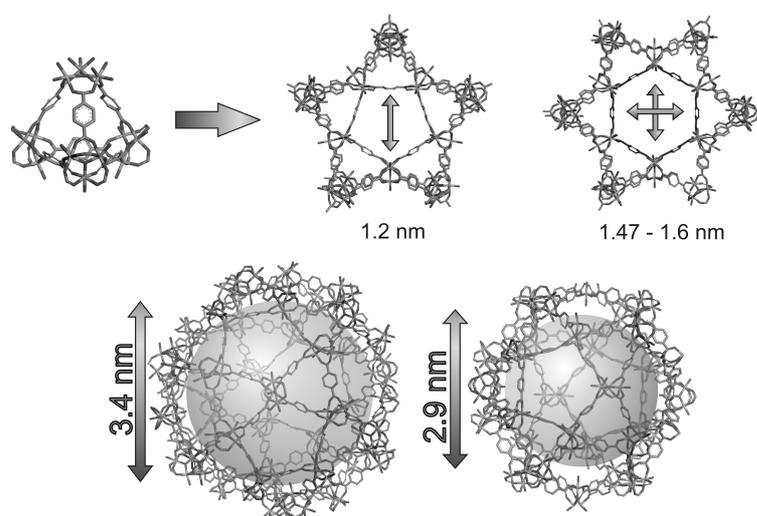
Figure 1. Construction of the pores and the cavities of MIL-101.

The synthesis of the metal@MOF or PCP systems is usually performed in two steps: Firstly, the sublimation or infiltration of a metal complex precursor into the porous network, and secondly, the consequent reduction of the imbedded precursor to metal NP with hydrogen or another reducing

agent. The MOCVD loading with metal complex precursors can proceed in a highly controlled way, even in a single crystal to single crystal reaction.[12] Hence, this step most likely is not causing the problems in terms of generating over-sized particles. Therefore, we thought that the conditions of the reduction step are crucial in terms of particle formation and became interested in understanding this key step better.

We have been interested in PCP or MOF synthesis for many years[13] and succeeded recently in the synthesis of Pt@MOF-177 via MOCVD.[11] Pt@MOF-177 shows an unusual high room temperature hydrogen storage capacity and is an efficient catalyst for the oxidation of alcohols using oxygen as an oxidant. Yet massive problems of catalyst stability encountered. Since water is formed as a byproduct in these oxidation reactions we addressed the instability of the MOF-177 host to the presence of water and switched to relatively water stable MIL-101.[14] It has been investigated as a host for metal NP by a variety of groups.[6],[8],[9],[15] The structure of MIL-101 is very complex: The connector consists of a chromium oxo trimer being connected to six other connectors via doubly deprotonated terephthalic acid linkers. The resulting tetrahedron is assembled to the so called "super tetrahedrons" leading to two different cavities with pore dimensions of about 2.9 and 3.4 nm and pore windows of 1.2 – 1.6 nm (Figure 1).

Herein, we report on the selective loading of MIL-101 with palladium NP via MOCVD and the dependence of the particle size from the reduction conditions. We were able to show that MIL -101 cavity conform Pd NP and smaller ones can be generated by altering the reaction conditions. The latter is especially interesting since bi- and multi-metallic NP might be grown starting from these under-sized particles. Furthermore, the behavior of the resulting Pd@MIL-101 hybrid materials as a catalyst in ketone hydrogenation is discussed.

4.2   Results and Discussion

4.2.1   Selective Pd loading of MIL-101

IR, XRD, and BET studies: The ICP-OES measurements of the loaded Pd@MIL-101 (Table 1 and Figure 2) nicely show the almost quantitative loading of the MIL-101 system with the Pd precursor. When applying dynamic vacuum, no difference to the usually applied static vacuum[6],[10] could be noticed. Both synthesis steps, the loading of MIL-101 and the hydrogenolysis of $[(\eta^5\text{-}C_5H_5)Pd(\eta^3\text{-}C_3H_5)]$@MIL-101, can be performed with up to 98% yield. The conditions during the reduction step are listed in Table 1. The comparison of the calculated values of the Pd loading with the observed values (Figure 2) nicely demonstrates the good adjustability of the metal content.

Table 1. Synthesized Pd@MIL-101 systems with initial weight ratio of Pd precursor and MIL-101 as well as conditions during reduction of the Pd precursor@MIL-101 systems. Abbreviation scheme: first two letters indicate temperature and H_2 pressure condition during reduction, H = high, L = low; the following two digits indicate reduction time in hours and the final two digits the wt.-% Pd loading. Longer reduction times were used for the LL-series due to milder reduction conditions.

run	Pd / Cr [a]	Conditions of reduction			Pd-content
		[°C]	[bar]	[h]	[wt.-%]
HH2609	0.20	70	70	26	9.3
HH2610	0.25	70	70	26	9.9
HH1545	1.68	70	70	15	44.5
HH2656	2.11	70	70	26	55.6
LL6012	0.25	21	5	60	12.4
LL4842	1.68	21	5	48	41.6
LL6058	2.13	21	5	60	57.5
Postmod [b]	0.50	21	5	20	
		50	30	24	17.5
VHTP-25[c]	0.81	220	110	1	24.9

[a] Pd precursor to Cr ratio. [b] Post modified: back to back two step reduction. After 20 h pressure and temperature were increased. [c] Very high temperature and pressure.
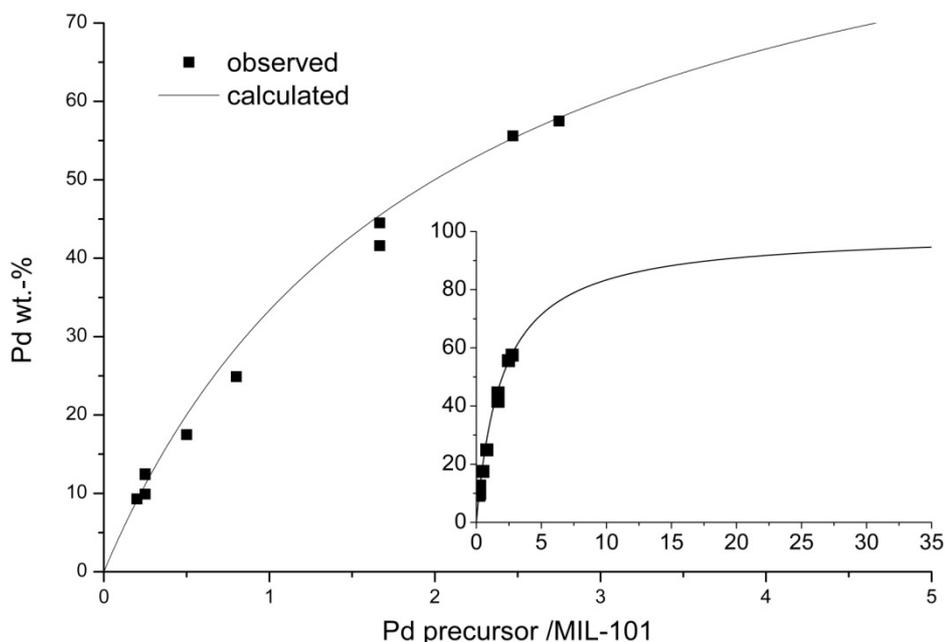
Figure 2. The initial weight ratio Pd precursor/MIL-101 is plotted against the Pd wt.-% of Pd@MOF. A good accordance of the measured (squares) and the calculated values (line) was observed. The loading of the MIL-101 system with the Pd precursor is almost quantitative.

The IR spectra (Figure 3) of the different Pd@MIL-101 systems indicate the intact structure of MIL-101 for all reduction protocols beside that of VHTP-25. For the VHTP-25 protocol additional peaks are visible, showing degradation of the host structure, which can be explained by the very high temperature applied during the reduction step.
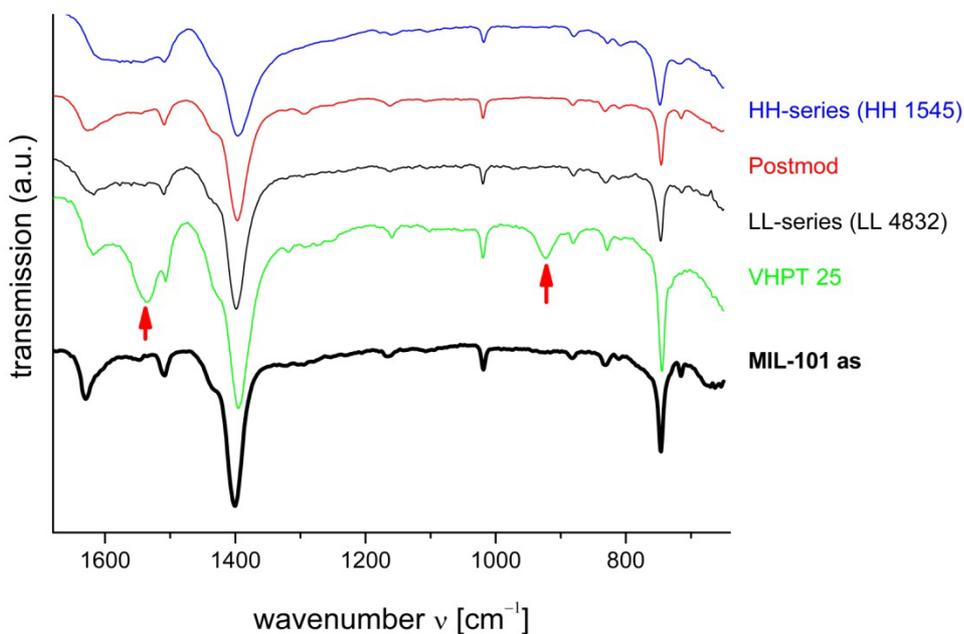
Figure 3. IR Spectra of Pd@MIL-101 (selected runs). The typical vibrations of MIL-101 (black) are still existent in the loaded systems. Yet one can see additional peaks for VHTP-25, assuming a degradation of the host structure (1537 and 925 cm^{-1} marked by arrows).
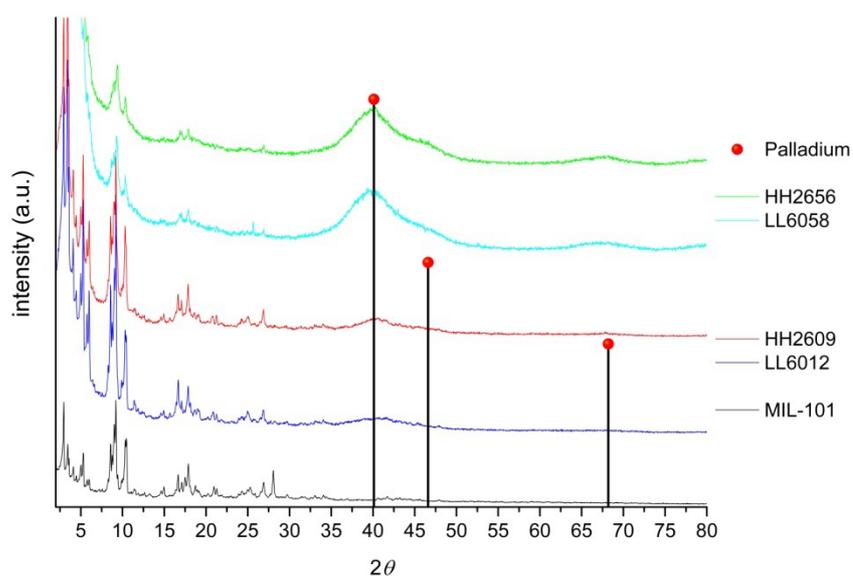
Figure 4. XRD pattern of Pd@MIL-101 (selected runs). Beside the *fcc* characteristic Pd pattern at $2\vartheta = 40°$, $2\vartheta = 46.6°$, and $2\vartheta = 68.2°$, one can clearly see the intact structure of MIL-101. The Pd reflections become more intense with higher metal loadings.

The XRD analysis (Figure 4) of the Pd@MIL-101 systems displays the characteristic MIL-101 pattern in the region $2\vartheta < 20°$. In addition, an intensified noise at higher loadings of Pd is observed. It can be explained by the absorption of diffracted intensities by palladium. The face-centered cubic (*fcc*) Pd peaks at $2\vartheta = 40°$, $2\vartheta = 46.6°$, and $2\vartheta = 68.2°$, respectively (111), (200), and (220) are visible for the Pd loaded systems. More intensive Pd based diffraction patterns were found for the highly Pd loaded systems. NP in the size regime of 1 or 3 nm can be assumed based on the full width at half maximum of the Pd diffraction patterns, which is in accordance with the dimensions of the cavities in MIL-101.

Table 2. Surface area measurements for the free and metal loaded MIL-101.

Sample	BET surface area (m^2g^{-1})	Pore volume (cm^3g^{-1})
MIL-101[a]	2180	1.06
HH2609	1314	0.63
HH2610	1339	0.63
HH1545	251	0.17
HH2656	223	0.11
LL6012	1263	0.64
LL4842	197	0.18
LL6058	220	0.11
Postmod	1141	0.24
VHTP-25	31	0.01

[a] As synthesized material.

The surface area for the different MIL-101 samples was calculated from the N_2 isotherm using the BET Model (Brunnauer-Emmett-Teller) and found to be around 2200 m²/g. It is definitely lower than the reported value by Férey *et al.*[14] but similar to those reported by others.[8],[18] The Pd loaded MIL-101 structures clearly show a smaller specific surface area. It is due to occupying of some cavities by Pd NP but also due to the fact that Pd increases the mass of the systems (especially with loadings up to 58 wt.-%). While systems with low loadings maintain at least 40% of their former specific surface area, systems with higher loadings drop to merely 10% of their former specific surface area. In the case of VHTP-25 no significant pore volume and surface area can be detected indicating the destruction of the host structure.

TEM studies: During the adjacent TEM measurements a massive deformation and destruction of the host structure by operating at high electron intensity could be observed. Thus we tried to measure at the lowest possible intensity to obtain reproducible results. For each of the different reduction protocols (except for VHTP-25) we could see the typical octahedron shaped crystallites of MIL-101 in the size regime of 100 nm – 5 µm.

1. Reduction protocol: Low temperature. The generation of Pd@MIL-101 at low temperatures (21 °C) and low H_2 pressure (5 bar) led to highly ordered structures. TEM micrographs of LL6012 and LL6058 show a very high regularity of the trapped Pd NP (Figure 5 A and B). The example with low metal loadings (LL6012) shows very small Pd NP (~ 2.7 nm) with a narrow size distribution. The mean particle size slightly increases with increasing metal loading (to about 2.9 nm), yet keeping a narrow size distribution.

2. Reduction protocol: High temperature. Adjusting the conditions to elevated temperature (70 °C) and higher pressure (70 bar) led to narrowly but differently distributed Pd NP within the pores/cavities of MIL-101 as shown in Figure 5. The NP distribution is again very narrow and the mean particle size (about 1.7 nm) is well below the dimensions of both cavities, the size being more in the size regime of the cavity windows (1.2 – 1.6 nm) albeit the particles are in average a little larger. When proceeding to higher loadings the saturation of the cavities increases. Again a similarly narrow Pd NP size distribution is observed with its mean particle size at 1.7 nm (Figure 5 C and D).

The reduction under (firstly) mild conditions and afterwards at elevated temperature led to an equally sharp distribution of very small Pd NP (Figure 5 E). The results are comparable to those obtained by the high temperature protocol. This implies a possible post modification of the NP. While the first reduction step leads to the formation of NP being in the size regime of 2 – 3 nm (similar to the results of the LL runs) the second step leads to a confinement of the particles to a mean particle size of around 1.7 nm.

3. Reduction protocol: Very high temperature. If applying extreme conditions like 220 °C and 110 bar (note the thermal stability of MIL-101 being higher than 275 °C) we observed a partly destruction of the host structure and an agglomeration of particles beyond the range of the cavity dimensions (Figure 5 F). A broad particle size distribution ranged from 2-11 nm is observed. In addition, surface particles being larger than 15 nm were found.

Despite the fact that TEM is an invasive analysis and the particle sizes can be modified by the electron beam a clear correlation between the reduction protocol and the resulting particle size can be observed. The reduction temperature seems to play an important role. In case of MIL-101 higher reduction temperatures lead to smaller particles. Especially with MIL-101 is the presence of cavities which are rather large in comparison to the size of its connecting windows (Figure 1). It is conceivable that at high (70 °C) but not too high temperatures the Pd NP are "dynamic" enough and the window size of the MIL-101 has a larger influence on the particle size than the cavity sizes and hence undersized particles can be obtained.
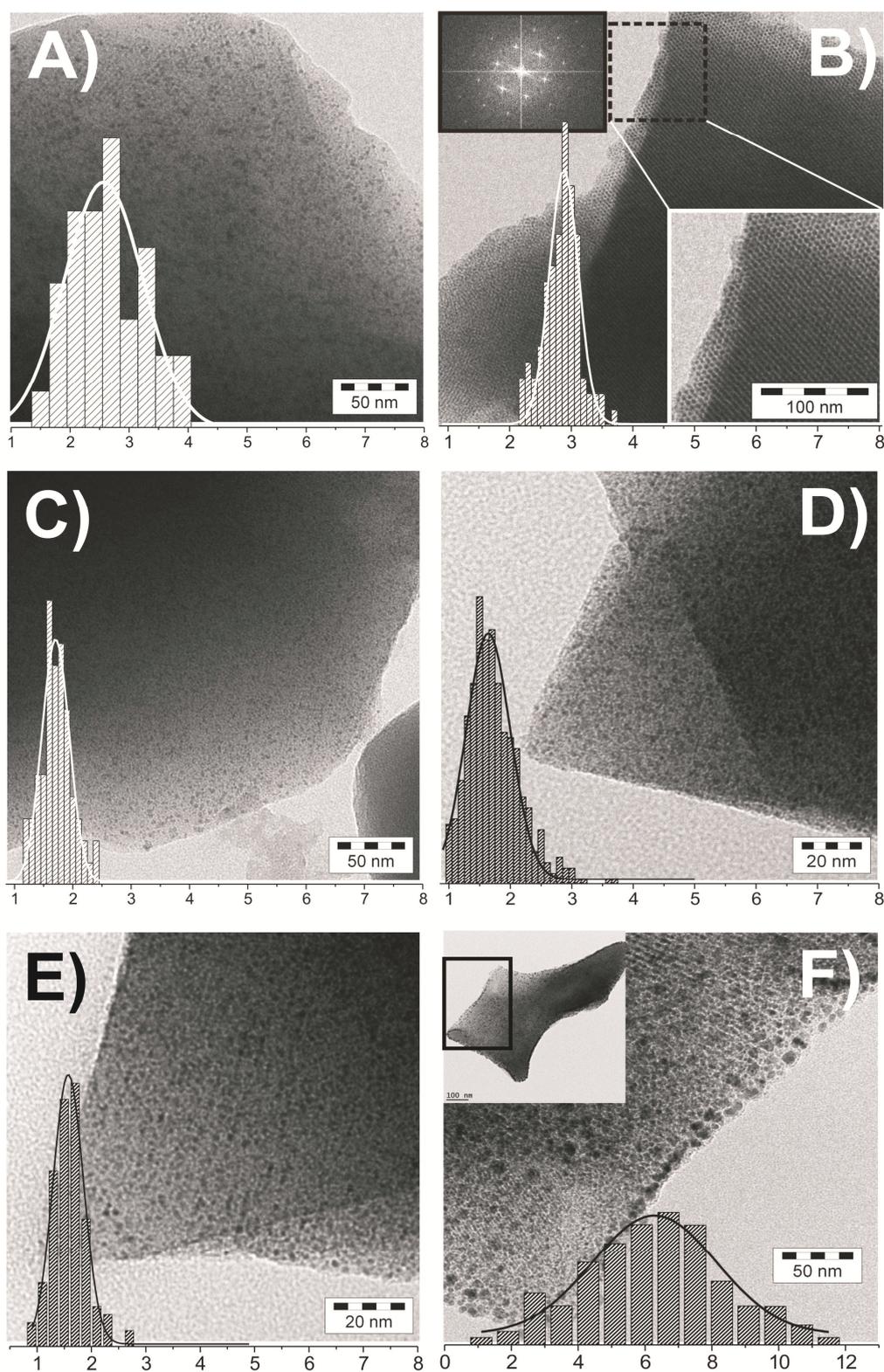
Figure 5. TEM analysis of Pd@MIL-101. A) LL6012; B) LL6058: The regular structure is not limited to one layer, but stretches throughout the whole crystallite (as indicative by the FTT); C) HH2609; D) HH1545: Narrow particle size distributions centered around 1.7 nm were found; E) Postmod; F) VHTP-25: The host structure is seriously damaged and samples show a layer of surface particles larger than 15 nm in diameter.

4.2.2 Catalytic Studies

Activity, selectivity, and substrate scope: The synthesized Pd@MIL-101 samples were investigated as catalysts in the solvent free reduction of ketones. Propiophenone was used as a substrate for initial studies. As no catalytic activity was detected with 1 bar H_2, higher pressure was applied. In-situ IR analysis of the reaction is indicative of nearly no induction period (Figure 6).
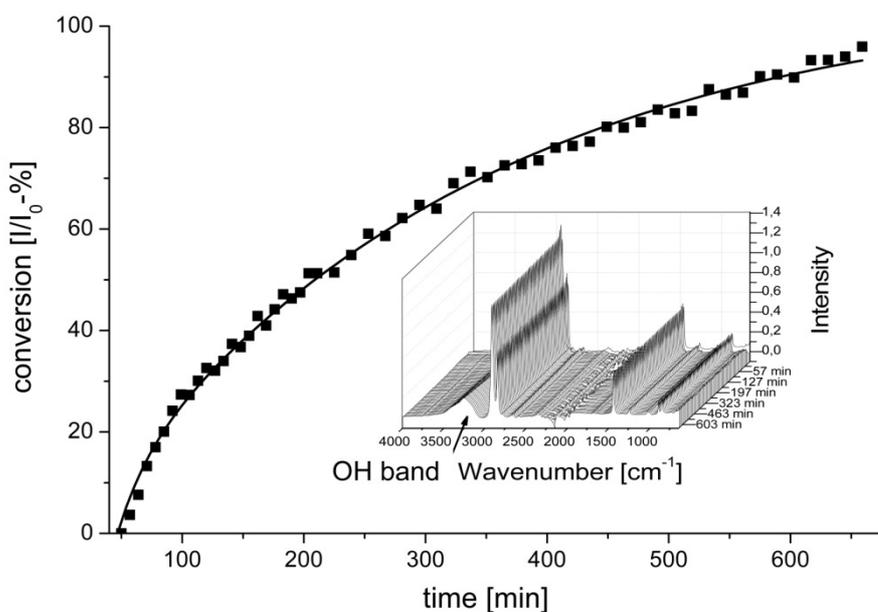
Figure 6. Kinetic studies of reduction of propiophenone via in-situ IR. The catalyst system HH1545 was used for the reduction of propiophenone; (70 °C, 4.8 bar H_2 atmosphere, 750 rpm, 76 h, 28 mg HH1545, 5 mL propiophenone).

Experiments of the catalyst system based on HH1545 and LL4842 with a variety of substrates showed a few interesting features (Table 3). While aromatic ketones were readily reduced aliphatic ketones didn't show any conversion. Electron rich aryl residues likewise decrease activity (N° 7-9). 4-Methylbenzophenone (N° 10) didn't show any conversions for LL4842 but for HH1545 indicating a hampered diffusion into the porous LL system. In General, system LL4842 shows higher conversions for smaller substrates (N° 1 and 2) and lower conversions for bigger substrates (N° 3-6, 9). The complete filling of the cavities restricts the accessible metal surface decreasing possible interactions with sterically demanding substrates. With time/temperature, the selectivity for both systems can be switched to the corresponding alkane (deoxygenation). For reactions with branched alkyl residues (N° 6) selectivity towards the alcohol stays dominant. Comparative experiments with MIL-101 as catalyst (without Pd NP) didn't show any conversion, excluding a possible activity of the MIL-101 himself in terms of ketone reduction.

Table 3. Reduction of various aryl-alkyl ketones to the corresponding alcohol and/or arylalkane at 39 – 80 °C (pressure 20 bar: time: 24 h); left: LL4842, right: HH1545 (0.1 mol-% Pd); conv = conversion [%], sel_1 = selectivity for the corresponding alcohol (**1**) [%], sel_2 = selectivity for the corresponding alkenes (2) [%]. R1= aryl residue, R2= aliphatic residue.

	LL4842		HH1545		
ketone	80 °C conv (sel_1/sel_2)	50 °C conv (sel_1/sel_2)	80 °C conv (sel_1/sel_2)	50 °C conv (sel_1/sel_2)	39 °C conv (sel_1/sel_2)
(1) acetophenone	100 (< 1/98)	100 (32/60)	100 (< 1/95)	99 (90/8)	90 (98/1)
(2) propiophenone	100 (< 1/80)	100 (80/18)	99 (10/65)	98 (92/6)	95 (97/2)
(3) valerophenone	98 (45/40)	57 (98/1)	100 (98/< 1)	100 (97/2)	68 (99/<1)
(4) heptanophenone	100 (25/72)	23 (90/8)	100 (50/48)	100 (99/<1)	70 (99/<1)
(5) isopropyl-phenylketone	100 (< 1/70)	72 (98/1)	100 (97/<1)	100 (98/<1)	
(6) 2,2-dimethylpropiophenone	99 (70/20)	22 (98/1)	100 (95/4)	100 (97/2)	
(7) 4'-fluoro-propiophenone	100 (30/69)	100 (50/48)	100 (91/7)	100 (89/10)	
(8) 4'-methyl-propiophenone	100 (< 1/98)	96 (25/72)	100 (12/83)	100 (20/79)	
(9) 4'-methoxy-propiophenone	100 (< 1/98)	30 (40/58)	100 (< 1/95)	100 (4/95)	
(10) 4-methyl-benzophenone	0 (0/0)	0 (0/0)	99 (88/10)	100 (95/4)	

Experiments in the reduction of alkyl residue varied ketones showed higher activity for sterically less hindered molecules, which are (most likely) able to access the active sites better (Figure 7). These observations are indicative of size selectivity as well. Hexanophenone shows a conversion of 23%, which is a third of the conversion of acetophenone at equal reaction conditions.
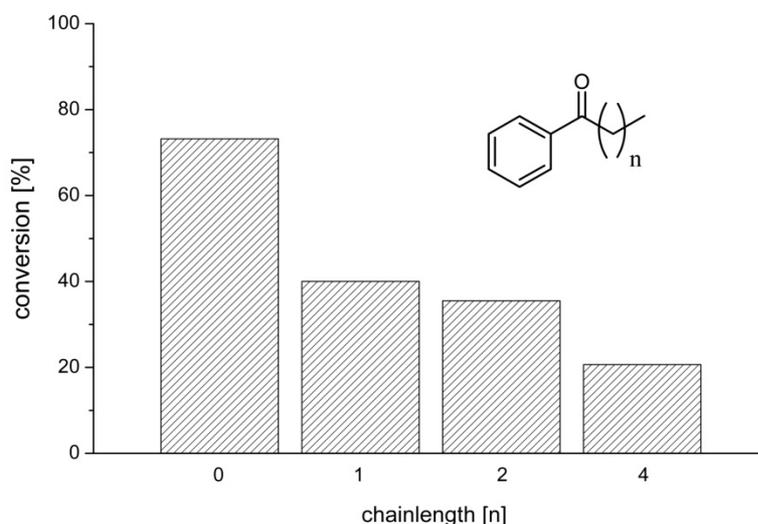
Figure 7. Plotting of conversion against the chain length of the alkyl residue. (50°C, 20 bar H_2 atmosphere, 750 rpm, 16 h, 0.09 wt.-% Pd, LL4842 catalyst).

Recyclability: The recyclability of the catalyst system HH1545 was tested in six consequent runs in which the reaction was stopped after ~ 50% conversion (9h). After six runs no significant decrease of activity could be detected (Figure 8). The detection of the formed byproducts stayed continuously low. A second experiment involved the examination of the system LL4842. Again no decrease of activity after 11 runs could be detected (Figure 9). Yields of 1-phenyl-1-propanol are around 90%. A higher activity of LL4842 in comparison to HH1545 is observed. To search for possible leaching effects we investigated the hydrogenation activity of the separated reaction mixture. No further conversion was detected. We therefore assume Pd leaching being rather low. ICP-OES measurements of the catalyst after 11 runs did not show a reduction of the Pd loading confirming our assumption. In contrast to the experiments, which were stopped after relatively short reactions times, 8 or 9h, experiments after prolonged catalysis showed a deactivation of the catalyst. This was accompanied by a coloring of the reaction mixture after 76 h, that can't be attributed to any product or educt (Figure 10).
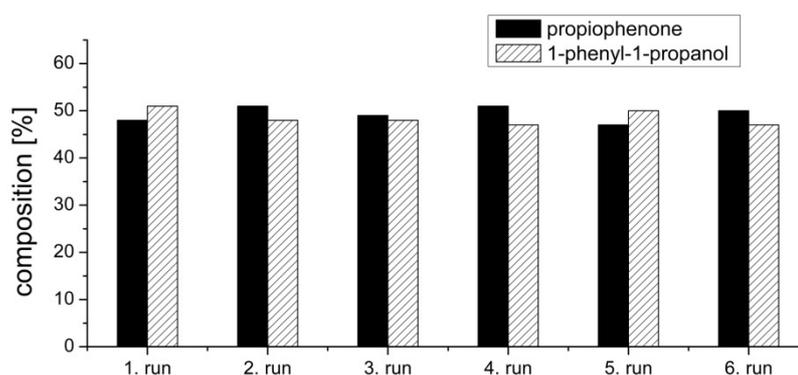
Figure 8. Recyclability test of HH1545 catalyst in the reduction of propiophenone. No significant decrease of activity after six runs was observed. Reaction conditions: 50 °C, 40 bar H_2 atmosphere and 750 rpm, 9 h, 18 mg HH1545, 4 mL propiophenone, 1mL dodecane.
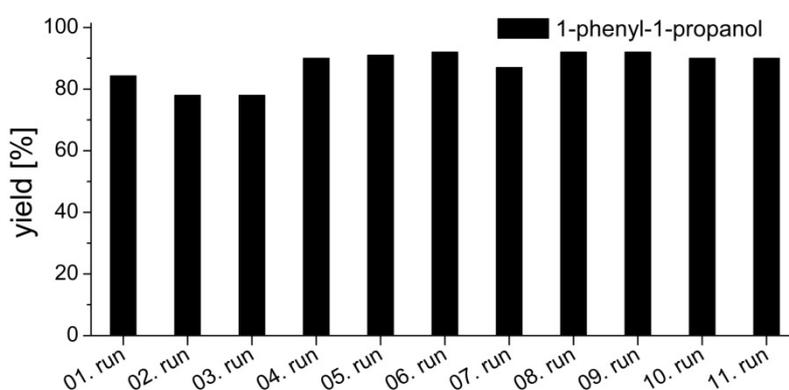
Figure 9. Recyclability test of LL4842 catalyst in the reduction of propiophenone. After eleven runs no significant decrease of activity could be detected. Reaction conditions: 50 °C, 40 bar H_2 atmosphere, 750 rpm, 8 h, 4 mg LL4842, 2 mL propiophenone, 0.113 mL dodecane.
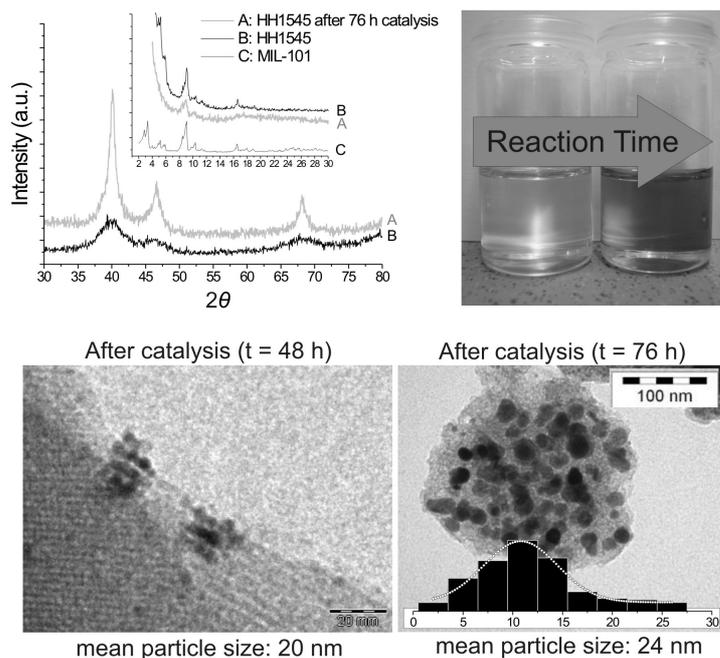
Figure 10. XRD pattern and TEM images of the catalyst system based on HH1545 after prolonged catalysis, reduction of propiophenone. Change of particle size after 48 h and 76 h catalysis time. Reaction conditions: 50 °C, 20 bar H_2 atmosphere, 76 h, 750 rpm.

The XRD pattern after 76 h of catalysis shows a narrowing of the *fcc* Pd signals indicating a growth of particle sizes. TEM images of the samples confirm an increase of the mean particle size of Pd beyond the confinement of the pore dimensions. These results seem to be in contrast to the recyclability tests earlier, yet this instability is relevant to prolonged catalysis only. TEM investigations after 48 h prolonged catalysis revealed the formation of bigger, 24 nm particles (Figure 11). They do not consist out of one big particle (as does the samples after 76 h) but of agglomerated particles of about 4 nm.

4.3 Conclusions

In summary, we have presented evidence for a selective loading of MIL-101 with Pd NP. The volatile Pd precursor complex [(η^5-C_5H_5)Pd(η^3-C_3H_5)] was introduced via MOCVD up to loadings higher than 50 wt.-% of Pd. Pd NP of different size could be generated by varying the reduction conditions especially the temperature. Reduction at low (room) temperature gave rise to cavity size conform particles and reduction at elevated temperature (70 °C) yielded Pd NP lower in size as given by the host cavities. We see some potential for these under-sized particles in terms of loading with a second (or third) metal to make multimetallic NP. Catalysis studies – hydrogenation of ketones – indicate that the Pd@MIL-101 catalysts are size selective. The catalysts can be recycled but decompose after (very long) reaction times during which the ketone and alcohol concentration becomes low.

4.4   Experimental Section

Analytical and spectroscopic methods: Elemental analysis was performed by standard protocols employing digestion in $HNO_3/HCl/H_2O_2$ and inductively coupled plasma optical emission spectrometry (ICP-OES) using a Varian, Vista-Pro radial. GC analyses were performed by using an Agilent 6890N gas chromatograph equipped with a flame ionization detector (FID) and an Agilent 19091 J-413 FS capillary column using dodecane as internal standard. All X-ray powder diffractograms were recorded by using a STOESTADI-P-diffractometer (CuK$_\alpha$ radiation, 1.54178 Å) in ϑ-2ϑ -geometry and with a position sensitive detector. All powder samples were introduced into glass capillaries ($\emptyset$ = 0.7 mm, Mark-tubes Hilgenberg No. 10) in a glove box and sealed prior to the measurements. FTIR-measurements were performed at a Perkin Elmer FTIR-Spectrum 100 over a range of 4400 cm^{-1} to 650cm^{-1}. In-situ IR measurements were carried out by using a ReactIR 4000 of Mettler Toledo with adamantine window over a range of 4400cm^{-1} to 650cm^{-1}. The Nitrogen physisorption isotherms were measured at 77 K using a Quantachrome Autosorb 1 apparatus. 25-80 mg of pre-degassed sample were transferred to a quartz cell and consequently degassed again at 100°C, 10^{-3} mbar for 24 h. Specific surface areas were calculated using five points by BET. The specific total pore volume was measured by the DFT calculations. Transmission electron microscopy (TEM) was carried out by using a Varian LEO 9220 (200 kV) instrument. The sample was suspended in chloroform and sonicated for 5 min. Subsequently a drop of the suspended sample was placed on a grid (Plano S 166–3) and allowed to dry.

Reactants and solvents: Terephthalic acid, propiophenone as well as the other ketones were purchased from Acros Organics. 1-phenyl-1-propanol was purchased from Sigma Aldrich chemicals. Chromium(III) nitrate nonahydrate ($Cr(NO_2)_3*9H_2O$) and allylpalladium(II) chloride dimer were purchased from ABCR. All manipulations and chemical reactions were conducted under an inert atmosphere [Schlenk-technique (Ar) and/or glove box technique (N_2, H_2O, O_2 < 0.1 ppm). Non-halogenated solvents were dried with sodium/benzophenone ketyl and halogenated solvents with CaH$_2$. Deuterated solvents were obtained from Cambridge Isotope Laboratories, degassed, dried with molecular sieves and distilled prior to use.

Starting materials synthesis: The Pd precursor [(η^5-C$_5$H$_5$)Pd(η^3-C$_3$H$_5$)] was synthesized under exclusion of light following a published procedure.[16] 2.5 g allylpalladium(II)chloride dimer was dissolved in 50 mL abs. THF and cooled to -60 °C. Drop wise addition of 6 mL NaCp (Cp = cyclopentadienyl) under constant cooling and stirring lead to a red coloring of the solution that was stirred for another 15 min at -20 °C and for 30 min at RT. The solvent was removed under vacuum and the residue was dissolved in 50 mL hexane and separated via cannula filtration. The solvent was removed under vacuum.

MIL-101 was synthesized and washed according to a published procedure.[17] 400 mg H_2BDC, 640 mg $Cr(NO_3)_3$ 9H_2O, 0.08 mL HF and 8 mL H_2O were mixed and sealed in a Teflon lined hydrothermal autoclave. The mixture was heated for 8 h at 220 °C, cooled down fast to 160 °C and slowly to 30 °C (cooling rate: 2.7°C/h). The resulting green mixture was filtered off over pore 3 filters to eliminate excessive crystallized terephthalic acid. The filtrate was again filtered off using a fine pore paper filter and washed with 50 mL water. Two times the resulting solid was refluxed in EtOH for 12 h and filtered off using a fine pore paper filter. The resulting solid was two times soaked in 1M NH_4F solution, stirred for 24 h at 70 °C and filtered hot. The resulting green powder was washed with water and evacuated at 10^{-5} bar to remove any solvent. All materials were stored under argon.

Infiltration of $[(\eta^5$-$C_5H_5)Pd(\eta^3$-$C_3H_5)]$ into MIL-101: preparation of $[(\eta^5$-$C_5H_5)Pd(\eta^3$-$C_3H_5)]$@MIL-101: Freshly evacuated MIL-101 powder and $[(\eta^5$-$C_5H_5)Pd(\eta^3$-$C_3H_5)]$ were placed in a two-chamber-tube separated by a glass frit and were kept at 25 °C in a 1.4 x 10^{-4} mbar (diffusion pump) dynamic vacuum for 3 – 8 h. The procedure yielded a dark green to black powder (depending on the loading of Pd), which was immediately processed in hydrogenolysis to yield Pd@MIL-101.

Preparation of Pd@MIL-101: quantitative hydrogenolysis of $[(\eta^5$-$C_5H_5)Pd(\eta^3$-$C_3H_5)]$ in MIL-101: The adjacent reduction of Pd(II) to Pd(0) was performed with hydrogen at defined pressure and temperature in a Parr Instruments steel autoclave (Table 1). To remove traces of the former ligands, the material was than evacuated for 24 h at 5 x 10^{-5} mbar (125°C).

Reduction of ketones using Pd@MIL-101 as catalyst: All reduction experiments were carried out for 24 h in a steel autoclave (Parr) with 20 bar H_2 and a temperature range from 39 °C - 80 °C. A typical experiment consisted of 1.00 mg catalyst and 3.7 mmol ketone [dissolved in 1 mL THF (21 °C – 60 °C) or toluene (80 °C) if solid]. The catalyst was weighed accurate to 0.01 mg. The conversion was determined by GC with dodecane as internal standard.

Recyclability of Pd@MIL-101 (HH1545 and LL4842): The reaction was stopped after 8 and 9 h respectively; the catalyst was separated from the reaction mixture via centrifugation and cleaned under reduced pressure and 70 °C for 15 h. The reaction mixture was tested for leaching. The conversion was determined by GC with dodecane as external standard.

In-situ IR spectroscopy: In-situ IR experiments were performed with 28 mg catalyst (HH1545), 5 mL propiophenone, and 400 ml cyclohexane. Reaction conditions were 70 °C, 4.8 bar H_2, 750 rpm. The conversion was determined by GC with dodecane as external standard.

4.5 Acknowledgements

4.6 References

[1] a) B. F. Abrahams B. F. Hoskins D. M. Michail, R. Robson, *Nature* **1994**, *369*, 727 − 729; b) B. F. Hoskins, R. Robson *J. Am. Chem. Soc.* **1989**, *111*, 5962–5964.

[2] H.Li, M. O'Keeffe, O.M. Yaghi, *Nature* **1999**, *402*, 276-279.

[3] a) J. R. Long, Omar M. Yaghi, *Chem. Soc. Rev.* **2009**, *38*, 1213-1214; b) M. O'Keeffe, *Chem. Soc. Rev*. **2009**, *38*, 1215 − 1217; c) A. M. Spokoyny, D. Kim, A. Sumrein and C. A. Mirkin, *Chem. Soc. Rev*. **2009**, *38*, 1218 − 1227; d) T. Uemura, N. Yanai and S. Kitagawa, Chem. Soc. Rev. **2009**, *38*, 1228 − 1236; e) T. Düren, Y.-S. Bae, R. Q. Snurr**,** *Chem. Soc. Rev.* **2009**, *38***,** 1237 − 1247; f) L. Ma, C. Abney and W. Lin, *Chem. Soc. Rev.* **2009**, *38***,** 1248 − 1256; g) A. U. Czaja, N. Trukhan, U. Müller, *Chem. Soc. Rev.* **2009,** *38***,** 1284 − 1293; h) L. J. Murray, M. Dincă and J. R. Long, *Chem. Soc. Rev.* **2009**, 38, 1294 − 1314; i) G. Férey and C. Serre, *Chem. Soc. Rev.* **2009**, 38, 1380 − 1399; j) J. Lee, O. K. Farha, J. Roberts, K. A. Scheidt, S. T. Nguyen, J. T. Hupp, *Chem. Soc. Rev.* **2009**, *38*, 1450-1459.

[4] a) S. Hermes, M.-K. Schröter, R. Schmid, L. Khodeir, M. Muhler, A. Tissler, R. W. Fischer and R. A. Fischer, *Angew. Chem. Int. Ed*. **2005**, *44*, 6237-6241; b) S. Hermes, M.-K. Schroeter, R. Schmid, L. Khodeir, M. Muhler, A. Tissler, R. W. Fischer, R. A. Fischer, *Angew. Chem*. **2005**, *117*, 6394–6397; c) M. Meilikhov, K. Yusenko, D. Esken, S. Turner, G. V. Tendeloo, R. A. Fischer, *Eur. J. Inorg. Chem.* **2010**, 3701-3714.

[5] D. Esken, S. Turner, O.I. Lebedev, G. V. Tendeloo, R.A. Fischer, *Chem. Mater.* **2010**, *22*, 6393-6401.

[6] a) M. Sabo, A. Henschel, H. Froede, E. Klemm and S. Kaskel*, J. Mater. Chem*. **2007**, *17*, 3827-3832; b) N. V. Maksimchuk, M. N. Timofeeva, M. S. Melgunov, A. N. Shmakov, Y. A. Chesalov, D. N. Dybtsev, V. P. Fedin, O. A. Kholdeeva, *J. Catal*. **2008**, *257*, 315-323; c) H. Liu, Y. Liu, Y. Li, Z. Tang, H. Jiang, *J. Phys. Chem. C*. **2010**, *114*, 13362–13369; d) Y. Pana, B. Yuana, Y. Li, D. He, *Chem. Commun.* **2010**, *46*, 2280-2282.

[7] T. Ishida, M. Nagaoka, T. Akita, M. Haruta, *Chem. Eur. J.* **2008**, *14*, 8456-8460.

[8] M. S. El-Shall, V. Abdelsayed, A. El Rahman S. Khder, H. M. A. Hassan, H. M. El-Kaderi and T. E. Reich, *J. Mater. Chem*. **2009**, *19*, 7625.

[9] Y. K. Hwang, D. Y. Hong, J. S. Chang, S. H. Jhung, Y. K. Seo, J. Kim, A. Vimont, M. Daturi, C. Serre and G. Férey, *Angew. Chem., Int. Ed*. **2008**, *47*, 4144-4148.

[10] a) S. Hermes, F. Schröder, S. Amirjalayer, R. Schmid, R. A. Fischer, *J. Mater. Chem.* **2006**, *16*, 2464-2472; b) S. Hermes, D. Zacher, A. Baunemann, C. Wöll, and R. A. Fischer, *Chem. Mater.* **2007**, *19*, 2168-2173; c) M. Müller, O. Lebedev and R. A. Fischer, *J. Mater. Chem.* **2008**, *18*, 5274-5281; d) M. Müller, S. Hermes, K. Kähler, M.W. E. van den Berg, M. .Muhler and R. A. Fischer, *Chem. Mater*. **2008**, *20*, 4576-4587; e) S. Turner, O. I. Lebedev, F. Schröder, D. Esken, R. A. Fischer, G. Van Tendeloo, *Chem. Mater.* **2008**, *20*, 5622-5627; f) F. Schroeder, D. Esken, M. Cokoja, M. W. E. van den Berg, O. I. Lebedev, G. van Tendeloo, B. Walaszek, G. Buntkowsky, H. H. Limbach, B. Chaudret and R. A. Fischer, *J. Am. Chem. Soc*. **2008**, *130*, 6119-6130; g) D. Esken, X. Zhang, O. I. Lebedev, F. Schröder and R. A. Fischer, *J. Mater. Chem.* **2009**, *19*, 1314-1319; h) F. Schröder, S. Henke, X. Zhang, R. A. Fischer, *Eur. J. Inorg. Chem.* **2009**, *21*, 3131-3140; i) M. Meilikhov, K. Yusenko, R. A. Fischer, *Dalton Trans*. **2010**, *39*, 10990–10999; j) M. Meilikhov, K. Yusenko, A. Torrisi, B. Jee, C. Mellot-Draznieks, A. Pöppl, R. A. Fischer, *Angew. Chem., Int. Ed*. **2010**, *49*, 6212 –6215.

[11] S. Proch, J. Herrmannsdörfer, R. Kempe, C. Kern, A. Jess, L. Seyfarth, J. Senker, *Chem. Eur. J.* **2008**, *14*, 8204 – 8212.

[12] a) H. Kim, H. Chun, G.-H. Kim, H.-S. Lee, K. Kim, *Chem. Commun*. **2006**, *26*, 2759–2761; b) M. Meilikhov, K. Yusenko, R. A. Fischer, *Dalton Trans*. **2010**, *39*, 10990–10999; c) M. Meilikhov, K. Yusenko, R. A. Fischer, *Dalton Trans*. **2009**, 600-602.

[13] a) T. Schareina, R. Kempe, *Z. Anorg. Allg. Chem.* **2000**, *626*, 1279-1281; b) T. Schareina, C. Schick, B. F. Abrahams, R. Kempe, *Z. Anorg. Allg. Chem.* **2001**, *627*, 1711-1713; c) T. Schareina, C. Schick, R. Kempe, *Z. Anorg. Allg. Chem.* **2001**, *627*, 131-133; d) B. Schoknecht, R. Kempe, *Z. Anorg. Allg. Chem.* **2004**, *630*, 1377-1379; e) R. Kempe, *Z. Anorg. Allg. Chem.* **2005**, *631*,1038-1040.

[14] G. Férey, C. Mellot-Draznieks, C. Serre, F. Millange, J. Dutour, S. Surblé, L. Margiolaki, *Science* **2005**, *309*, 2040-2042.

[15] a) B. Yuan*,* Y. Pan*,* Y. Li*,* B. Yin*,* H. Jiang*, Angew. Chem. Int. Ed.* **2010***, 49,* 4054 –4058; b) Y. Pan*,* B. Yuan*,* Y. Li*,* D. He*, Chem. Commun.* **2010***, 46,* 2280 –2282*.*

[16] Y. Tatsuno, T. Yoshida, Seiotsuka, N. Al-Salem, B. L. Shaw, in *Inorganic Synthesis*, Vol.19 (Ed: D.F. Shriver), WILEY-VCH, Weinheim, **1979**, p. 220-223.

[17] A. Henschel, K. Gedrich, R. Kraehnert, S. Kaskel, *Chem. Commun*. **2008**, 4192-4194.

[18] J. Ehrenmann, S. K. Henninger, C. Janiak, *Eur. J. Inorg. Chem.* **2011**, 471–474.

5 Ni/Pd@MIL-101: Synergistic Catalysis with Cavity-Conform Ni/Pd Nanoparticles

Justus Hermannsdörfer[a], Martin Friedrich[a], Nobuyoshi Miyajima[b], Rodrigo Q. Albuquerque[c],[d], Stephan Kümmel[c], Rhett Kempe*[a]

[a] Lehrstuhl für Anorganische Chemie, Universität Bayreuth, Universitätsstraße 30, 95440 Bayreuth (Germany), Fax: (+49) 921-55-2157, Email: kempe@uni-bayreuth.de
[b] Bayerisches Geoinstitut, Universität Bayreuth, Universitätsstraße 30, 95440 Bayreuth (Germany)
[c] Theoretische Physik IV, Universität Bayreuth, Universitätsstrasse 30, 95440 Bayreuth (Germany)
[d] Institute of Chemistry of São Carlos, University of São Paulo, 13560-970 São Carlos (Brazil)

Abstract: A perfect fit: Cavity-conform bimetallic Ni/Pd nanoparticles of different composition were generated in the metal–organic framework MIL-101. Experimental evidence and molecular dynamic simulations indicate the existence of mixed bimetallic particles. Pronounced synergistic effects have been observed in liquid-phase catalysis.

Abstract in German: Passgenaue Katalyse: Kavitätenkonforme dimetallische Ni/Pd-Nanopartikel unterschiedlicher Zusammensetzung wurden im Metall-organischen Gerüst MIL-101 erzeugt. Experimentelle Befunde und MD-Simulationen belegen das Vorliegen durchmischter dimetallischer Partikel, die ausgeprägte synergetische Effekte in der Flüssigphasenkatalyse zeigen.

5.1 Introduction

Porous coordination polymers (PCP)[1] or metal-organic frameworks (MOF)[2] are currently investigated intensively, for instance, regarding gas storage,[3] separation,[4] sensing[5] and as catalysts.[6] In view of catalytic applications PCP/MOFs are well suited to stabilize very small metal nano-particles (MNP) without blocking their surface by strongly binding ligands. The cavities and windows of the PCP/MOFs can regulate the particle size and simultaneously guarantee access to the catalytically active sites of the MNP. In comparison to loading via solution infiltration,[7] solid grinding,[8] microwave irradiation,[9] and surface grafting,[10] the MOCVD method (Metal Organic Chemical Vapor Deposition) developed by Fischer and co-workers is of advantage especially in terms of control and high metal loadings (> 5 wt.-%).[11] Mainly the host structures MOF-5,[2] MOF-177[26] and MIL-101[27] have been used for loading with different MNP (Fe,[12-15] Co,[15,16] Cu,[12,13,17] Zn,[12,13,17,18] Sn,[12] Pt,[12,14], Au,[12,19], Pd,[12-14,20-23] Ru[14,24] and Ni.[25] The significantly higher hydrolysis stability of MIL-101 in comparison to MOF-5 and MOF-177 makes it attractive for the synthesis of robust catalyst systems.[22,23] Debatable (independent from the loading method used) is the question: are the generated MNP localized inside the PCP/MOF cavities or not. Frequently, MNP larger than the cavities and particles localized on the outer surface of the PCP/MOF crystallite were observed. Recently, we could show that one can synthesize MIL-101 cavity conform Pd NP by applying the MOCVD method using the precursor $[(C_5H_5)Pd(C_3H_5)]$ followed by reduction with H_2 at room temperature (Figure 1, left).[23] If the reduction is carried out at 70 °C significantly smaller Pd NP were generated. Their diameter seems to be determined by the window sizes and not so much by the cavity sizes (Figure 1, centre).[23] This observation allows to conclude that the remaining space can be used to load a second metal. Thus, bimetallic NPs in the sub nanometer range (< 10 nm) are accessible (Figure 1, right). This is interesting for catalytic applications due to a few reasons. Very small NPs have a very large surface to volume ratio. The dilution of costly noble metals by inexpensive metals like Ni is economical. Bimetallic NP catalysts can show synergistic effects regarding activity and/or selectivity as (for instance) observed for Au/Pt NP supported on spherical polyelectrolyte brushes.[28]
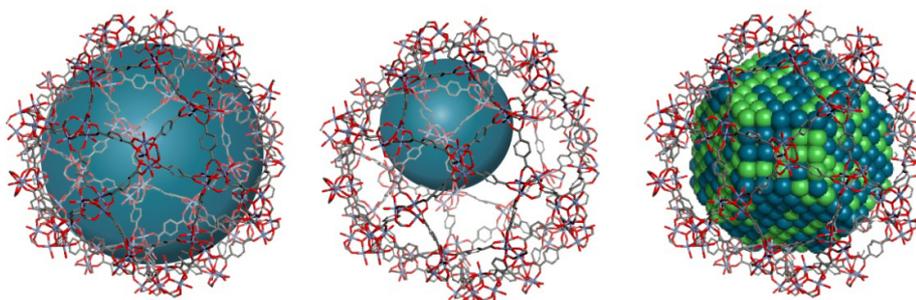
Figure 1. Size selective cavity loading of MIL-101 (left: cavity conform, centre: undersized cavity loading, right introduction of a second metal)

5.2   Results and Discussion

We report here on the generation of cavity conform Ni/Pd NP of different composition and their synergism in the catalytic hydrogenation of alkyl-alkyl ketones. The synthesis of bimetallic NP in PCP/MOF via MOCVD is not much investigated.[14] Catalytic synergy effects of cavity conform bimetallic MNP stored in PCP/MOF cavities are not known. PCP/MOFs were used as support (localization of the MNP also at the outer surface of the PCP/MOF supports and/or regarding the size not cavity conform) for bimetallic Au/Pd and Ag/Au NP and catalytic synergism could be observed.[29,30] The optimal synthesis of the Ni/Pd@MIL-101 catalysts was firstly investigated with respect to two loading versions, successively and simultaneously. The successive loading seems attractive since the undersized Pd NP offer enough room to form cavity conform bimetallic particles. Admittedly, the Pd NP could function as agglomeration sites and initiate excessive particle grows. The simultaneous loading becomes difficult due to the different reduction behaviour of the two precursors. A 1:1 loading with Pd and Ni precursors {[(C$_5$H$_5$)Pd(C$_3$H$_5$)], [(C$_5$H$_5$)$_2$Ni]} shows for both variants (after reduction) mainly NP in the size range of the MIL-101 cavities (SI Figure S1). For the successive loading comparably more oversized particles were generated. PXRD (powder X-ray diffraction) shows two separated Ni and Pd 111 peaks for the successive loading (SI Figure S2) with the Ni peak being considerable weaker. In contrast, the simultaneous loading shows a single broad 111 peak indicating bimetallic NP. The synthesis of the Pd$_x$Ni$_y$@MIL-101 catalyst systems with an exact adjustment of the Pd to Ni ratio via substitution of Pd by Ni in 20 weight percent steps (SI Figure S3) was therefore carried out applying the simultaneous loading. Firstly, the reduction was carried out at 70 °C and 50 bar H$_2$ pressure for 20 h (1. generation).[23] TEM (transition electron microscopy) confirm NP from 2 to 3 nm (SI Figure S4-6) for the systems with high Pd content (Pd > Ni).

Additionally, the formation of large particles at the outer surface of the MIL-101 crystals (SI Figure S7) is observed at high Ni contents. Pure Ni@MIL-101 follows this tendency and shows NP which are clearly over the size of the MIL-101 cavities. Due to an increasing particle size with increasing Ni content the reduction conditions were optimized. Cavity conform bimetallic NP could be generated by increasing the temperature and reducing the pressure (2. generation, Figure 2). PXRD and IR investigations confirm the stability of the support under the relatively harsh reduction conditions (SI Figure S11, 12, 14). Elemental analysis shows a average metal loading of 18 wt.-% which matches with the calculated metal content (SI Figure S15). Already a small amount of Pd changes the reduction behaviour of [(C$_5$H$_5$)$_2$Ni] and prevents the formation of larger Ni particles. HR TEM EDS measurements of Pd$_4$Ni$_1$@MIL-101 und Pd$_3$Ni$_2$@MIL-101 indicate bimetallic particles. EDS investigations of the whole sample and a few of the single particles show identical Ni:Pd ratios (Figure 3).
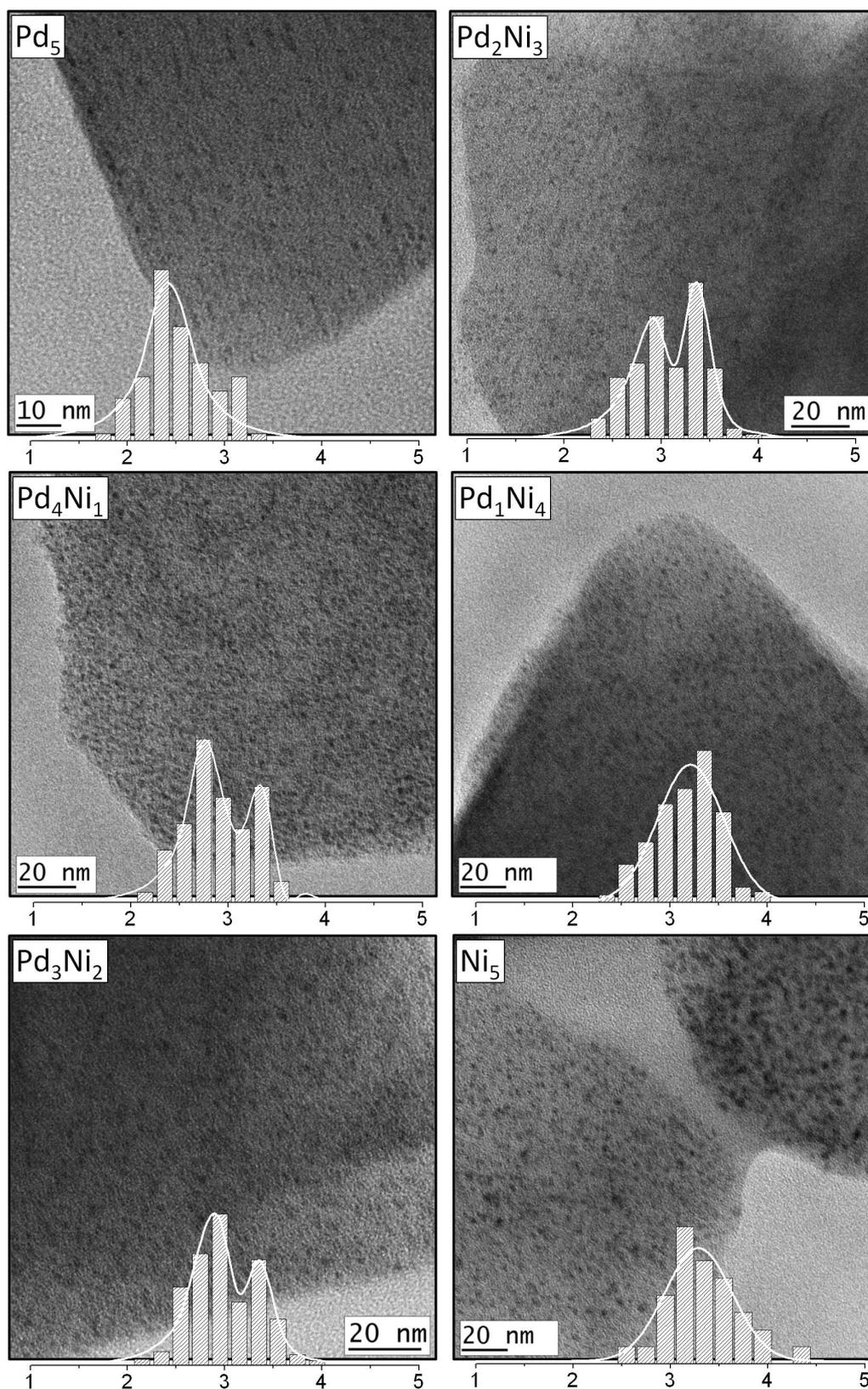
Figure 2. TEM investigations of the Pd_xNi_y@MIL-101 catalyst systems using the optimized reduction conditions (2. generation). With increasing Ni content the reduction temperature is increased and the pressure is reduced (Pd_5, Pd_4Ni_1, Pd_3Ni_2 = 70 °C/50 bar; Pd_2Ni_3 = 70 °C/5 bar; Pd_1Ni_4, Ni_5 = 90 °C/5 bar). The reduction time was 20 h. The averaged metal loading is 18 wt.-%. The substitution of Pd by Ni was carried out in 20 weight percent steps.
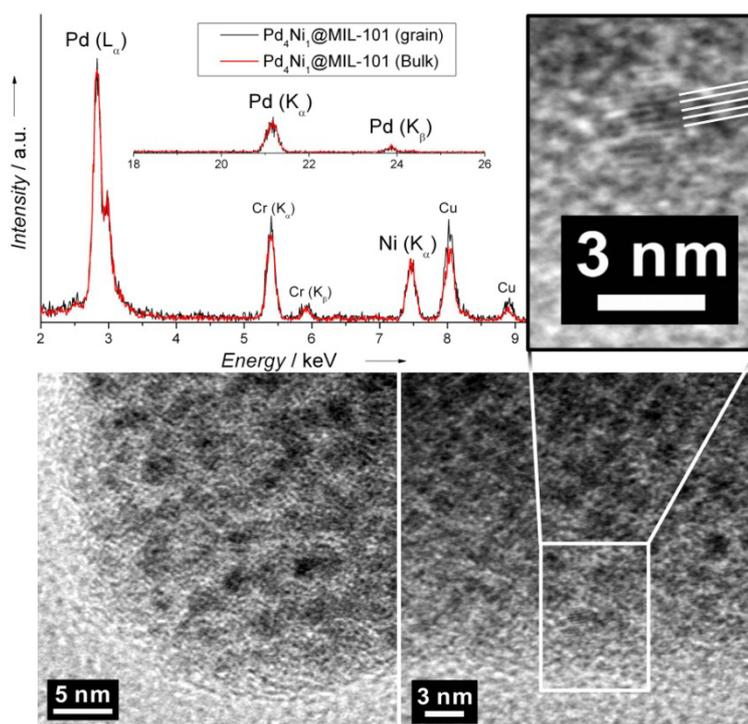
Figure 3. HR TEM EDS analysis of Pd_4Ni_1@MIL-101. The Ni:Pd ratio is identical if the bulk sample is considered and if single particles are analyzed. The d-spacing (fringes) of the Ni/Pd NP observed by TEM {e.g. for Pd_3Ni_2@MIL-101 [111] 2.19(5) Å} matches with the expected value and the PXRD data (SI Figure S14).

In combination with the catalytic activity and the calculations carried out (*vide infra*) bimetallic Ni/Pd NP can be concluded. In comparison to pure MIL-101, N_2 physisorption shows a lowered surface for the loaded systems which results from a higher sample weight and the occupation of pores by MNP (SI Table 2). Interestingly, pure Pd@MIL-101 und pure Ni@MIL-101 show a larger specific surface than the mixed systems. It might be explained by the localization of some MNP on the outer surface for Ni@MIL-101 and the formation of undersized MNP in case of Pd@MIL-101.

The Pd_xNi_y@MIL-101 catalyst systems were investigated in different hydrogenation reactions. For the reduction of phenol as well as cyclic ketones (Figure 4) and alkyl-alkyl ketones (Table 1) a clearly pronounced synergistic effect is observed. The mixed Ni/Pd catalysts are definitely more active than the pure Pd or Ni catalysts. Generally, the hydrogenation of alkyl-alkyl ketones is difficult to accomplish by heterogeneous catalysts.[31] Aryl-alkyl ketones are hydrogenated without problems by these catalysts.[23] Neither 3-heptanone nor cyclohexanone are reduced by the Ni@MIL-101 catalyst under the used conditions. Also Pd@MIL-101 shows clearly lower conversions, comparable to that of Pd on coal (Pd/C). In contrast, the combination of both metals in the bimetallic Pd_xNi_y@MIL-101 catalyst systems shows high conversions also at 25 °C (Table 1, entry 1). Table 1 shows the results of the reduction of 3-heptanone under different conditions.
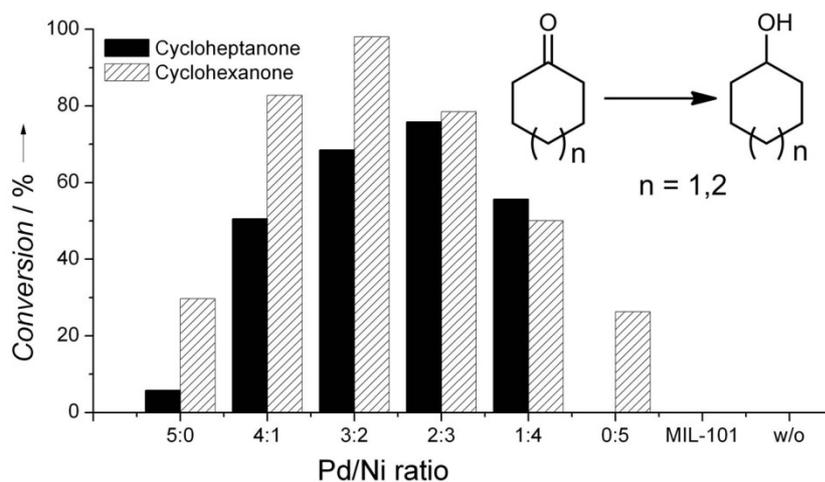
Figure 4. Reduction of cyclohexanone (0.18 mg Pd (0.52 10^{-3} mol-%), 350 µL, 60 °C, 24 h,) and cycloheptanon (0.36 mg Pd (0.8 10^{-3} mol-%), 500 µL, 60 °C, 48 h) at 20 bar H_2; w/o = without catalyst.

Table 1. Catalytic results of the reduction of 3-heptanone with Pd_xNi_y@MIL-101.

Entry	System	T [°C]	t [h]	Conversion [%]	Pd/ketone [mol-% 10^{-3}]
1	Pd_3Ni_2	25	27	50	2.88
2	Pd_3Ni_2	35	20	80	2.88
3	Pd_3Ni_2	60	20	75	1.44
4	$Pd_5 + Ni_5$	35	20	14	2.88
5	$Pd_5 + Ni_5$	35	40	25	2.88
6	Pd/C + Ni pwd	35	20	12	2.88
7	Pd_3Ni_2	35	20	80	2.88
8	Pd_4Ni_1	35	20	72	2.88
9	Pd_3Ni_2 (sL)	35	20	22	2.88
10	Pd_5	35	20	1	4.75
11	$Pd_5 + Ni_5$	60	20	10	1.85
12	Pd/C + Ni pwd	60	20	8	1.85
13	Pd_3Ni_2	60	20	60	1.13
14	Pd_4Ni_1	60	20	52	1.13
15	Pd_2Ni_3 (G1)	60	20	12	1.13
16	Pd_1Ni_4 (G1)	60	20	5	1.13
17	Ni_5 (G1)	60	20	0	1.13

T = temperature; sL = successive loading; $Pd_5 + Ni_5$ = Pd_5@MIL-101 + Ni_5@MIL-101; Pd/C = Pd on coal (5 wt.-% Pd); Ni pwd = Nickel powder (Merck); G1 = 1. generation.

The use of a mixture of pure Pd@MIL-101 and pure Ni@MIL-101 in a 3:2 ratio (entry 4, 5 and 11) shows a clearly lower catalytic activity than the corresponding catalyst Pd_3Ni_2@MIL-101 and as Pd_4Ni_1@MIL-101 (7 and 8). The conversions of a corresponding mixture of Pd/C and Ni powder (Merck) (6, 12) are more lower. The lower conversions (under analogous conditions) of the mixture of pure Pd@MIL-101 and Ni@MIL-101 catalyst in comparison to the bimetallic cavity conform Pd_xNi_y@MIL-101 catalyst systems indicate a synergistic catalysis effect which is based on bimetallic particles. A comparison between successive and simultaneous loading (8, 9) shows that the successive loading leads to catalytically less active Pd-Ni NP structures. Experiments with 1. generation Pd_xNi_y@MIL-101 (15-17) yielded also lower conversions than that of the 2. generation. The adjustment of the reduction conditions towards cavity conform NP has a positive influence on the activity as well.
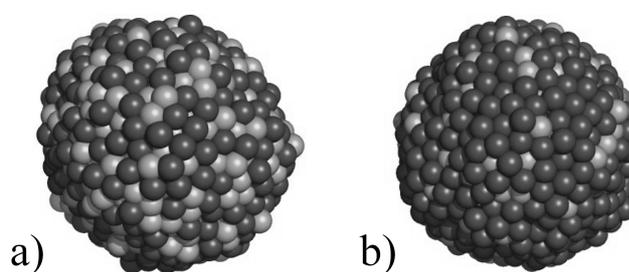
Figure 5. Structures of bimetallic Ni/Pd NP based on MD simulations. a) A bimetallic mixed structure of low energy for $Pd_{775}Ni_{514}$. b) A structure of higher energy that was simulated starting from a Ni core Pd shell particle and already shows Ni atoms (grey) on the surface.

The hypothesis of the formation of bimetallic Ni/Pd NP is also supported by molecular dynamic (MD) calculations. NP with 1289 atoms (which means a number of atoms that allows to form a closed octahedron in the experimentally relevant size range of 3.5 nm) were constructed in three different ways: on the one hand side as Ni core Pd shell NP, on the other hand as Ni shell and Pd core NP and as NP with a random distribution of the atoms. 3:2 was chosen as the Pd to Ni ratio in accordance with the ratio at which experimentally high conversions were observed. All structures were first heated to 1400 K and afterwards slowly tempered to generate energetically favourable structures. Two examples are shown in Figure 5. The left structure (a) is the energetically most favourable structure that we found by tempering. It is characterized by a strong mixing of the Ni and Pd atoms and a correspondingly corrugated surface. The right structure (b) was formed via tempering of a Ni core Pd shell particle. Ni atoms have migrated towards the surface during tempering and the particle does not have a core shell structure any more. Its surface is still Pd rich and its energy is about 120 eV (2 %) higher than that of the particle shown in Figure 5, left. If one changes the Pd to Ni ratio to 3:5 a truncated octahedron with a perfect Ni core of 805 atoms and a closed Pd shell with 484 atoms can be constructed. These special "magic" numbers of atoms should make core shell NP energetically

more favourable. The energy differences between a core shell particle and randomly mixed NP become smaller but tempering again leads to mixed bimetallic NP as energetically preferred structures. Hence, the MD simulations support the existence of bimetallic Ni/Pd NP. Ni/Pd NP are different in comparison to (for instance) Au/Pt or Au/Pd NP which were also used in catalysis. For these, NP having an Au shell were predicted to be the energetically more stable ones on the basis of empirical potentials and DFT.[32] The differences in size of the Ni and the Pd atoms could also be a reason for the mixing of the atoms in the Ni/Pd NP.[32b] Thus, "well fitted surface boundaries" are difficult to create. The resulting corrugated structure could enable the observed synergistic catalysis effects. According to the phase diagram, Ni and Pd are miscible in the relevant temperature range.[33] The reusability tests were carried out for the synergistically interesting Pd_3Ni_2@MIL-101 system (hydrogenation of 3-heptanone). After each catalytic experiment the catalyst was centrifuged, the reaction mixture was decanted off and the catalyst was washed with THF. The catalyst was again separated from THF via decanting and dried at 10^{-3} bar and 30 °C for 2 h. Reusability studies at 60 °C and 35 °C show no significant decrease in the conversion in 7 or 10 catalytic cycles, respectively (SI Figure S24, 25). PXRD investigations confirm the stability of the MIL-101 support (SI Figure S26). TEM investigations show no increase in the particle size after multiple use in catalysis (SI Figure S27). Similarly, ICP-OES analyses show stable Ni/Pd, Pd/Cr and Ni/Cr ratios (SI Table 4). The specific surface doesn't change also after multiple cycles (SI Table 2).

5.3 Conclusions

In summary, we introduce a bimetallic synergistically acting catalyst system. Via MOCVD, the sublimable metal-organic precursors $[(C_5H_5)Pd(C_3H_5)]$ and $[(C_5H_5)_2Ni]$ can be loaded quantitatively and in different mixtures into the porous host structure of MIL-101. Cavity conform Ni/Pd NP of different composition were generated via an optimized reduction of the loaded precursors by H_2. The so formed catalysts are active in the hydrogenation of alkyl-alkyl ketones. High catalytic efficiency is only observed if both metals operate synergistically and are nearly atomically dispersed. The bimetallic Ni/Pd NP catalysts are reusable. The MIL-101 support combines ideally stability and good access of the educts to the catalytically active sites. The synthesis of such "naked" (bi)metallic NP, tuneable regarding their size, is generally of great interest.[34]

5.4 Acknowledgements

5.5 Supporting Information

5.5.1 Experimental Section

Reactants and solvents: Terephthalic acid (H$_2$BDC) was purchased from Acros Organics. Ethylbenzene and cyclohexanone were purchased from Sigma-Aldrich chemicals. Chromium(III) nitrate nonahydrate (Cr(NO$_2$)$_3$·9H$_2$O), allylpalladium(II) chloride dimer, and bis(cyclopentadienyl) nickel(II) were purchased from ABCR. 3-heptanone and cycloheptanone were purchased from Alfa Aesar. Phenol was purchased from Riedel-de Haen. All manipulations and chemical reactions were conducted under an inert atmosphere [Schlenk-technique (Ar) and/or glove box technique (H$_2$O, O$_2$ < 0.1 ppm). Non-halogenated solvents were dried with sodium/benzophenone ketyl and halogenated solvents with CaH$_2$.

Analytical and spectroscopic methods: Elemental analysis was performed by standard protocols employing digestion in HNO$_3$/HCl/H$_2$O$_2$ and inductively coupled plasma optical emission spectrometry (ICP-OES) using a Varian Vista-Pro radial. GC analyses were performed using an Agilent 6890N gas chromatograph equipped with a flame ionization detector (FID) and an Agilent 19091 J-413 FS capillary column using dodecane as external standard. All X-ray powder diffractograms were recorded using a STOE STADI-P-diffractometer (CuK$_\alpha$ radiation, 1.54178 Å) in ϑ-2ϑ-geometry with a position sensitive detector. FTIR-measurements were performed at a Perkin Elmer FTIR-Spectrum 100 over a range of 4000 cm^{-1} to 550 cm^{-1}. The nitrogen physisorption isotherms were measured at 77 K using a Quantachrome Nova 2000e apparatus. 25 mg of the pre-degassed sample were transferred to a quartz cell and consequently degassed again at 100 °C, 10^{-4} mbar for 24 h. Transmission electron microscopy (TEM) was carried out by using a Varian LEO 9220 (200 kV) instrument. TEM-EDS (*energy dispersive X-ray spectroscopy*) measurements were carried out by using a CM20FEG (200 kV) with NORAN System 7 X-ray Microanalysis System at Bayerisches Geoinstitut. The sample was suspended in chloroform and sonicated for 5 min. Subsequently a drop of the suspended sample was placed on a grid and allowed to dry.

Starting materials synthesis: The Pd precursor [(η^5-C$_5$H$_5$)Pd(η^3-C$_3$H$_5$)] was synthesized under exclusion of light following a published procedure.[35] 2.5 g of allylpalladium(II) chloride dimer were dissolved in 50 mL of abs. THF and cooled to -60 °C. Dropwise addition of 6 mL NaCp (Cp = cyclopentadienyl) dissolved in 20 mL of abs. THF under constant cooling and stirring lead to a red coloring of the solution that was stirred for another 15 min at -20 °C and for 30 min at RT. The solvent was removed under vacuum and the residue was dissolved in 50 mL of abs. hexane followed by cannula filtration. The solvent was removed under vacuum. The Ni precursor [Ni(η^5-C$_5$H$_5$)$_2$] was further purified by sublimation and stored at -35 °C under N$_2$ prior to infiltration.

MIL-101 was synthesized and washed according to a published procedure.[36] 1.64 g H_2BDC, 4 g of $Cr(NO_3)_3 \cdot 9H_2O$, 0.5 mL of HF and 50 mL of H_2O were mixed and sealed in a Teflon lined hydrothermal autoclave. The mixture was heated for 8 h at 210 °C. Fast cooling to 160 °C followed by slow cooling (2.7 °C/h) to 30 °C led to crystallization of unreacted terephthalic acid, which could be removed from the resulting green mixture via filtration over pore 3 filter. The filtrate was again filtered using a fine pore paper filter. The resulting solid was washed with 50 mL of water, refluxed two times in EtOH for 12 h each and filtered off using a fine pore paper filter. The resulting green powder was washed with water and evacuated at 10^{-5} mbar to remove any solvent. All materials were stored under argon.

Infiltration of $[(\eta^5\text{-}C_5H_5)Pd(\eta^3\text{-}C_3H_5)]$ and $[Ni(\eta^5\text{-}C_5H_5)_2]$ into MIL-101: Freshly evacuated MIL-101 powder, $[(\eta^5\text{-}C_5H_5)Pd(\eta^3\text{-}C_3H_5)]$, and $[Ni(\eta^5\text{-}C_5H_5)_2]$ were placed in a three-chamber-tube separated by a glass frit and were kept at 25 °C in a 10^{-4} mbar dynamic vacuum for 3 – 8 h. Dynamic vacuum was used to minimize possible deposition of metal precursor on the outer surface of MIL-101. Exclusion of light minimal temperature was used to prevent premature reduction of metal precursors. The procedure yielded a dark green to black powder, which was immediately processed in hydrogenolysis to yield Pd_xNi_y@MIL-101.

Preparation of Pd_xNi_y@MIL-101: The adjacent reduction of M(II) (M = Pd, Ni) to M(0) was performed with hydrogen at defined pressure, temperature and time in a Parr Instruments steel autoclave. To remove traces of the ligands, the material was evacuated for 24 h at $5 \cdot 10^{-5}$ mbar (125 °C).

Reduction of ketones using Pd_xNi_y@MIL-101 as catalyst: All reduction experiments were carried out in a steel autoclave (Parr) with 20 bar H_2 pressure. The catalyst was weighed accurate to within 0.01 mg. The conversion was determined by GC with dodecane as external standard.

Recyclability of Pd_xNi_y@MIL-101: The catalyst was separated from the reaction mixture via centrifugation, cleaned with THF, and dried at 30 °C for 2 h at 10^{-3} mbar before the next run. The conversion was determined by GC with dodecane as external standard.

5.5.2   Optimization of the loading conditions
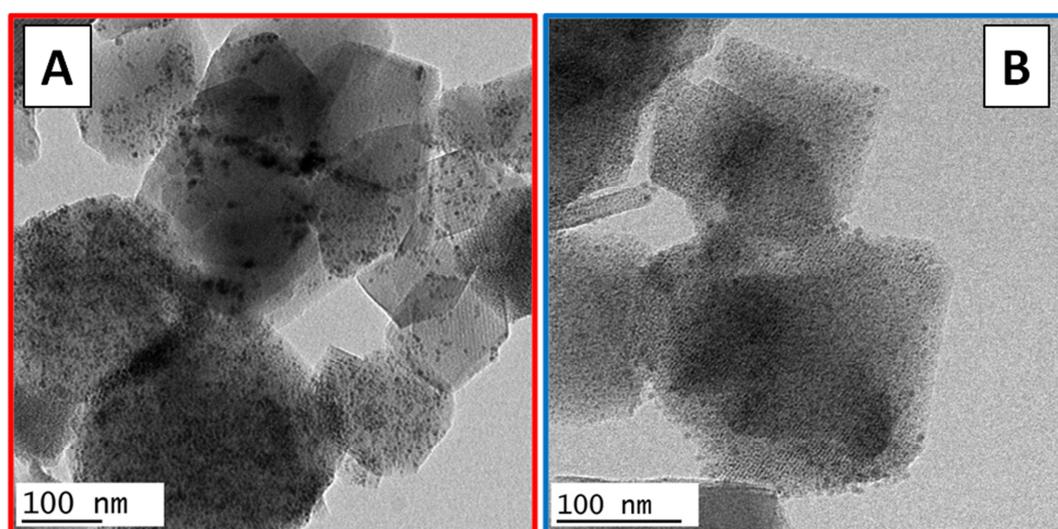
Figure S1: TEM pictures of $Pd_{2.5}Ni_{2.5}$@MIL-101. A: Successive loading of Pd and Ni shows slightly bigger metal nanoparticles (MNP), which are randomly placed. B: Simultaneous loading shows smaller particles within the cavities of MIL-101.
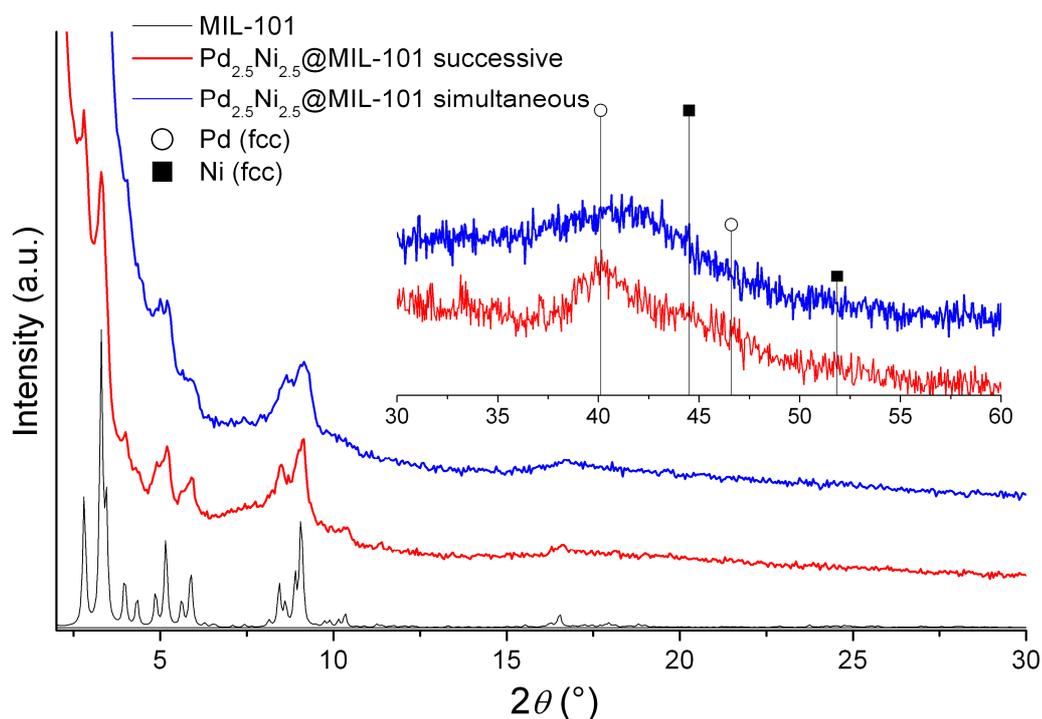
Figure S2: PXRD of $Pd_{2.5}Ni_{2.5}$@MIL-101. Successive loading of $[(C_5H_5)Pd(C_3H_5)]$ and $[(C_5H_5)_2Ni]$ into MIL-101 shows separated (111) reflections for Pd and Ni, indicating non bimetallic particles. Simultaneous loading shows broader reflections without separation. Broadening of MIL-101 reflections is due to metal infiltration.
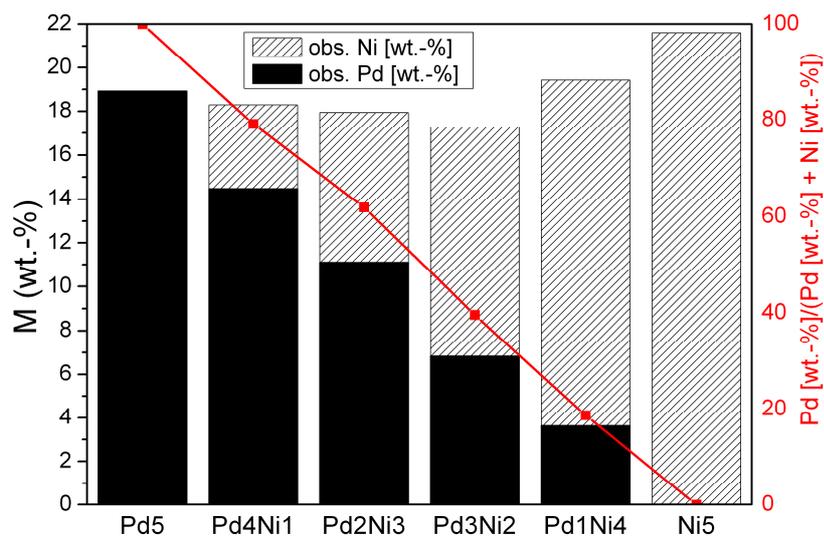
Figure S3: ICP-OES analysis of Pd_xNi_y@MIL-101 synthesized according to standard protocol (70 °C, 50 bar, 20 h). The average metal weight content is 19 wt.-%. The substitution of Pd with Ni is performed in 20 wt.-% steps.
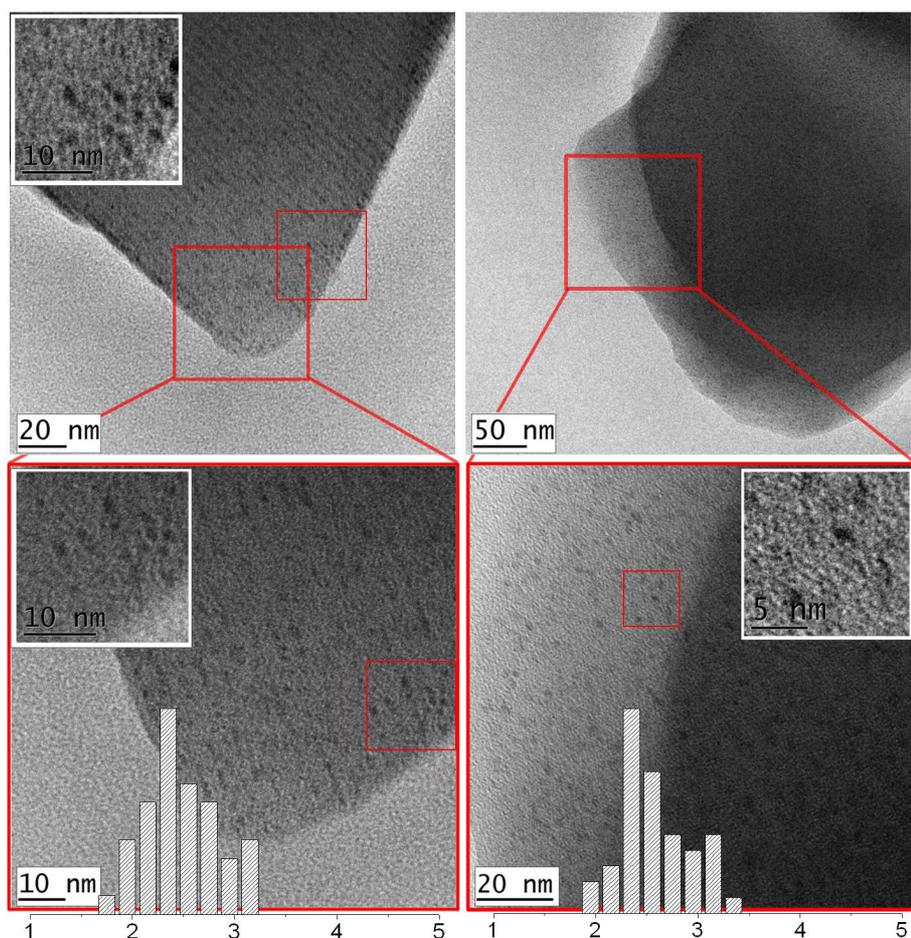
Figure S4: TEM analysis of Pd_5@MIL-101 synthesized according to standard protocol (70 °C, 50 bar, 20 h). Pd-nanoparticles (NPs) of 2-3 nm in diameter are visible. The regular order of MNP suggests incorporation of MNP within the cavities of MIL-101.
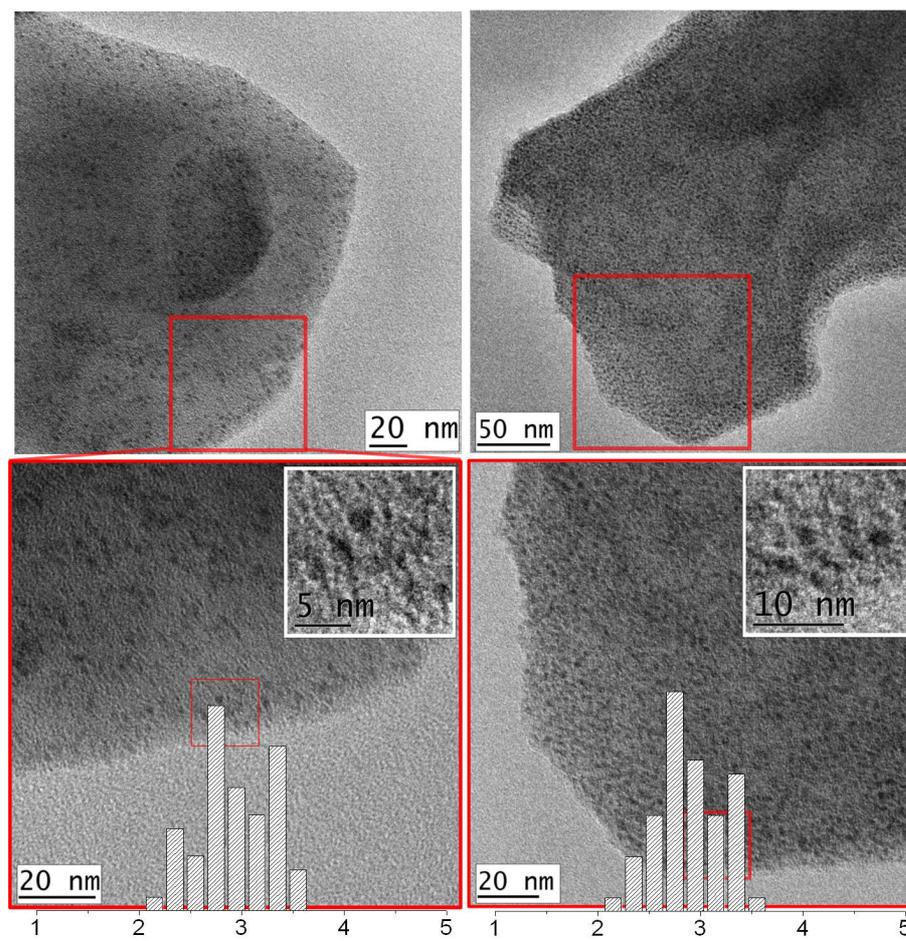
Figure S5: TEM analysis of Pd_4Ni_1@MIL-101 synthesized according to standard protocol (70 °C, 50 bar, 20 h). Pd NPs of 2-3.5 nm in diameter are visible. The regular order of MNP suggests incorporation of MNP within the cavities of MIL-101.
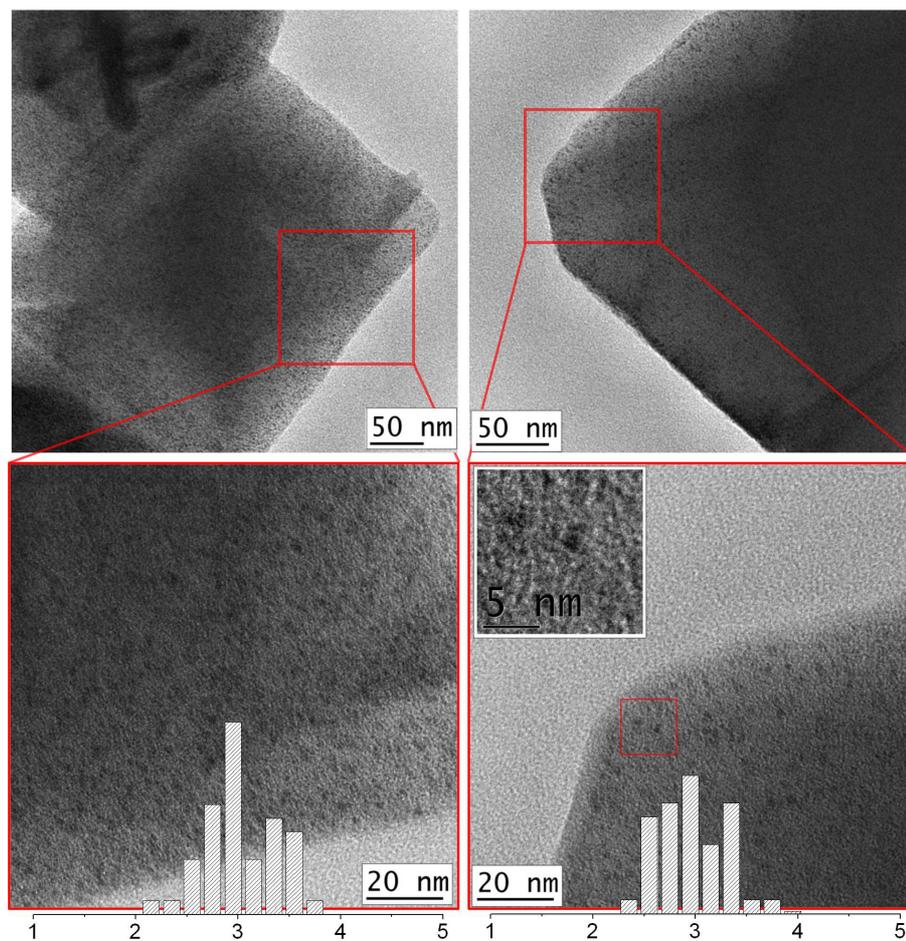
Figure S6: TEM analysis of Pd$_3$Ni$_2$@MIL-101 synthesized according to standard protocol (70 °C, 50 bar, 20 h). Pd NPs of 2.5-3.5 nm in diameter are visible. The regular order of MNP suggests incorporation of MNP within the cavities of MIL-101.
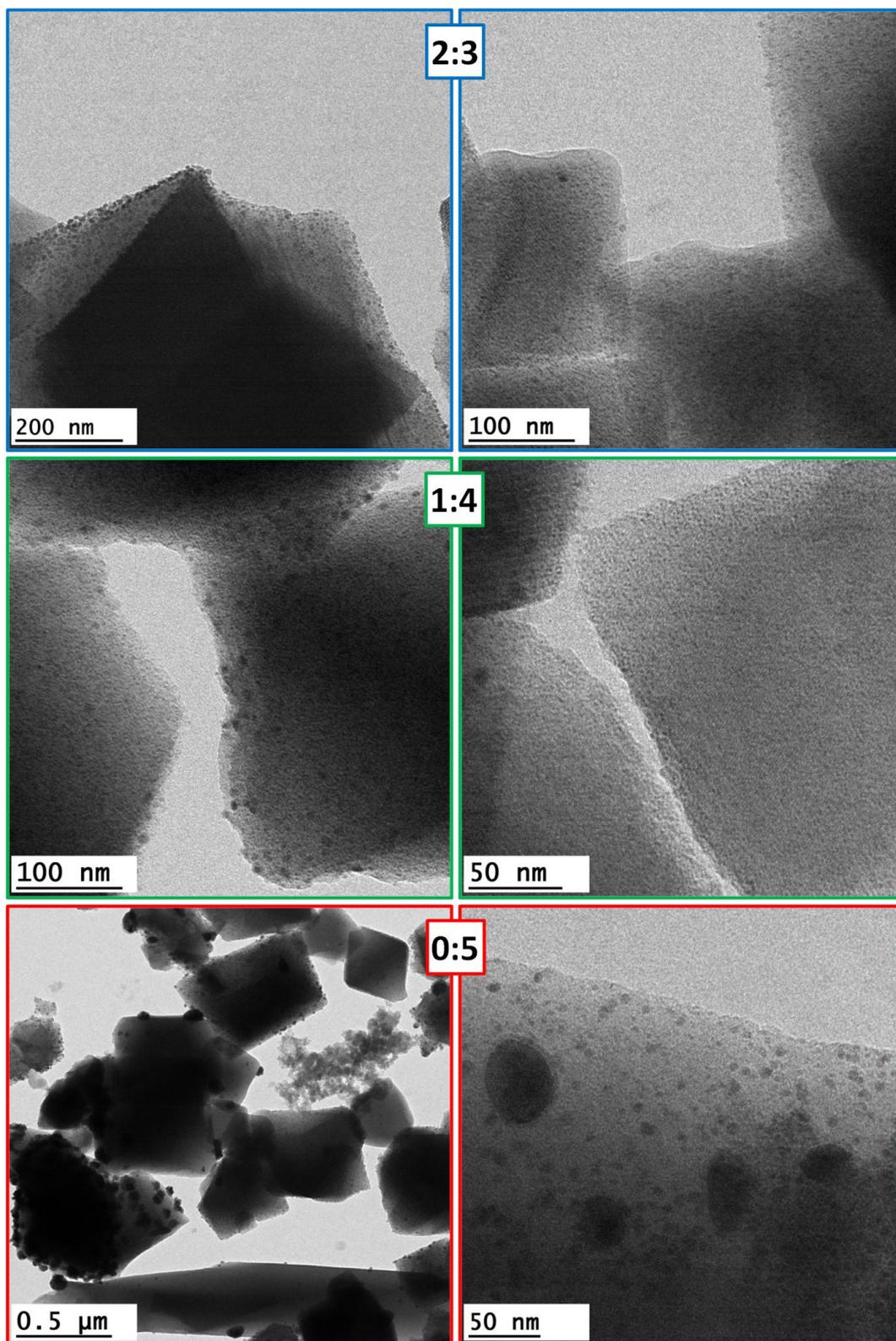
Figure S7: TEM analysis of Pd_2Ni_3@MIL-101 (blue), Pd_1N_4@MIL-101 (green), and Ni_5@MIL-101 (red) synthesized according to standard protocol (70 °C, 50 bar, 20 h). Though some NPs of 3 nm in diameter are visible, many bigger particles at the outer surface of MIL-101 crystallites are present, requiring an adjustment of the reduction protocol.

5.5.3 Characterization of the Pd/Ni@MIL-101 catalyst synthesized via the optimized loading and reduction conditions (2nd Generation)
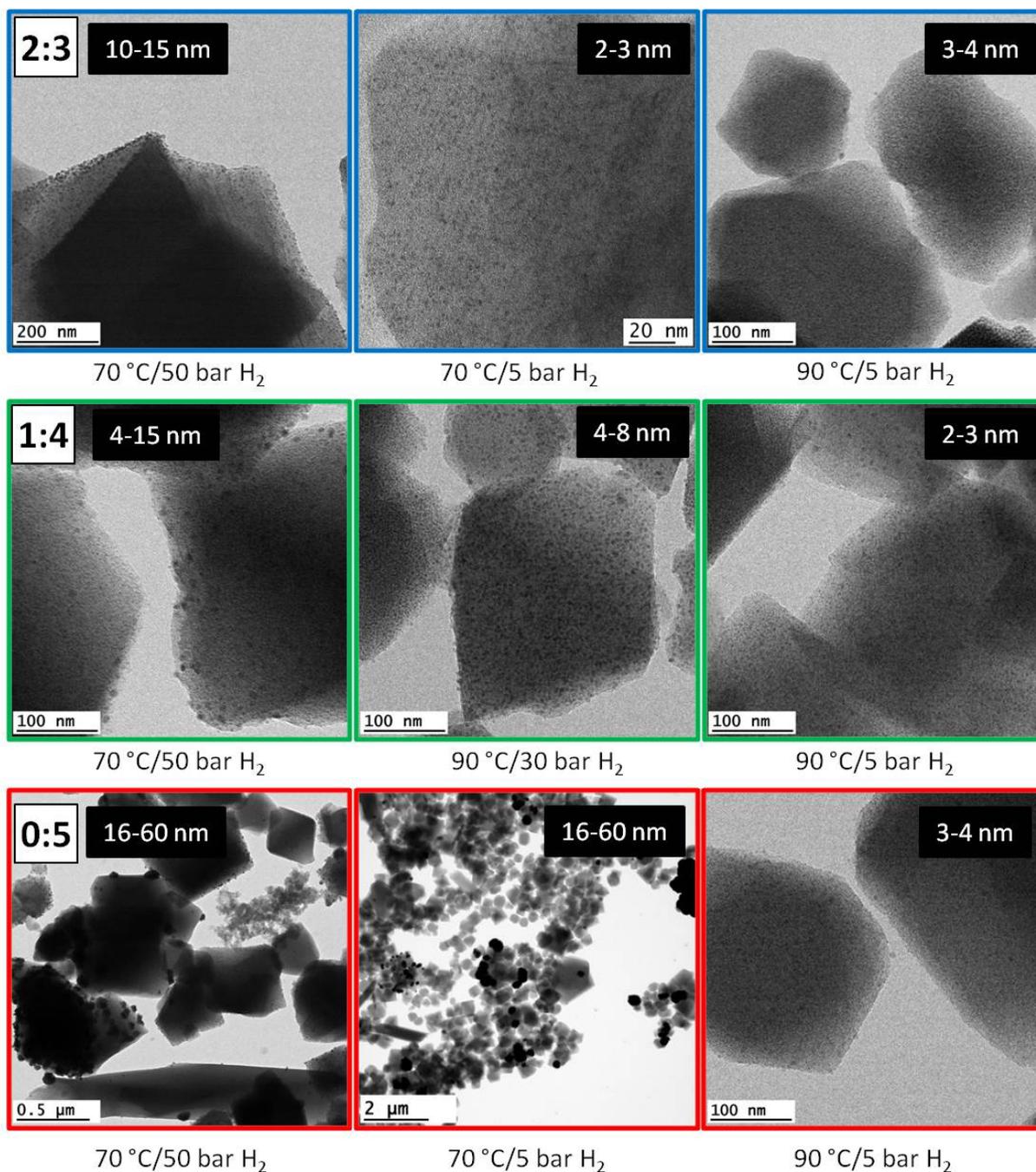
Figure S8: TEM analysis of different reduction protocols for Ni dominated systems Pd_2Ni_3@MIL-101 (blue), Pd_1N_4@MIL-101 (green), and Ni_5@MIL-101 (red). Mean particle size is depicted within graphs. Reduction with H_2 must be carried out with less pressure and higher temperature to yield small, cavity conform NP. MNP sizes depicted in black boxes indicate approximate values based on single measurements. Histograms for optimized reduction protocol are shown separately in Figure S9, S10 and S11.
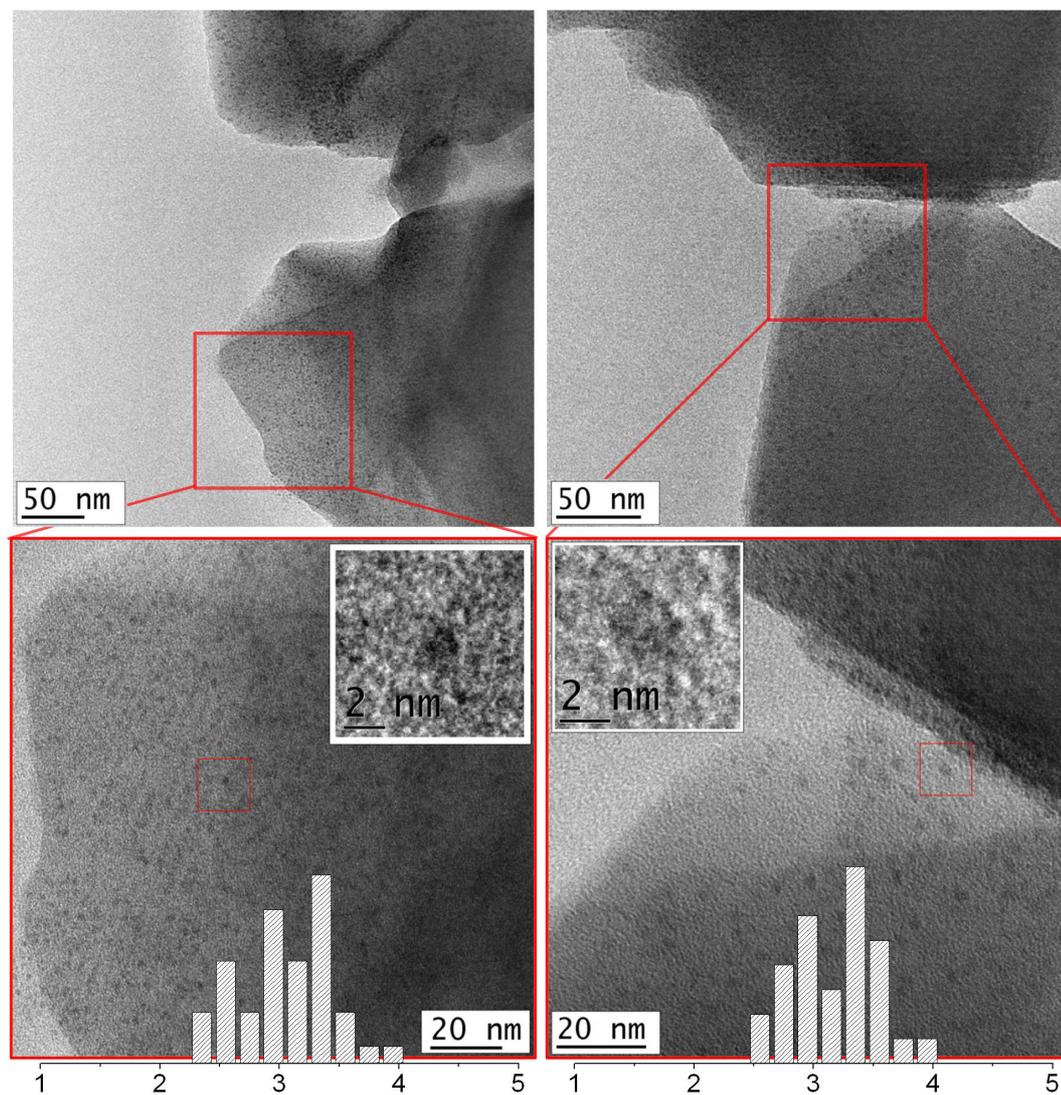
Figure S9: TEM analysis of Pd$_2$Ni$_3$@MIL-101 synthesized according to optimized reduction protocol (70 °C, 5 bar, 20 h). Pd NPs of 2.5-3.5 nm in diameter are visible. The regular order of MNP suggests incorporation of MNP within the cavities of MIL-101.
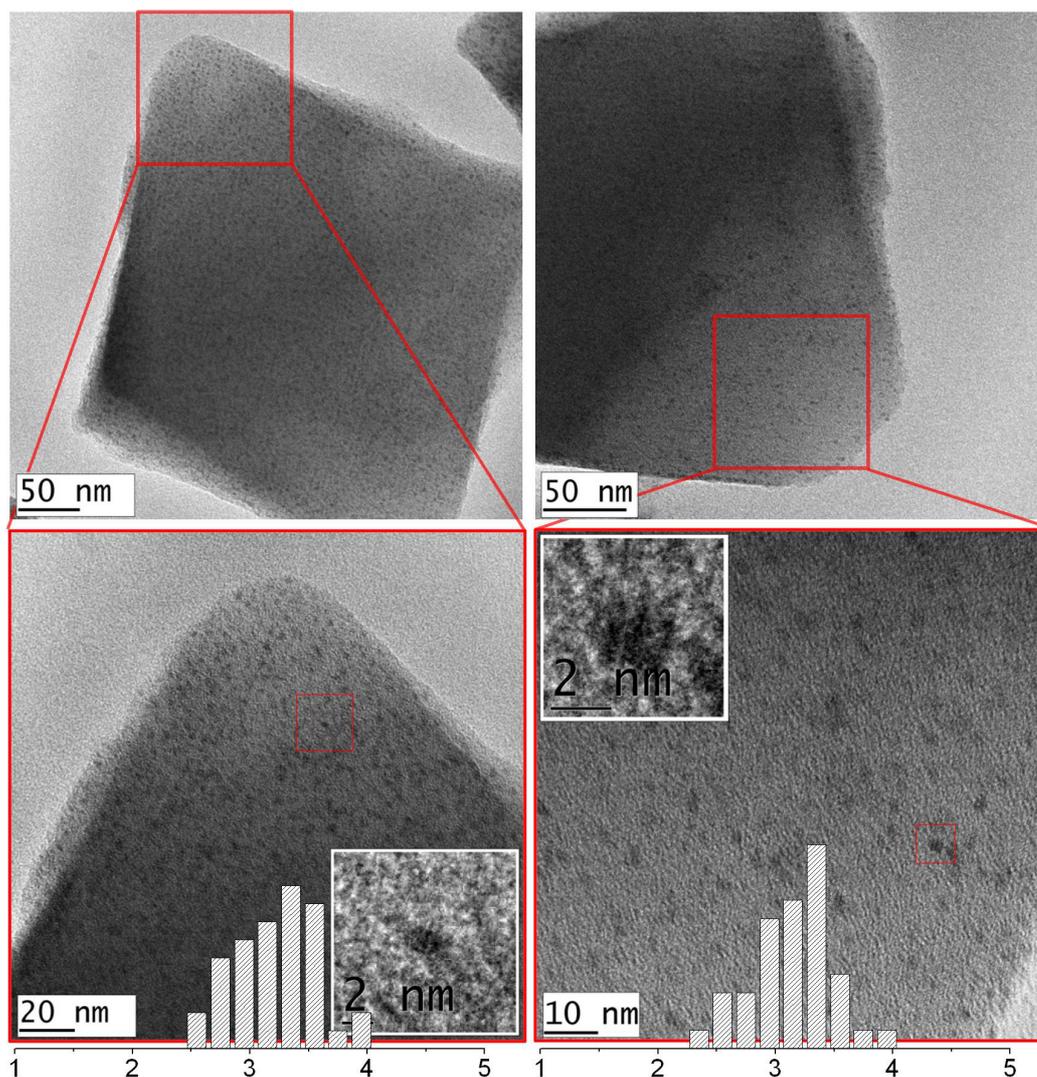
Figure S10: TEM analysis of Pd_1Ni_4@MIL-101 synthesized according to optimized reduction protocol (90 °C, 5 bar, 20 h). Pd NPs of 2.5-3.5 nm in diameter are visible. The regular order of MNP suggests incorporation of MNP within the cavities of MIL-101.
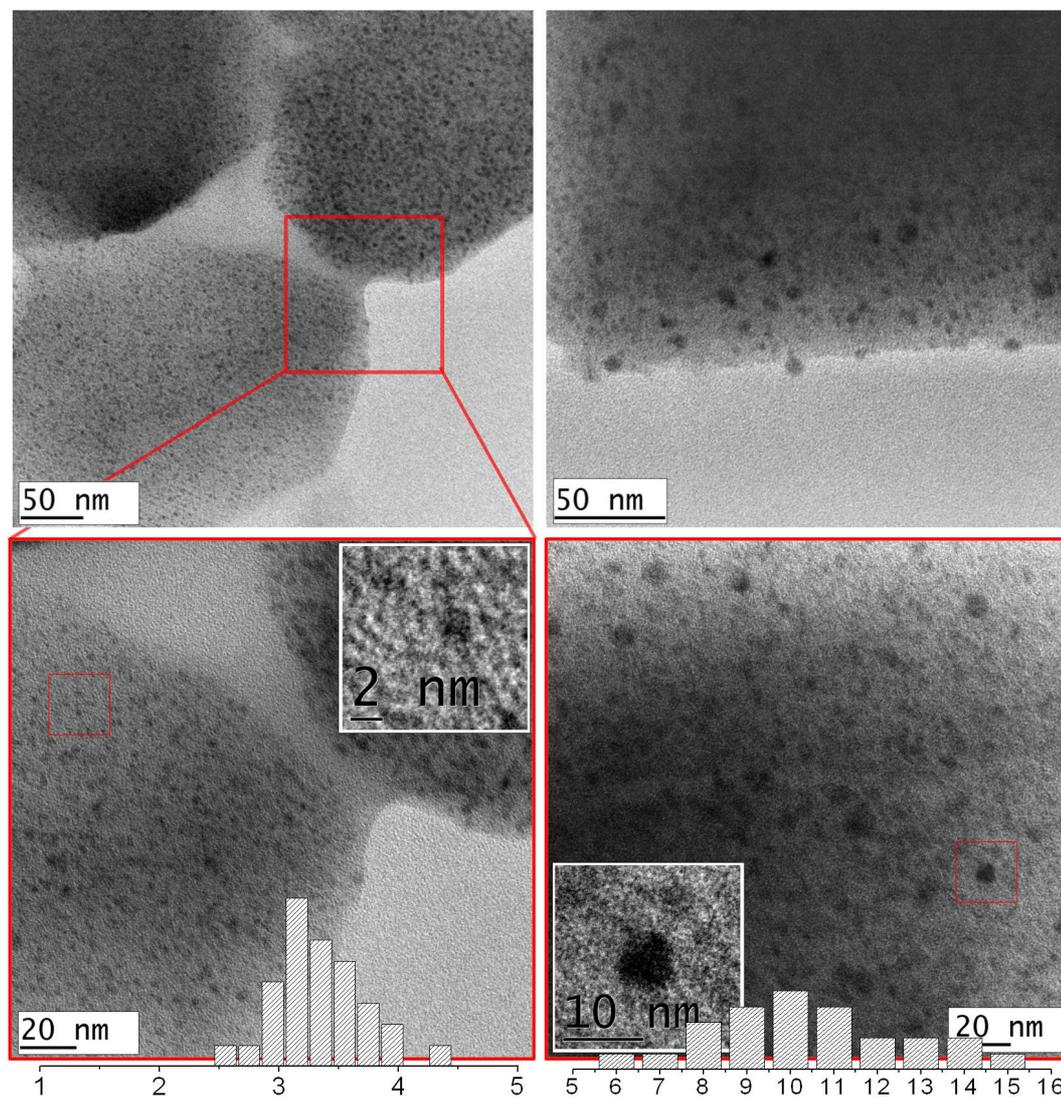
Figure S11: TEM analysis of Ni$_5$@MIL-101 synthesized according to optimized protocol (90 °C, 5 bar, 20 h). Pd NPs of 3-4 nm in diameter are visible. The pictures on the right side show MNP with an average particle size of 10 nm.
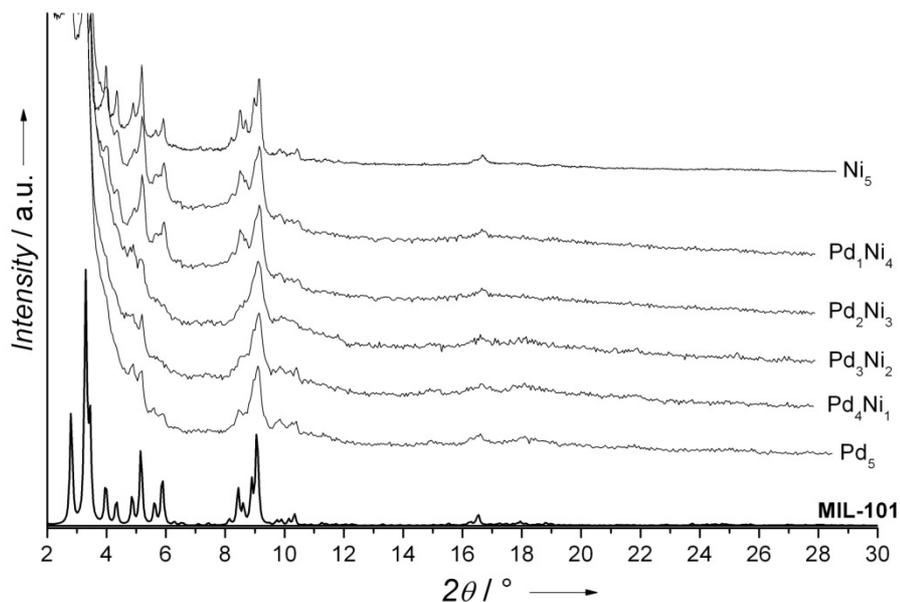
Figure S12: PXRD analysis of Pd_xNi_y@MIL-101 synthesized according to optimized reduction protocol. The reflections of MIL-101 of the metal loaded and reduced systems are stable under the chosen conditions. Broadening of MIL-101 reflections is due to metal infiltration. Reflections become sharper with increasing Ni content.
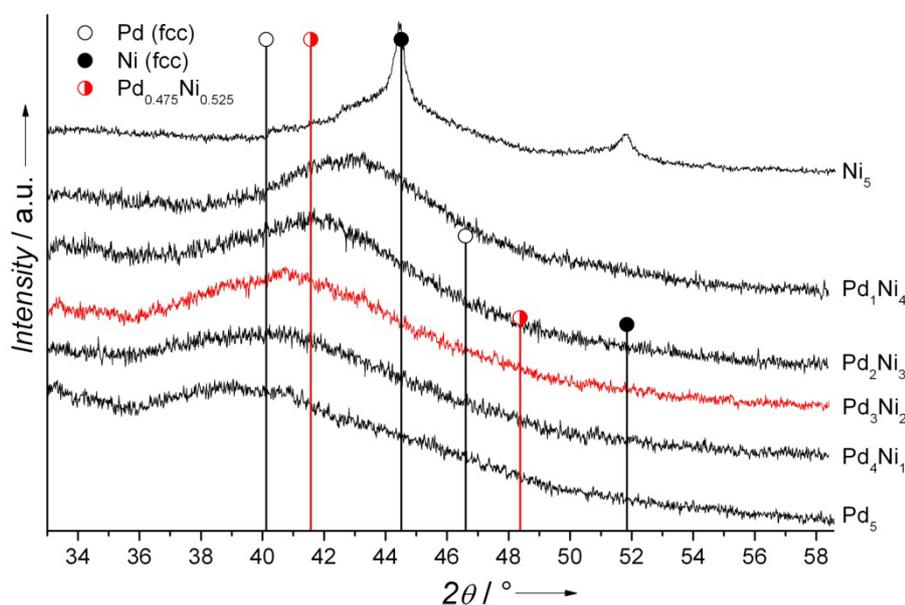
Figure S13: PXRD analysis of Pd_xNi_y@MIL-101 synthesized according to optimized reduction protocol. The broad *fcc* signals indicate very small nanoparticles. With increasing Ni content the 111 reflection shifts from 38° 2ϑ (pure Pd) towards 44° 2ϑ (pure Ni). Pure Ni_5@MIL-101 shows additional sharp reflections at 44° 2ϑ and 52° 2ϑ with narrow FWHM above the broad halo indicating a mixture of small NP with some bigger particles. The downshift of reflections (in comparison to literature) is due to small particle size. $Pd_{0.475}Ni_{0.525}$ (Literature) is settled between Pd and Ni reflections and is in accordance to our observations.
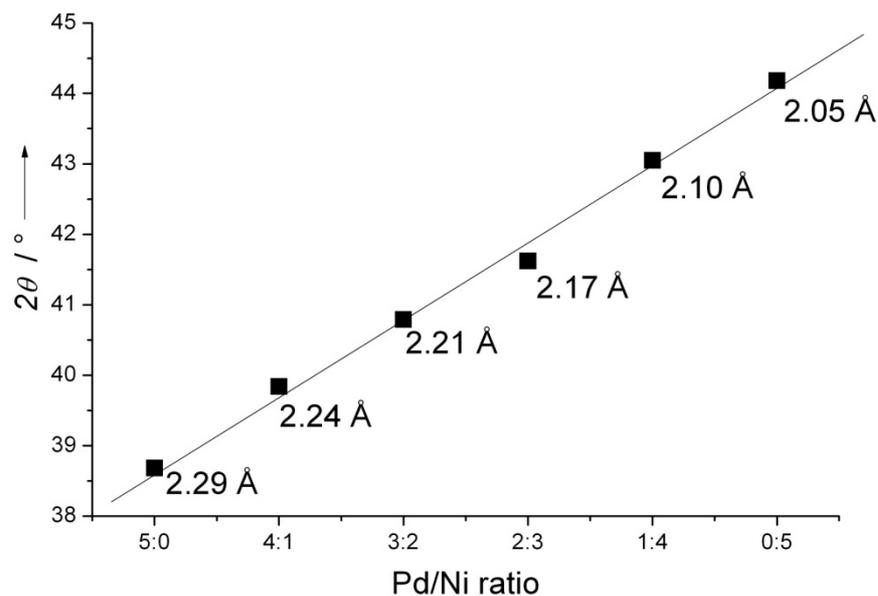
Figure S14: Shift of the (111) peak of the Pd/Ni@MIL101 catalysts with increasing Ni content and lattice spacing. With increasing Ni content the (111) reflection shifts from 38° (pure Pd) towards 44° (pure Ni).
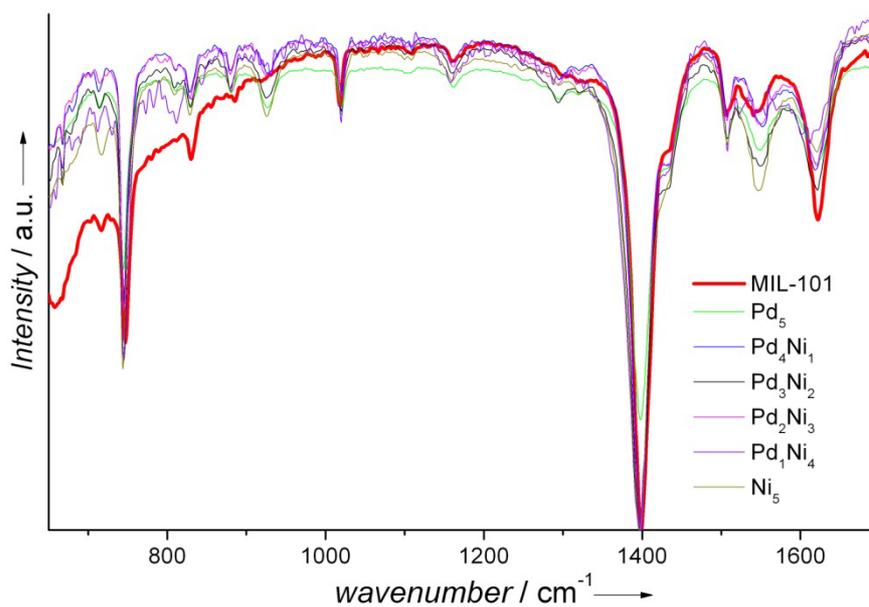
Figure S15: IR analysis of Pd_xNi_y@MIL-101. The lattice vibrations of MIL-101 are not disturbed by the loading with the metal precursors and their reduction.
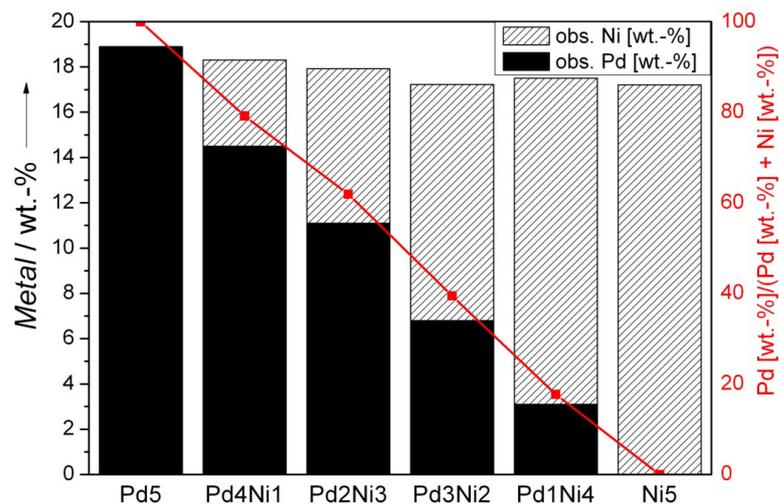
Figure S16: ICP-OES analysis of Pd_xNi_y@MIL-101 synthesized with optimized reduction protocol (90 °C, 1-5 bar, 20 h). The average metal weight content is 18 wt.-%. The substitution of Pd with Ni is performed in 20 wt.-% steps.
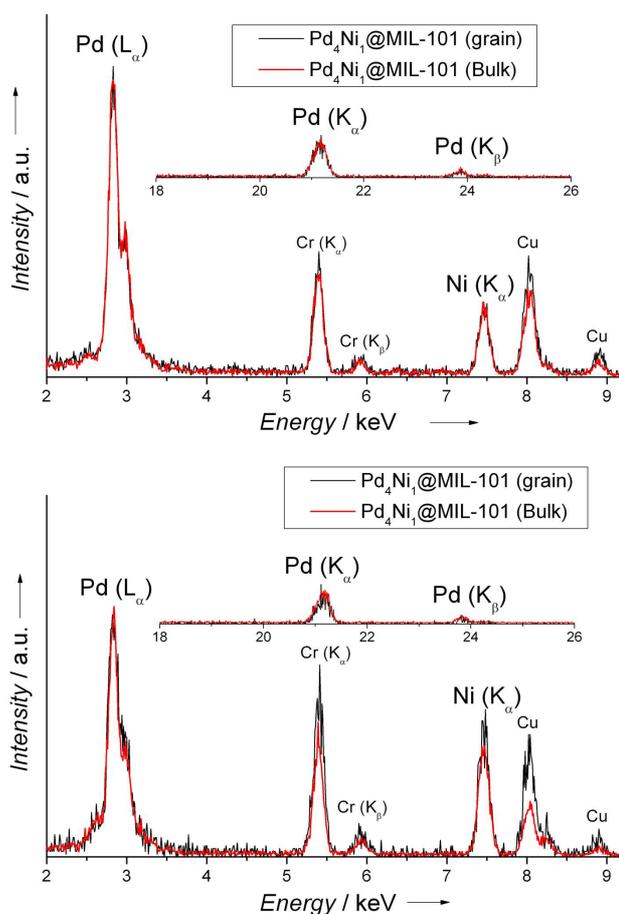
Figure S17: TEM-EDS analysis of Pd_4Ni_1@MIL-101 (top) and Pd_3Ni_2 (bottom). Pd/Ni-ratio in bulk (red) and single NP (black) is identical assuming bimetallic particles.
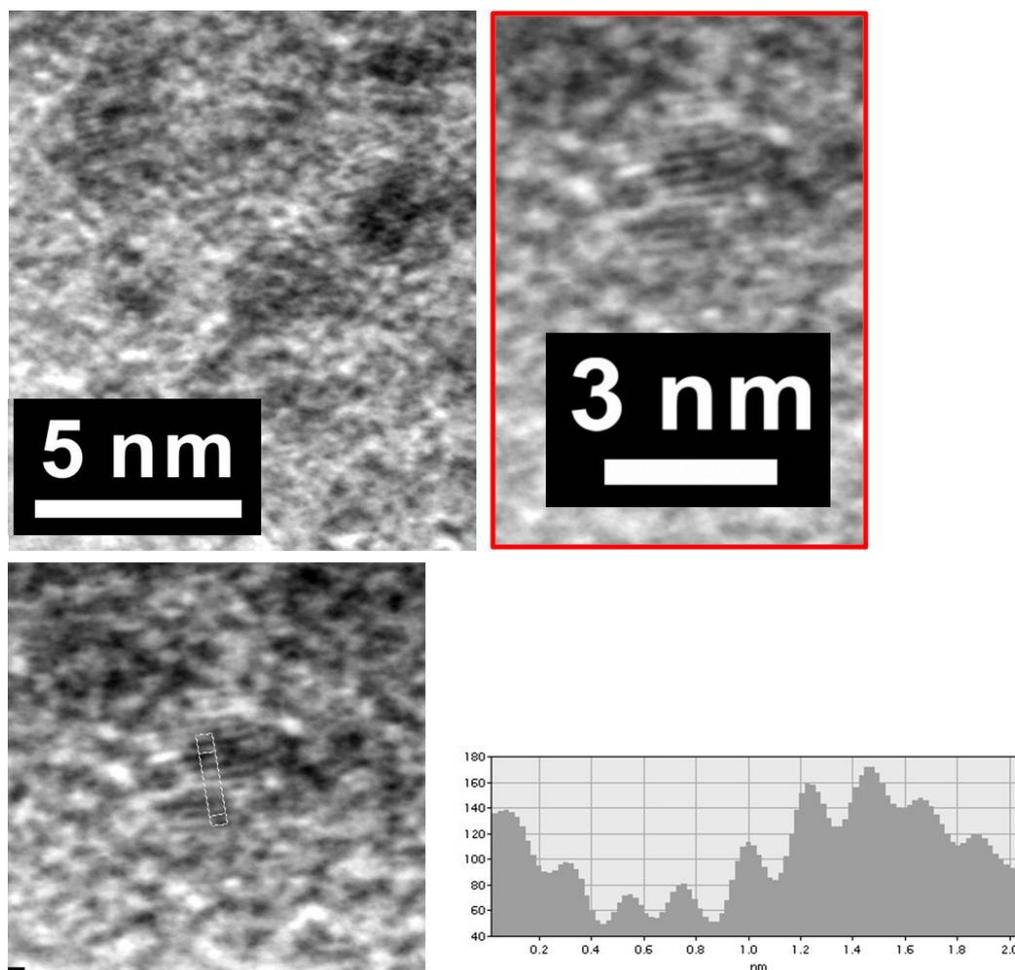
Figure S18: HR-TEM analysis of Pd_4Ni_1@MIL-101. Top left: multiple particles, Top right: single particle, bottom left: single particle and d spacing grit, bottom right resulting d spacing profile [d spacing [111] 2.26(6) Å] calibrated using graphite.
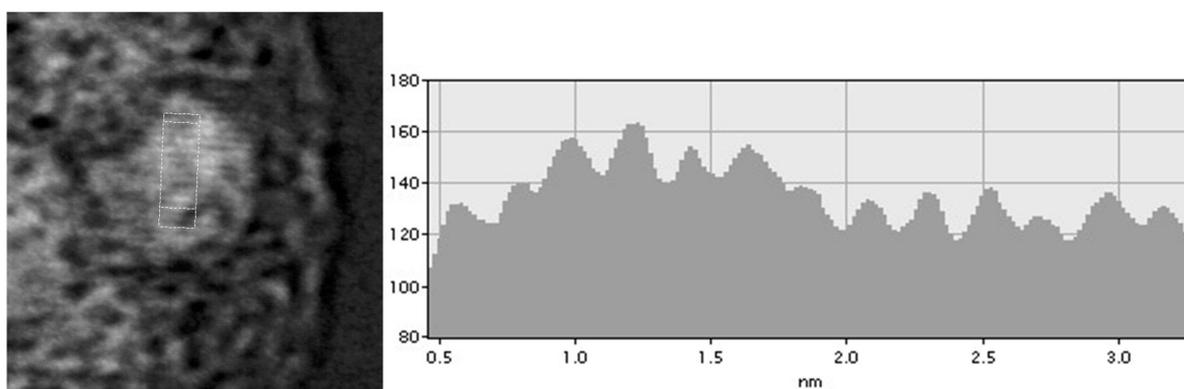
Figure S19: HR-TEM analysis of Pd_3Ni_2@MIL-101. Left: single particle and d spacing grit, right resulting d spacing profile [d spacing [111] 2.19(5) Å] calibrated using graphite.

Table S1: Optimized reduction conditions for $[(\eta^5\text{-}C_5H_5)Pd(\eta^3\text{-}C_3H_5)]$ /$[Ni(\eta^5\text{-}C_5H_5)_2]$@MIL-101. Palladium dominated systems can be reduced via previously published procedure.[23] With increasing Ni content temperature must be increased whilst pressure is decreased. Reduction time is 20 h for each system.

Pd/Ni	Temperature	Pressure
5:0	70 °C	50-70 bar
4:1	70 °C	40 bar
3:2	70 °C	40 bar
2:3	70 °C	5 bar
1:4	90 °C	5 bar
0:5	90 °C	5 bar

Table S2: Specific surface area of Pd_xNi_y@MIL-101. Pure Pd and Ni loaded MIL-101 show the highest surface area, whilst mixed systems have a decreased surface area.

	Specific Surface area [m²/g]	Pore volume [cm³/g]
Pd_5@MIL-101	1145	0.58
Pd_4Ni_1@MIL-101	828	0.49
Pd_3Ni_2@MIL-101	874	0.46
Pd_2Ni_3@MIL-101	755	0.47
Pd_1Ni_4@MIL-101	1106	0.59
Ni_5@MIL-101	1333	0.71
MIL-101	2554	1.51
Pd_3Ni_2@MIL-101 (after 10 times 5 h catalysis)	892	0.47

5.5.4 Catalytic studies
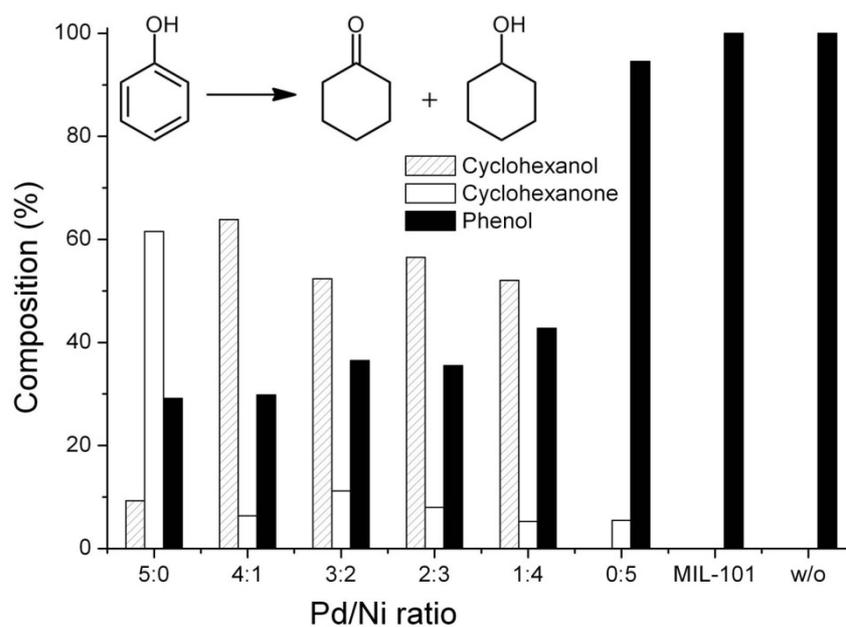
Figure S20: Reduction of phenol (0.18 mg Pd ($0.52 \cdot 10^{-3}$ mol-%), 350 µL phenol, 60 °C, 48 h, 20 bar H_2; w/o = without catalyst).
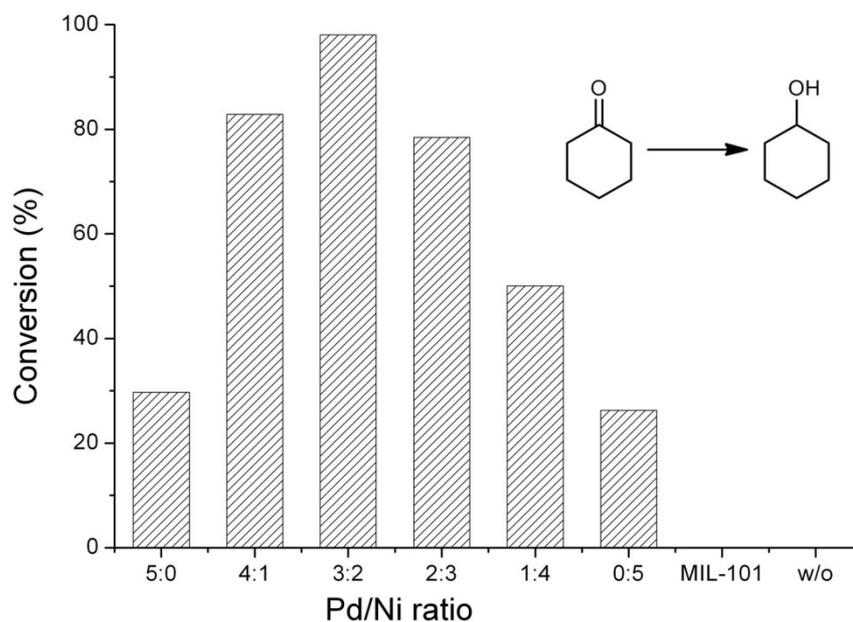
Figure S21: Reduction of cyclohexanone (0.18 mg Pd ($0.50 \cdot 10^{-3}$ mol-%), 350 µL cyclohexanone, 60 °C, 24 h, 20 bar H_2; w/o = without catalyst).
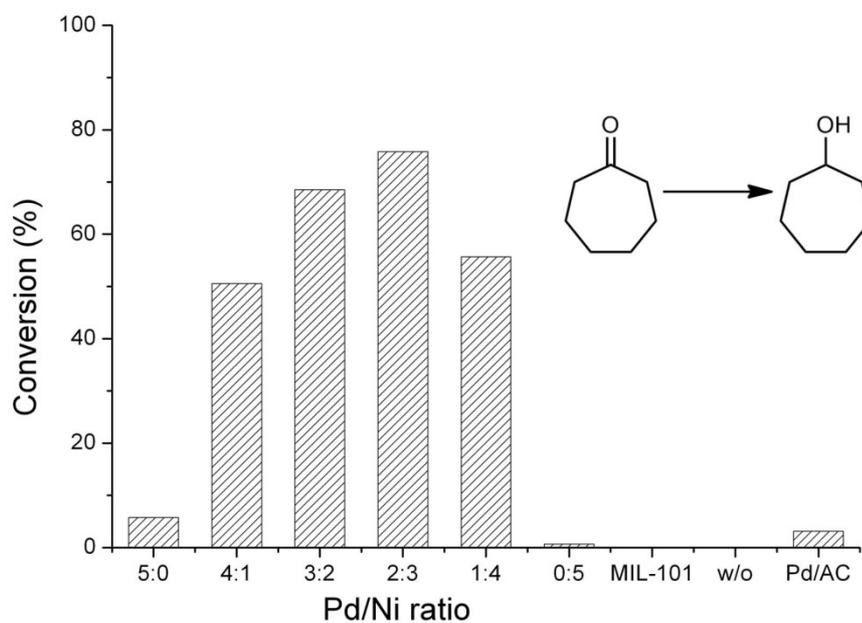
Figure S22: Reduction of cycloheptanone (0.36 mg Pd (0.80 · 10^{-3} mol-%), 500 µL cycloheptanone, 60 °C, 48 h, 20 bar H_2. Pd/C = Pd on active charcoal; w/o = without catalyst).
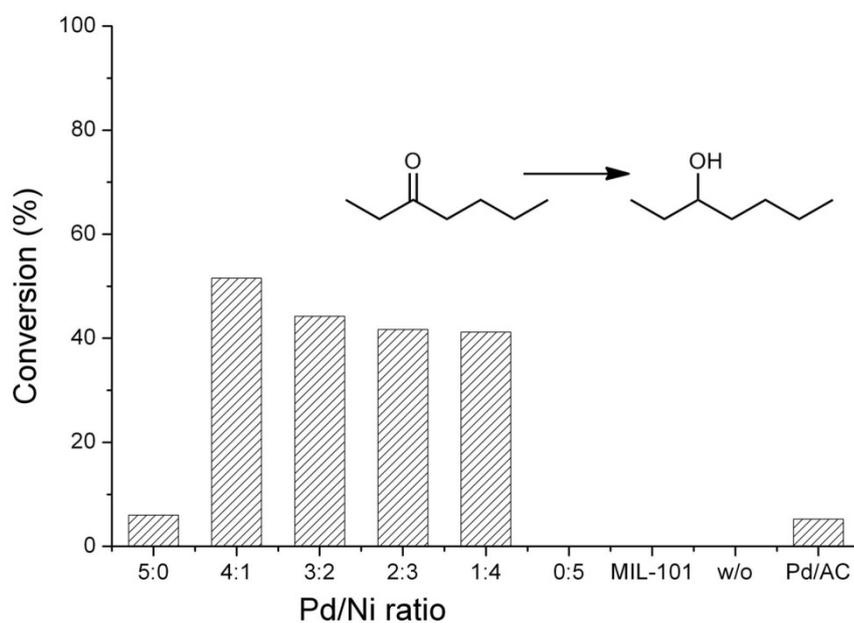
Figure S23: Reduction of 3-heptanone (0.36 mg Pd (0.94 · 10^{-3} mol-%), 500 µL 3-heptanone, 60 °C, 48 h, 20 bar H_2. Pd/C = Pd on active charcoal; w/o = without catalyst).

Table S3: Catalytic results from reduction of 3-heptanone with Pd_xNi_y@MIL-101. Temp. = temperature; conv. = conversion; sl = successive loading; Pd/C = Pd on active charcoal (5 wt.-% Pd); Ni pwd = nickel powder; G1 = 1. generation.

entry	system	Temp. [°C]	t [h]	Conv. [%]	Pd/3-Heptanon [g/mol]
1	Pd_3Ni_2@MIL-101	25	27	50	0.306
2	Pd_3Ni_2@MIL-101	35	20	80	0.306
3	Pd_3Ni_2@MIL-101	60	20	75	0.153
4	Pd_5@MIL-101+ Ni_5@MIL-101	35	20	14	0.306
5	Pd_5@MIL-101+ Ni_5@MIL-101	35	40	25	0.306
6	Pd/C + Ni pwd	35	20	12	0.306
7	Pd_3Ni_2@MIL-101	35	20	80	0.306
8	Pd_4Ni_1@MIL-101	35	20	72	0.306
9	Pd_3Ni_2@MIL-101 (sl)	35	20	22	0.306
10	Pd_5@MIL-101	35	20	1	0.506
11	Pd_5@MIL-101+ Ni_5@MIL-101	60	20	10	0.197
12	Pd/AC + Ni pwd	60	20	8	0.197
13	Pd_3Ni_2@MIL-101	60	20	60	0.120
14	Pd_4Ni_1@MIL-101	60	20	52	0.120
15	Pd_2Ni_3@MIL-101 (G1)	60	20	12	0.120
16	Pd_1Ni_4@MIL-101 (G1)	60	20	5	0.120
17	Ni_5@MIL-101 (G1)	60	20	0	0.120
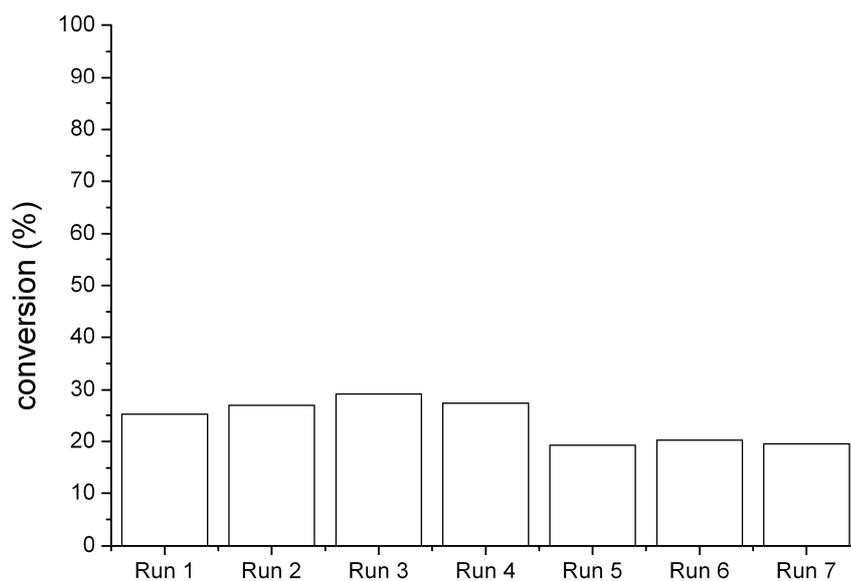
Figure S24: Reusability test of Pd$_3$Ni$_2$@MIL-101 (2.4 mg Pd (3.70 · 10^{-3} mol-%), 0.85 mL 3-heptanone, 60 °C, 3 h, 20 bar H$_2$). Used catalyst was centrifuged, washed in THF and dried 2 h at 10^{-3} mbar prior to the next run.
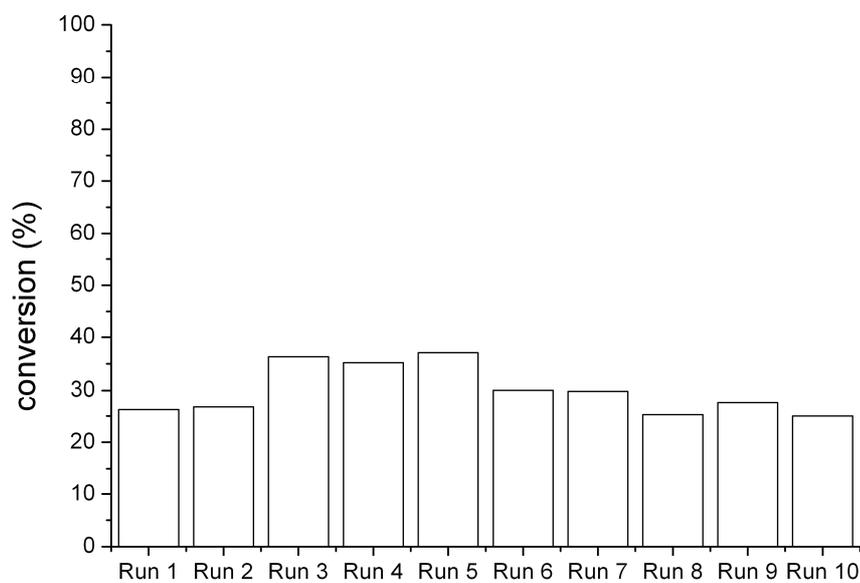
Figure S25: Reusability test of Pd$_3$Ni$_2$@MIL-101 (4.5 mg Pd (11.80 · 10^{-3} mol-%), 0.5 mL 3-heptanone, 35 °C, 5 h, 20 bar H$_2$). Used catalyst was centrifuged, washed in THF and dried 2 h at 10^{-3} mbar prior to the next run.
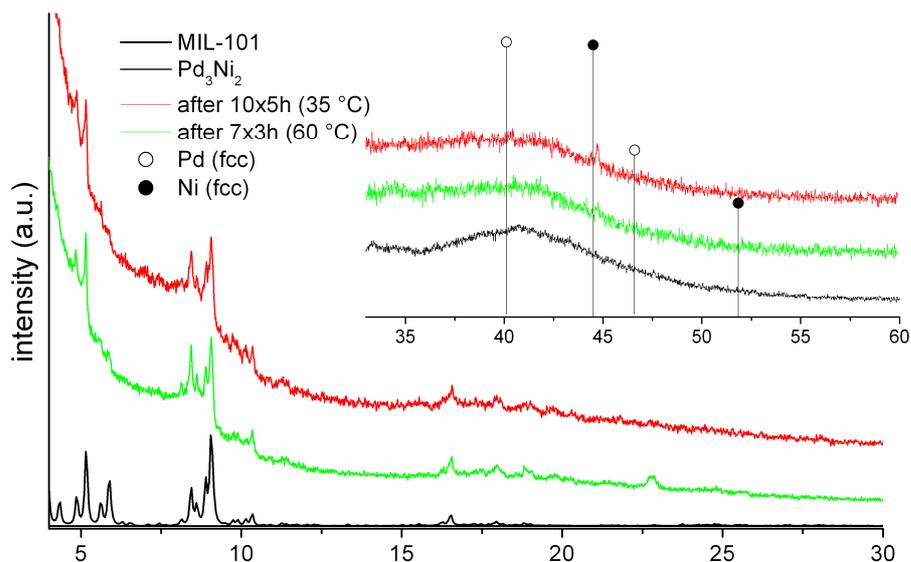
Figure S26: PXRD analysis of Pd$_3$Ni$_2$@MIL-101 before and after catalysis. The reflections of MIL-101 of the used systems do not change confirming the stability of the host MIL-101. *fcc* reflections of Ni/Pd remain broad. An additional small but sharp reflex shows the formation of some bigger Ni particles after 10 · 5 h. As no bigger particles are observed in TEM, we assume minor growth of particles.
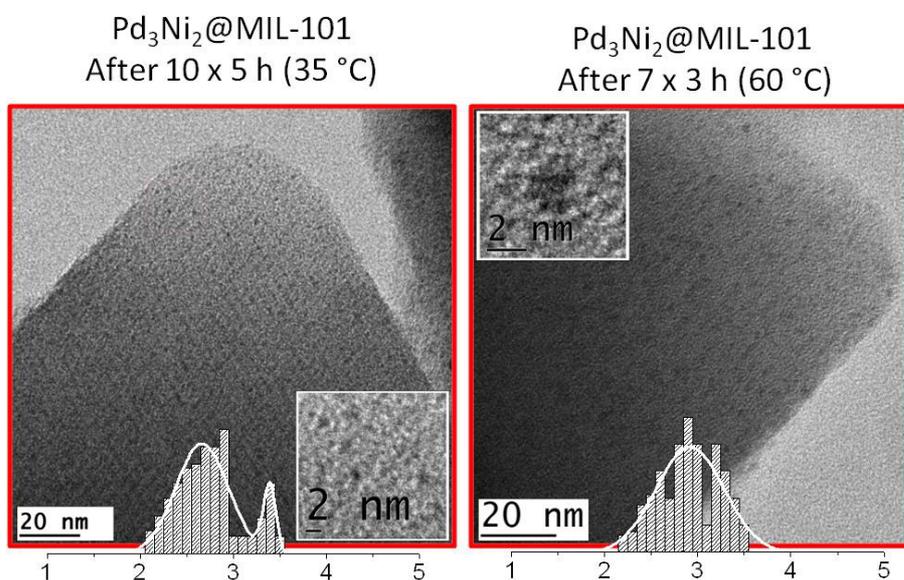
Figure S27: TEM analysis of Pd$_3$Ni$_2$@MIL-101 before and after catalysis. Neither increasing size of NPs nor agglomeration of NPs is visible, confirming the stability of the system. No bigger Ni particles are observed as already implied by PXRD analysis (small sharp reflex of Ni).

Table S4: ICP OES measurement of used Pd$_3$Ni$_2$@MIL-101 catalyst after 7 times 3 h (60 °C) and 10 times 5 h (35 °C).

	Pd/Ni	Pd/Cr	Ni/Cr
Pd$_3$Ni$_2$@MIL-101	65:35	51:49	39:61
After 7 times 3 h at 60 °C	62:38	58:42	42:58
After 10 times 5 h at 35 °C	64:36	55:45	40:60
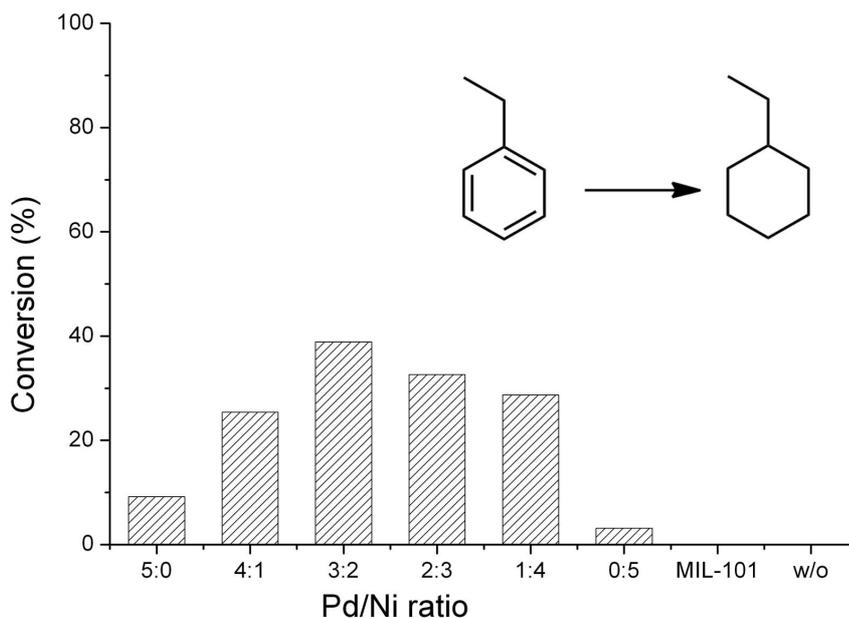
Figure S28: Reduction of ethylbenzene (0.36 mg Pd (0.83 · 10^{-3} mol-%), 500 µL ethylbenzene, 60 °C, 48 h, 20 bar H$_2$. Pd/AC = Pd on active charcoal; w/o = without catalyst).

5.5.5   Molecular Dynamics

The Molecular Dynamics (MD) simulations, as well as the Simulated Annealing (SA) were carried out using the LAMMPS Molecular Dynamics Simulator.[37] For all simulations, timesteps of 1 fs were used and the interactions among atoms in each nanoparticle (NP) were described by using the embedded-atom model (EAM) many-body potential.[38] According to the EAM, the total energy of a given atom depends on a pair-wise potential involving this atom and each neighbour, as well as on the electron density around it. The cutoff distances shown inside the potential tables containing the EAM parameters[39] were used here, i.e., 5.3 Å for Pd and 4.8 Å for Ni. The default combination rules between the parameters of each metal were used in order to describe the alloy. The NVT ensemble and Nose-Hoover thermostat were chosen and all NPs were simulated in vacuum. The following protocols were used, with each nanosecond corresponding to 10^6 MD steps:

a) MD at 360 K: A Gaussian distribution of velocities corresponding to 50 K was generated for the atoms. The NP was heated up to 360 K at 1.55×10^{-2} K.fs^{-1} for 20 ps, then was equilibrated for 2 ns, followed by the production phase of 5 ns.

b) SA from 1400 K to 10 K: A Gaussian distribution of velocities corresponding to 50 K was generated for the atoms. The NP was heated up to 1400 K at 1.35×10^{-3} K.fs^{-1} for 1 ns, then the molten NP was equilibrated for 3 ns at 1400 K and slowly cooled down to 10 K at 1.39×10^{-4} K.fs^{-1} for 10 ns. At 10 K the NP was equilibrated for further 1 ns.

In order to check whether this setup indeed allows to find the stable structures of NPs we have carried out a SA calculation for a pure Pd NP following the protocol described above and using a cooling rate of 1.39×10^{-5} K.fs^{-1}. After melting and slowly cooling, a very regular truncated octahedron is found again. This demonstrates that our setup indeed allows us to find relevant structures.

$$\text{input (Pd}_{1289}\text{)} \qquad 1400\ \text{K} \qquad 10\ \text{K}$$
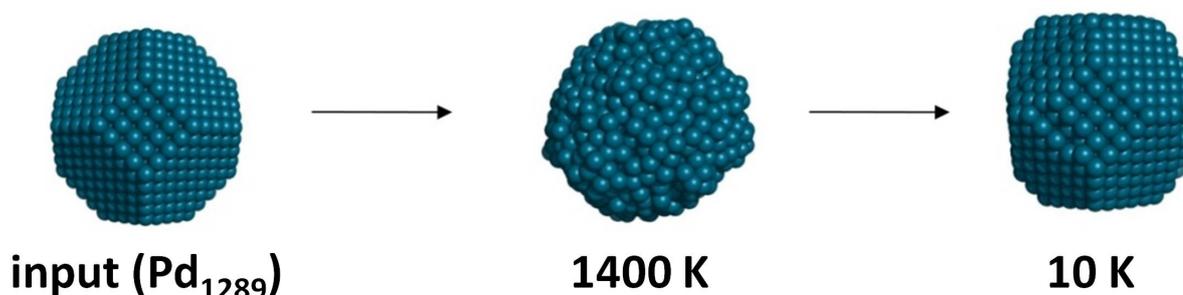
Figure S29: Tempering of Pd NP

5.6 References

[1] a) B. F. Abrahams, B. F. Hoskins, D. M. Michail, R. Robson, *Nature* **1994**, *369*, 727–729; b) B. F. Hoskins, R. Robson, *J. Am. Chem. Soc.* **1989**, *111*, 5962–5964.

[2] H. Li, M. Eddaoudi, M. O'Keeffe, O. M. Yaghi, *Nature* **1999**, *402*, 276–279.

[3] M. P. - Suh, H. J. Park, T. K. Prasad, D.-W. Lim, *Chem. Rev.* **2012**, *112*, 782–835.

[4] J.-R. Li, J. Sculley, H.-C. Zhou, *Chem. Rev*. **2012**, *112*, 869–932.

[5] L. E. Kreno, K. Leong, O. K. Farha, M. Allendorf, R. P. Van Duyne, J. T. Hupp, *Chem. Rev.* **2012**, *112*, 1105–1125.

[6] a) M. Yoon, R. Srirambalaji, K. Kim, *Chem. Rev.* **2012**, *112*, 1196–1231; b) A. Dhakshinamoorthy, H. Garcia, *Chem. Soc. Rev.* **2012**, *41*, 5262-5284.

[7] a) M. Sabo, A. Henschel, H. Froede, E. Klemm and S. Kaskel*, J. Mater. Chem*. **2007**, *17*, 3827-3832; b) N. V. Maksimchuk, M. N. Timofeeva, M. S. Melgunov, A. N. Shmakov, Y. A. Chesalov, D.

N. Dybtsev, V. P. Fedin, O. A. Kholdeeva, *J. Catal*. **2008**, *257*, 315-323; c) H. Liu, Y. Liu, Y. Li, Z. Tang, H. Jiang, *J. Phys. Chem. C.* **2010**, *114*, 13362–13369; d) Y. Pana, B. Yuana, Y. Li, D. He, *Chem. Commun.* **2010**, *46*, 2280-2282; e) A. Henschel, K. Gedrich, R. Kraehnert, S. Kaskel, *Chem. Commun*. **2008**, 4192-4194.

[8]   T. Ishida, M. Nagaoka, T. Akita, M. Haruta, *Chem. Eur. J.* **2008**, *14*, 8456-8460.

[9]   M. S. El-Shall, V. Abdelsayed, A. El Rahman S. Khder, H. M. A. Hassan, H. M. El-Kaderi, T. E. Reich, *J. Mater. Chem*. **2009**, *19*, 7625.

[10] Y. K. Hwang, D. Y. Hong, J. S. Chang, S. H. Jhung, Y. K. Seo, J. Kim, A. Vimont, M. Daturi, C. Serre and G. Férey, *Angew. Chem. Int. Ed*. **2008**, *47*, 4144-4148.

[11] a) S. Hermes, M.-K. Schröter, R. Schmid, L. Khodeir, M. Muhler, A. Tissler, R. W. Fischer, R. A. Fischer, *Angew. Chem.* **2005**, *117*, 6394–6397; b) M. Meilikhov, K. Yusenko, D. Esken, S. Turner, G. V. Tendeloo, R. A. Fischer, *Eur. J. Inorg. Chem.* **2010**, 3701–3714.

[12] S. Hermes, F. Schröder, S. Amirjalayer, R. Schmid, R. A. Fischer, *J. Mater. Chem.* **2006**, *16*, 2464-2472.

[13] M. Müller, O. Lebedev, R. A. Fischer, *J. Mater. Chem.* **2008**, *18*, 5274-5281.

[14] F. Schröder, S. Henke, X. Zhang, R. A. Fischer, *Eur. J. Inorg. Chem.* **2009**, *21*, 3131-3140.

[15] M. Meilikhov, K. Yusenko, R. A. Fischer, *Dalton Trans*. **2010**, *39*, 10990–10999.

[16] M. Meilikhov, K. Yusenko, A. Torrisi, B. Jee, C. Mellot-Draznieks, A. Pöppl, R. A. Fischer, *Angew. Chem. Int. Ed*. **2010**, *49*, 6212 –6215.

[17] M. Müller, S. Hermes, K. Kähler, M.W. E. van den Berg, M. Muhler, R. A. Fischer, *Chem. Mater*. **2008**, *20*, 4576-4587.

[18] D. Esken, H. Noei, Y. Wang, C. Wiktor, S. Turner, G. V. Tendeloo, R. A. Fischer, *J. Mater. Chem.* **2011**, *21*, 5907–5915.

[19] a) D. Esken, S. Turner, O. I. Lebedev, G. Van Tendeloo, R. A. Fischer, *Chem. Mater.* **2010**, *22*, 6393- 6401; b) M. Mueller, S. Turner, O. I. Lebedev, Y. Wang, G. van Tendeloo, R. A. Fischer, *Eur. J. Inorg. Chem.* **2011**, *12*, 1876-1887.

[20] a) S. Hermes, D. Zacher, A. Baunemann, C. Wöll, R. A. Fischer, *Chem. Mater.* **2007**, *19*, 2168-2173; b) D. Esken, X. Zhang, O. I. Lebedev, F. Schröder, R. A. Fischer, *J. Mater. Chem.* **2009**, *19*, 1314.

[21] S. Turner, O. I. Lebedev, F. Schröder, D. Esken, R. A. Fischer, G. Van Tendeloo, *Chem. Mater.* **2008**, *20*, 5622-5627.

[22] S. Proch, J. Herrmannsdörfer, R. Kempe, C. Kern, A. Jess, L. Seyfarth, J. Senker, *Chem. Eur. J.* **2008**, *14*, 8204 – 8212.

[23] J. Hermannsdörfer, R. Kempe, *Chem. Eur. J*. **2011**, *17*, 8071–8077.

[24] F. Schroeder, D. Esken, M. Cokoja, M. W. E. van den Berg, O. I. Lebedev, G. van Tendeloo, B. Walaszek, G. Buntkowsky, H. H. Limbach, B. Chaudret, R. A. Fischer, *J. Am. Chem. Soc*. **2008**, *130*, 6119-6130.

[25] a) Y. K. Park, S. B. Choi, H. J. Nam, D. Y. Jung, H. C. Ahn, K. Choi, H. Furukawa, J. Kim, *Chem. Commun.* **2010**, *46*, 3086–3088; b) P.-Z. Li , K. Aranishi, Q. Xu, *Chem. Commun.* **2012**, *48*, 3173–3175.

[26] H. K. Chae, D. Y. Siberio-Pérez, J. Kim, Y. B. Go, M. Eddaoudi, A. J. Matzger, M. O'Keeffe, O. M. Yaghi, *Nature* **2004**, *427*, 523-527.

[27] G. Férey, C. Mellot-Draznieks, C. Serre, F. Millange, J. Dutour, S. Surblé, I. Margiolaki, *Science* **2005**, *306*, 2040-2042.

[28] M. Schrinner, S. Proch, Y. Mei, R. Kempe, N. Miyajima, M. Ballauff, *Adv. Mater.* **2008**, *20*, 1928.

[29] X. Gu, Z.-H. Lu, H.-L. Jiang, T. Akita, Q. Xu, *J. Am. Chem. Soc.* **2011**, *133* , 11822–11825.

[30] H.-L. Jiang, T. Akita, T. Ishida, M. Haruta, Q. Xu, *J. Am. Chem. Soc.* **2011**, *133*, 1304–1306.

[31] M. J. Jacinto, R. Landers, L. M. Rossi, *Catal. Commun.* **2009**, *10*, 1971–1974.

[32] a) D. T. Tran, R.L. Johnston, *Proc. R. Soc. A* **2011**, *467*, 2004-2019; b) R. Ferrando, J. Jellinek, R. L. Johnston, *Chem. Rev.* **2008**, *108*, 845–910; c) H. B. Liu,U. Pal, J.A. Ascencio, *J. Phys. Chem. C*, **2008**, *112*, 19173; d) L. Leppert, S. Kümmel, *Phys. Chem. C* **2011**, *115*, 6694-6702; e) J. Kaiser, L. Leppert, H. Welz, F. Polzer, S. Wunder, N. Wanderka, M. Albrecht, T. Lunkenbein, J. Breu, S. Kümmel, Y. Lu, M. Ballauff, *Phys. Chem. Chem. Phys.* **2012**, *14*, 6487-6495.

[33] M. Hansen, K. Anderko, "Constitution of Binary Alloys", McGraw-Hill, New York, 1958.

[34] a) C. Vollmer, C. Janiak, Coord. *Chem. Rev.* **2011**, *255*, 2039-2057; b) S. F. L. Mertens, C. Vollmer, A. Held, M. H. Aguirre, M. Walter, C. Janiak, T. Wandlowski, *Angew. Chem. Int. Ed.* **2011**, *50*, 9735-9738.

[35] Y. Tatsuno, T. Yoshida, S. Otsuka, N. Al-Salem, B. L. Shaw, in *Inorganic Synthesis*, Vol. 19 (Ed: D.F. Shriver), WILEY-VCH, Weinheim, **1979**, pp. 220-223.

[36] A. Henschel, K. Gedrich, R. Kraehnert, S. Kaskel, *Chem. Commun.* **2008**, 4192-4194.

[37] S. Plimpton, *J. Comp. Phys.* **1995**, *117*, 1-19.

[38] S. J. Plimpton, A. P. Thompson, *MRS Bulletin* **2012**, *37*, 513-521.

[39] http://www.ctcms.nist.gov/potentials.

6 Colloidal Size Effect and Metal Particle Migration in M@MOF/PCP Catalysis

Justus Hermannsdörfer[a], Martin Friedrich[a], Rhett Kempe*[a]

[a] Lehrstuhl für Anorganische Chemie, Universität Bayreuth, Universitätsstraße 30, 95440 Bayreuth (Germany), Fax: (+49) 921-55-2157, Email: kempe@uni-bayreuth.de

Abstract: MIL-101 crystallites have been synthesized in different sizes and infiltrated with the Pd precursor complex [Pd(C$_5$H$_5$)(C$_3$H$_5$)]. Reduction of the Pd precursor complex gave rise to Pd nanoparticles inside the cavities of MIL-101 crystallites. Catalytic studies showed a clear dependence of the catalytic activity on the MIL-101 crystallite size. Furthermore, Pd-nanoparticle migration from MIL-101 crystallite to crystallite was observed under mild conditions.

Abstract in German: MIL-101 Kristallite wurden in verschiedenen Größen synthetisiert und mit dem Pd Präcursor Komplex [Pd(C$_5$H$_5$)(C$_3$H$_5$)] infiltriert. Die Reduktion des Pd Präcursor Komplexes führte zu Bildung von Pd Nanopartikeln in den Kavitäten der MIL-101 Kristallite. Die katalytischen Untersuchungen zeigen eine eindeutige Abhängigkeit der katalytischen Aktivität von der Kristallitgröße des MIL-101. Desweiteren konnte eine Migration von Pd Nanopartikeln von MIL-101 Kristallit zu MIL-101 Kristallit unter milden Bedingungen beobachtet werden.

6.1 Introduction

Porous coordination polymers (PCPs) or metal organic frameworks (MOFs) are interesting catalyst components.[1] The pore or cavity systems of these crystalline high specific surface area materials are well suited to generate small metal nano-particles (MNP) without blocking of the MNP surface by strongly binding ligands. Most of the catalytic applications in which M@PCP/MOF-based catalyst have been used so far are solution phase processes. Heterogeneous solution phase catalysis is relatively less understood [2] and PCP/MOF based catalysts might be good model system to improve our understanding of these processes. Here we report (firstly) on the dependence of the catalytic activity on the size of the M@PCP/MOF crystallite (colloidal size effect) and confirm (secondly) Pd-particle migration from PCP/MOF crystallite to crystallite under very mild reaction conditions. MIL-101(Cr)[3] was used as the PCP/MOF host system due to its robustness in liquid-phase catalysis.[4] The key is the synthesis of MIL-101 in different crystallite size distributions, which have the same specific (internal) surface, and its highly controlled loading with Pd NP. The different MIL-101 crystallite size distributions were synthesized by varying the H_2BDC/HF ratio (H_2BDC=terephthalic acid). Metal Organic Chemical Vapor Deposition (MOCVD) was used for Pd loading. MOCVD is a very attractive metal loading method since it allows quantitative loading over a large metal wt.-% range.[5],[6] Pd@MIL-101 catalyst having different MIL-101 crystallite size distributions were used as hydrogenation catalysts in liquid phase. A correlation of the mean (outer) MIL-101 crystallite size surface of the Pd@MIL-101 catalyst from the catalytic activity was observed if diffusion control was avoided. The Pd NP migration was confirmed by using large crystallites of Pd@MIL-101 and mixing them with very small non-Pd loaded MIL-101 crystallites. TEM analysis of the very small MIL-101 crystallites after catalysis indicates the presence of Pd NP in the small formerly not Pd loaded MIL-101 crystallites and, hence, confirms particle migration.

The synthesis of MOFs/PCPs with different crystallite sizes can be controlled by various means. Several specific strategies,[7] like reverse microemulsion methods,[8] addition of a co-solvent into the reaction mixture,[9] use of microwaves[10] or ultrasound,[11] and addition of a modulator such as a polymer or surfactant[12],[13],[14],[15] have been reported for the synthesis of so-called nano MOFs (crystallite size < 100 nm). The effects of water concentration and acidity as well as other synthesis methods (conventional heating, microwave irradiation) have been studied for porous MIL-101.[13] However, research has mainly focused on improving yield and phase purity by optimizing the reaction time, temperature and reactant concentrations. Possible effects on catalysis were mentioned but not investigated. Synthesis of nano-sized MIL-101 (20 - 100 nm) with enhanced selectivity for CO_2 over N_2, could, for example, be achieved by the addition of monocarboxylic acids like benzoic or perfluorobenzoic acid.[14] Whilst high concentrations of monocarboxylic acids in the

synthesis restricts nucleation and enable the formation of large crystals,[15] low concentrations lead to small crystals, with the monocarboxylate acting as an etching agent.[16]

6.2   Results and Discussion

The standard protocol for synthesizing MIL-101(Cr) involves extensive washing to remove excessive terephthalic acid (H_2BDC), which decreases surface area either by occupying the pores or by crystallizing in solution. After this procedure, phase pure MIL-101 crystallites with specific surface areas (Brunauer–Emmett–Teller, BET) up to 3000 m^2g^{-1} and an average crystallite size of 700 nm were obtained. By controlling the amount of HF (H_2BDC/HF ratio) we were able to selectively change this average crystallite size (Table 1 and Table S1 in the Supporting Information). System notation shall be S (support) for MIL-101 followed by a number indicating the average crystallite size in nm (e.g., S150). By increasing the molar ratio of H_2BDC/HF, we end up with an average crystallite size of 150 nm. Alternatively, it is possible to obtain particle sizes of 1 - 2.5 µm by using lower ratios. The effective water concentration (H_2BDC/H_2O) plays a minor role in controlling crystallite size. Higher dilution leads to slightly increased crystallite size and more importantly narrows the size distribution (Figure 1/SI Figure S1, S2 in the Supporting Information).

Table 1: Adjustment of [H_2BDC/H_2O] and [H_2BDC/HF] allows synthesis of different crystallite sizes of MIL-101. Solvent for all synthesis was water (8 mL). Surface area for unloaded MIL-101 is around 2700 m^2/g, which is in accordance with literature.

MIL-101 system	Crystallite size [nm]	$Cr(NO_3)_3$ [mg]	H_2BDC [mg]	HF [µL]	H_2BDC/H_2O [mmol/mol]	H_2BDC/HF [mol/mol]	s. a.[1] [$m^2\,g^{-1}$]	s. a.[2] [$m^2\,g^{-1}$]
S150	150	640	264	10	3.58	2.76	2600	1030
S180	180	480	198	10	2.68	2.07	2500	1090
S250	250	320	132	10	1.79	1.38	2550	1240
S400	400	480	198	40	2.68	0.52	2750	1200
S700	700	640	264	60	3.58	0.46	2700	1050
S1400	1400	400	165	60	2.23	0.29	2900	1080

$Cr(NO_3)_3$ = $Cr(NO_3)_3 \cdot 9H_2O$; H_2BDC = terephthalic acid; HF = hydrofluoric acid (46 wt.-%); s. a.[1] = surface area of unloaded systems; s. a.[2] = surface area of loaded systems.

Smaller and bigger crystallites alike come along with undesired by-products, which decrease the surface area to 1200 m^2g^{-1}. The by-products were determined by HRTEM and PXRD (Figure S3, S5, S6 in the Supporting Information). For larger crystallites, terephthalic acid is formed which can effectively be removed through excessive washing with an ethanol/water mixture (90/10). For smaller crystallites (lower concentrations of HF) additional reflections in the powder X-ray diffraction (PXRD) at 19.5 2ϑ and above could be identified as non-porous grimaldite α-CrOOH which is known

to be formed under these conditions.[17] α-CrOOH can be easily isolated as greyish precipitate after centrifugation, whereas the small crystallites (S150, S180, S250) remain stable in solution and can be isolated by decantation. The stability and sedimentation kinetics of different MIL-101 crystallite sizes in EtOH and H_2O were examined with a particle separation analyser (Figure S4 in the Supporting Information). α-CrOOH deposits completely after 5 min, whereas crystallites of porous MIL-101 are deposited first (S1400) after 10 min; smaller crystallites remained stable in solution even after longer centrifugation times. Through repetitive differential centrifugation different sizes were accumulated and crystallite-size distribution was narrowed (Figure S2 in the Supporting Information). As-synthesized S150 had to be centrifuged multiple times to secure good separation and a higher yield. PXRD analysis of washed MIL-101 does not show any reflections belonging to the thermodynamically stable phase of MIL-53, terephthalic acid or α-CrOOH. No changes in reflection position or intensity caused by altered amounts of HF can be detected. As expected, reflections are sharper for bigger crystallites (Figure S8, S9 in the Supporting Information).
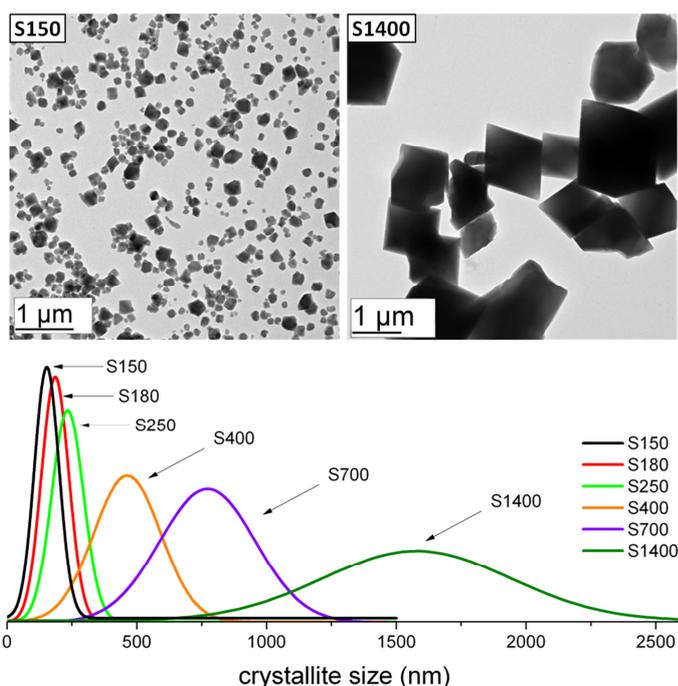
Figure 1: Top: TEM analysis of MIL-101 (S150 and S1400). Crystallites are larger for higher HF concentrations. Bottom: Crystallite size distribution of MIL-101 based on TEM analysis (Gaussian fit). S1400 shows a comparatively broad distribution.

N_2-physisorption measurements of washed MIL-101 gave surface areas in the range of 2500 - 3000 m^2g^{-1} with small variations in the sorption behaviour (Figure 2). For bigger MIL-101 crystallites a characteristic sorption for microporous systems (type I) can be seen. Surface area mainly derives from micropores in the range of 0.02 - 0.22 P/P_0. After refilling of micropores the isotherm proceeds

in a horizontal plateau. Isotherms of small crystallites like S180 do not show a horizontal plateau but rather a gentle ascent caused by adsorption between MIL-101 crystallites. These additional mesopores (size range of 4 - 15 nm) provide only a minor contribution to the overall specific surface as can be seen in pore size distribution analysis (DFT, Figure S8 in the Supporting Information).
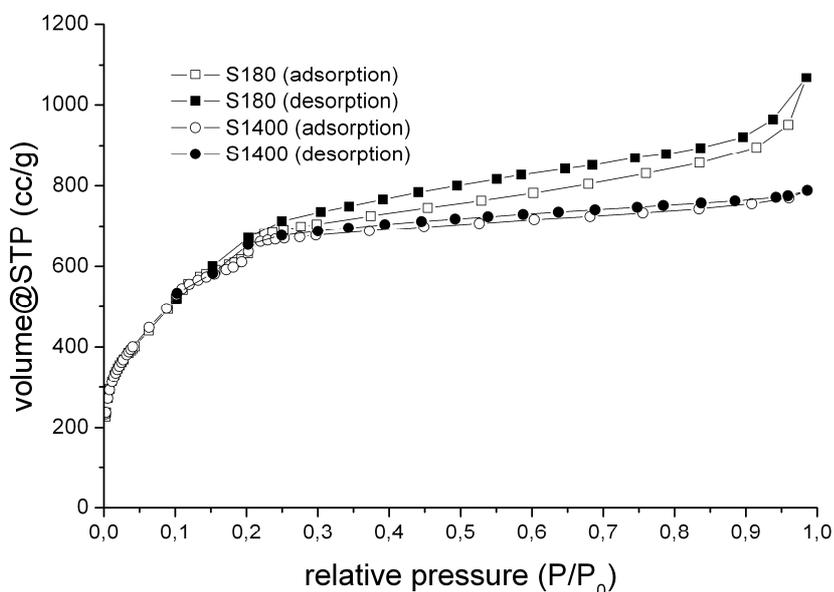
Figure 2: N_2-physisorption measurements of MIL-101. Bigger crystallites show characteristic curves for microporous systems. S180 shows additional hysteresis. The increase at higher P/P_0 values is due to adsorption of higher external surface area.

The loading of MIL-101 with $[(C_5H_5)Pd(C_3H_5)]$ via MOCVD at room temperature resulted in a blackish green solid which was immediately transferred under glove-box conditions into a steel autoclave. The reduction towards Pd@MIL-101 was performed under 50 bar H_2 and 70 °C for 20 h. Immediate evacuation at 100 °C and 10^{-4} mbar resulted in the active catalyst, which was stored under Nitrogen to avoid decomposition. System notation for Pd loaded MIL-101 shall be K (from the German word for catalyst) followed by a number indicating the average crystallite size in nm (e.g. K150). Inductively coupled plasma–optical emission spectroscopy (ICP-OES) analysis gave an average Pd loading of 15 wt.-% and a chromium content of 14 wt.-% (Table 2). N_2-physisorption measurements of Pd@MIL-101 show decreased surface areas, caused by Pd loading. Pd NPs occupy the pores and increase the weight, reducing the surface area by around 60 %. PXRD analysis (Figure S11 in the Supporting Information) of Pd@MIL-101 shows the typical reflections of MIL-101 confirming the stability of the systems under the chosen conditions (50 bar H_2, 70 °C). A slight broadening of the reflections is due to infiltration with Pd. Reflections for bigger crystallites again are sharper. The *fcc* reflections of Pd are very broad, which is due to the small Pd NP (Figure S12 in the Supporting Information). No sharp reflections are visible, which rules out the formation of bulk Pd. TEM analysis

(Figure 3 and Figure S13, S14 in the Supporting Information) indicate the presence of metal nanoparticles in the size range of 2 - 3.5 nm. Furthermore, a good dispersion throughout the MIL-101 crystallites is observed. No increase in the MNP concentration at the edges or the external surface was detected. The matching sizes of the MNPs and pores suggest the Pd NPs are specifically loaded within the pores. TEM analysis of MOFs/PCPs is characteristic for having a strong negative influence of electron beam. Strong radiation causes structural changes in the MOFs/PCPs. The loading of the cavities with MNP may stabilize and facilitate analysis. However, bigger MIL-101 crystallites can only be measured under cryo conditions, due to local damage by the electron beam and the resulting tensions within one MIL-101 crystallite. For K1400, additional problems arise, because the contrast between Pd NPs and the support is decreased due to the increased sample thickness.

Table 2: Pd loaded MIL-101 crystallites. S denotes unloaded MIL-101 crystallites; K denotes Pd loaded MIL-101 crystallites. The Cr and Pd contents are roughly at 14 and 16 wt.-% respectively. The surface area of Pd loaded MIL-101 drops to 1100 m² g^{-1}, which is 60 % of the unloaded systems.

Pd@MIL-101	MIL-101	Crystallite size [nm]	Cr [wt.-%]	Pd [wt.-%]	s. a.^{2}[m^2 g^{-1}]
K150	S150	150	13,3	16,3	1030
K180	S180	180	14,8	14,2	1090
K250	S250	250	14,8	15,0	1240
K400	S400	400	13,5	16,4	1200
K700	S700	700	13,6	16,9	1050
K1400	S1400	1400	14,4	16,0	1080

wt.-% = weight percent based on ICP-OES; s. a.^{2} = surface area of loaded systems.
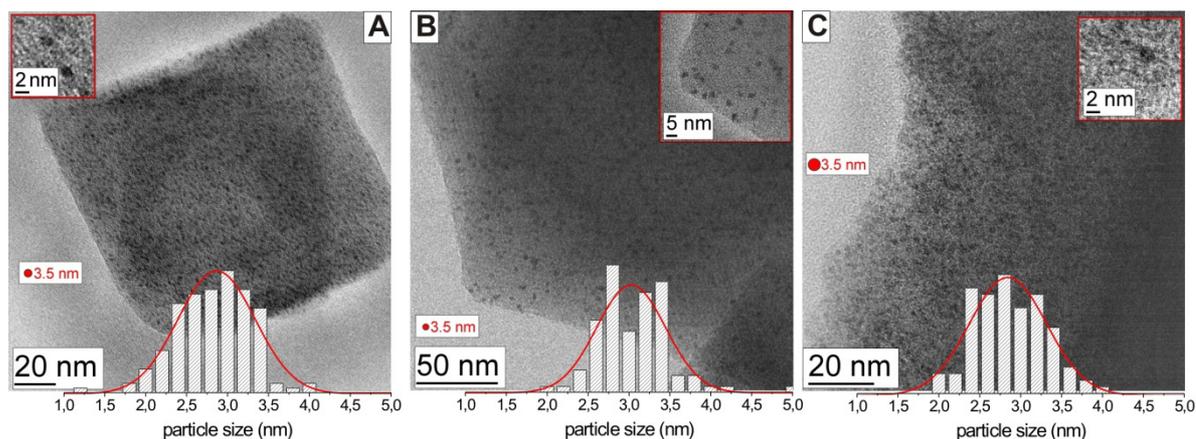
Figure 3: TEM analysis of Pd@MIL-101 with different crystallite sizes. A) = 150 nm; B) = 400 nm; C) = 1400 nm. The inset shows higher resolution of Pd NP. The particle size distribution show that the MNPs are in the same size regime as the cavities. The red/black spot has a diameter of 3.5 nm, which is the maximum particle size available for cavity-conforming MNPs. Higher resolution images are difficult to obtain for larger MIL-101 crystallites, due to local damage by the electron beam and the fact that the increased thickness of the sample minimizes the contrast between the MNPs and the support. K1400 was analyzed under cryo conditions.

Hydrogenation of ketones was used as the catalytic test reaction. The following reaction conditions were applied: 50 °C, 20 bar H_2, 24 h, and 800 rpm. A clear dependence of the catalytic activity/conversion on the MIL-101 crystallite size is observed for the reduction of benzophenone and propiophenone in n-hexane or toluene (Figure 4). Interestingly, the MIL-101 crystallite size dependence is in good accordance with a normalized surface-to-bulk ratio (number of cavities) of an octahedron-shaped MIL-101 crystallite (Figure 4, solid line). The MIL-101 crystallite-size effect is also controlled by the concentration of dissolved hydrogen. If the hydrogen pressure was reduced to 10 bar no dependence on the crystallite size is observed (Figure S17 in the Supporting Information). The H_2-solubility becomes the rate-determining step (diffusion control). The same effect can be seen for solvent-free catalysis. Even at 20 bar, without the addition of nonpolar solvents with good H_2-solubility, no crystallite size effects were observed for the reduction of propiophenone.
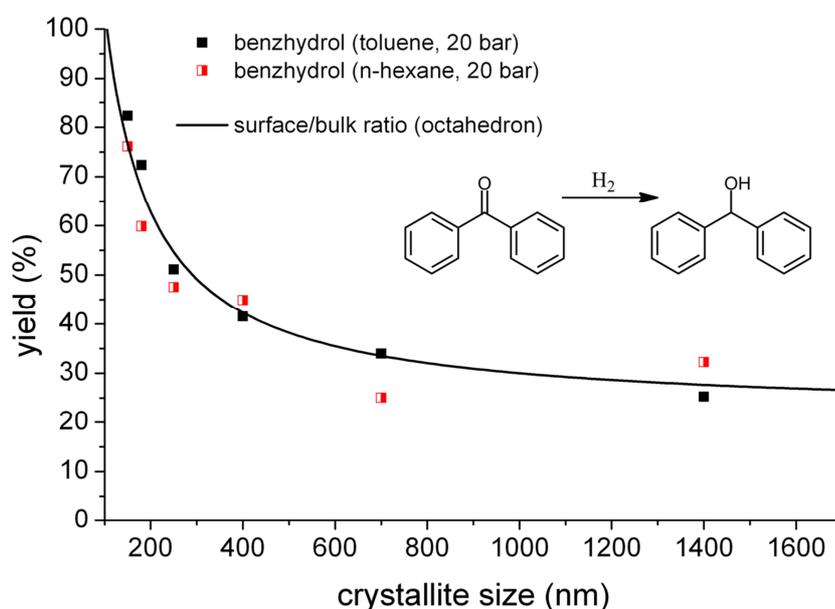
Figure 4: Reduction of benzophenone with Pd@MIL-101 (24 h, 20 bar, 800 rpm, 50 °C, 3 mg catalyst, 0.5 g benzophenone dissolved in either 0.61/0.12 mL *n*-hexane/THF or in 0.73 mL toluene; 0.15 mol-% Pd). A decrease in conversion/activity is observed for larger crystallites.

Two possible reaction pathways might be responsible for this PCP/MOF crystallite size-activity effect (Figure 5). (A) The reaction takes place at the surface of the Pd NP and the MIL-101 crystallite size effect results from slow diffusion of the ketones/alcohols through the micropores of the MIL-101 host. (B) Catalysis is based on leached metal atoms or clusters, which are more easily leached out due to higher external (outer) surface area of K150 compared to K1400. Leaching of MNP is highly relevant as it may influence the catalysts long-term stability or contaminate reaction products. The catalyst systems were recovered from the reaction mixture after catalysis by centrifugation. Treatment of the supernatant under identical catalytic conditions did not show any further

conversion of the substrate. In addition, no dissolved or dispersed Pd species were detected in the supernatant by ICP-OES. This observation indicates that reintegration or redeposition seems to be likely if route (B) dominates. To examine such effects, we added unloaded MIL-101 to the reaction mixture. To discriminate between catalyst and scavenger, small crystallites (S150) were added to Pd-loaded K1400 and large crystallites (S1400) to Pd-loaded K150. TEM analysis of the used catalyst (20 bar, 50 °C, 66 h) shows Pd NPs within the originally unloaded MIL-101, indicating particle migration and redeposition of Pd NPs. Reusability tests performed with the catalyst systems K180, K400, K700 and K1400 under identical conditions show no decrease in activity after repeat runs of 5×24 h and 3×66 h (Figures S20 and S21 in the Supporting Information). MIL-101 with its high surface area is suitable for collecting leached metal species so that no precious metal is lost during catalysis and the constant activity/reusability of the catalyst system is ensured.
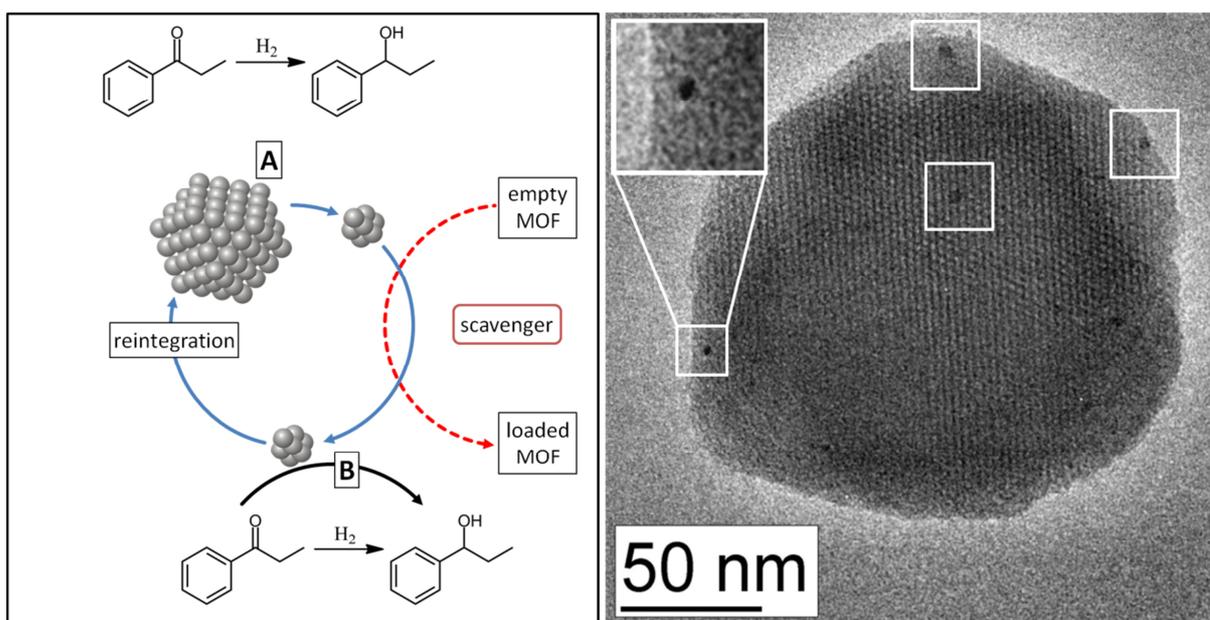
Figure 5: Experiments on leaching of MNP. Left: Possible reaction pathways for the reduction of aromatic ketones with Pd@MIL-101. (A): reaction takes places at the surface of MNP. (B): Reaction takes place on leached atoms or clusters, which may be reintegrated into the original MNP. If a 'scavenger' (MIL-101 of a different crystallite size distribution) is added, leached Pd NPs can be trapped. Right: TEM Analysis of scavenger MIL-101 (S150) after catalysis (Pd@MIL-101 (K1400); 66 h, 50 °C, 20 bar H_2, 800 rpm). NPs are clearly visible in the structure of the scavenger S150.

6.3   Conclusions

In conclusion, size-selective synthesis of MIL-101 crystallites was achieved by controlled addition of specific amounts of HF to the reaction mixture. Varying the amount of HF does not alter the structure of MIL-101. Non-porous by-products like terephthalic acid for higher concentrations of HF and α-CrOOH for lower concentrations of HF were found in significant amounts. These by-products could

be removed by differential centrifugation and/or extensive washing with EtOH. The crystallites with different sizes were loaded with Pd using MOCVD. There is a clear dependence of the liquid-phase hydrogenation activity of Pd@MIL-101 on the MIL-101 crystallite size. Yet, careful adjustment of reaction conditions (diffusion control has to be avoided) must be done in order to observe these effects. Furthermore, migration and redeposition of Pd species under catalytic conditions was recorded. Migration of MNPs out of the support and into empty MIL-101 crystallites was observed at temperatures as low as 50 °C. However, no deactivation of the catalyst system was observed, since the leached particles were recollected by the MIL-101 host.

6.4   Acknowledgements

6.5 Supporting Information

6.5.1 Experimental Section

Reactants and solvents: Terephthalic acid (H$_2$BDC), benzophenone and propiophenone were purchased from Acros Organics. Chromium (III) nitrate nonahydrate (Cr(NO$_2$)$_3$·9H$_2$O) and allylpalladium(II) chloride dimer were purchased from ABCR. All manipulations and chemical reactions were conducted under an inert atmosphere [Schlenk-technique (Ar) and/or glove box technique (H$_2$O, O$_2$ < 0.1 ppm). Non-halogenated solvents were dried with sodium/benzophenone ketyl and halogenated solvents with CaH$_2$.

Analytical and spectroscopic methods: Elemental analysis was performed by standard protocols employing digestion in HNO$_3$/HCl (3:1) and inductively coupled plasma optical emission spectrometry (ICP-OES) using a Varian Vista-Pro radial. GC analyses were performed using an Agilent 6890N gas chromatograph equipped with a flame ionization detector (FID) and a Mn HP-5 capillary column (30.0 m x 320 μm x 0.25 μm) using dodecane as external standard. All X-ray powder diffractograms were recorded using a STOE STADI-P-diffractometer (CuK$_\alpha$ radiation, 1.54178 Å) in ϑ-2ϑ-geometry with a position sensitive detector. The nitrogen physisorption isotherms were measured at 77 K using a Quantachrome Nova 2000e apparatus. 25 mg of the pre-degassed sample were transferred to a quartz cell and consequently degassed again at 100 °C, 10^{-4} mbar for 24 h. Transmission electron microscopy (TEM) was carried out by using a Varian LEO 9220 (200 kV) instrument. The sample was suspended in ethanol and sonicated for 5 min. Subsequently a drop of the suspended sample was placed on a grid and allowed to dry. The stability measurements in EtOH and water were performed in a LUMiFuge® 114 (LUM) with a rotation frequency of 1800 rpm (rounds per minute) and 50 min.

Starting materials synthesis: The Pd precursor [(η^5-C$_5$H$_5$)Pd(η^3-C$_3$H$_5$)] was synthesized under exclusion of light following a published procedure.[18] 2.5 g of allylpalladium(II) chloride dimer were dissolved in 50 mL of abs. THF and cooled to -60 °C. Dropwise addition of 6 mL NaCp (Cp = cyclopentadienyl) dissolved in 20 mL of abs. THF under constant cooling and stirring lead to a red coloring of the solution that was stirred for another 15 min at -20 °C, and for 30 min at 25 °C. The solvent was removed under vacuum and the residue was dissolved in 50 mL of abs. hexane followed by cannula filtration. The solvent was removed under vacuum. Red crystals were obtained and stored under exclusion of light and air at -30 °C.

MIL-101 was synthesized according to Table S1. H$_2$BDC and Cr(NO$_3$)$_3$ 9H$_2$O were weighed equimolar in a Teflon lined hydrothermal autoclave. A specific amount of HF and H$_2$O was added and sealed. The mixture was heated for 8 h at 210 °C. Fast cooling to 160 °C followed by slow cooling (2.7 °C/h) to 30 °C led to crystallization of unreacted terephthalic acid, which could be removed from the

resulting green mixture via filtration over pore 3 filter. The aqueous filtrate was centrifuged at 1800 rpm for 45 min and water was removed by decantation. The resulting solid was refluxed two times in EtOH/H_2O (9/1) for 12 h each and centrifuged at 1800 rpm for 45 min. Small crystallites of MIL-101 stayed in solution and could be separated from byproduct α-CrOOH via decantation. Repetitive centrifugation was applied to increase the yield. No α-CrOOH was detected for larger crystallites which deposited readily and could be separated from ethanol by decantation. The resulting green powder was evacuated at 10^{-5} mbar to remove any solvent. All materials were stored under argon.

Infiltration of $[(\eta^5\text{-}C_5H_5)Pd(\eta^3\text{-}C_3H_5)]$: Freshly evacuated MIL-101 powder and $[(\eta^5\text{-}C_5H_5)Pd(\eta^3\text{-}C_3H_5)]$ were placed in a two-chamber-tube separated by a glass frit and were kept at 25 °C in a 10^{-4} mbar dynamic vacuum for 20 h. Dynamic vacuum was used to minimize possible deposition of metal precursor on the outer surface of MIL-101. Exclusion of light was used to prevent premature reduction of metal precursors. The procedure yielded a dark green to black powder, which was immediately processed in hydrogenolysis to yield Pd@MIL-101.

Preparation of Pd@MIL-101: The adjacent reduction of Pd(II) to Pd(0) was performed with hydrogen at 50 bar, 70 °C for 20 h in a Parr Instruments steel autoclave. To remove traces of the ligands, the material was evacuated for 24 h at $5 \cdot 10^{-5}$ mbar (125 °C).

Reduction of ketones using Pd@MIL-101 as catalyst: All reduction experiments were carried out in a steel autoclave (Parr) with H_2 (5.0) atmosphere at 50 °C. The catalyst was weighed to within 0.01 mg. The conversion was determined by GC with dodecane as external standard.

Leaching test with Pd@MIL-101: All leaching experiments were carried out in a steel autoclave (Parr) with H_2 (5.0) atmosphere (20 bar) at 50 °C, 800 rpm. 2 mg of unloaded MIL-101 (S150/S1400) was added to the reaction mixture of 1.1 mg of Pd@MIL-101 (K1400/K150). After 66 h of catalysis, the catalyst mixture was separated from the reaction mixture via centrifugation at 12.000 rpm for 10 min. After the clear supernatant has been removed, the system was dried in vacuum (10^{-3} mbar) for 16 h.

Reusability test with Pd@MIL-101 (24 h/66 h): All reusability experiments were carried out in a steel autoclave (Parr) with H_2 (5.0) atmosphere (20 bar) at 50 °C, 800 rpm. 12 mg of Pd@MIL-101 (K180, K400, K700, K1400) was added to the reaction mixture of 2.0 mL of propiophenone and 2.4 mL of n-hexane. After 24 h/66 h of catalysis, the catalyst was separated from the reaction mixture via centrifugation at 12.000 rpm for 10 min. The catalyst system was dispersed in THF and centrifuged again. After the clear supernatant has been removed, the catalyst system was dried in vacuum (10^{-3} mbar) for 16 h.

Table S1: Adjustment of [H_2BDC/H_2O] and [H_2BDC/HF] allows synthesis of different crystallite sizes of MIL-101. Solvent for all synthesis was water (8 mL). Surface area for unloaded MIL-101 is around 2700 m^2/g, which is in accordance with literature.

MIL-101 system	Crystallite size [nm]	$Cr(NO_3)_3$ [mg]	H_2BDC [mg]	HF [µL]	H_2BDC/H_2O [mmol/mol]	H_2BDC/HF [mol/mol]	s. a.[1] [$m^2\,g^{-1}$]	s. a.[2] [$m^2\,g^{-1}$]	pH
S150	150	640	264	10	3.58	2.76	2600	1030	1.60
S180	180	480	198	10	2.68	2.07	2500	1090	1.99
S250	250	320	132	10	1.79	1.38	2550	1240	2.28
S400	400	480	198	40	2.68	0.52	2750	1200	2.33
S700	700	640	264	60	3.58	0.46	2700	1050	2.20
S1400	1400	400	165	60	2.23	0.29	2900	1080	2.39

$Cr(NO_3)_3$ = $Cr(NO_3)_3 \cdot 9H_2O$; H_2BDC = terephthalic acid; HF = hydrofluoric acid (46 wt.-%); s. a.[1] = surface area of unloaded systems.

6.5.2   Analytical Section
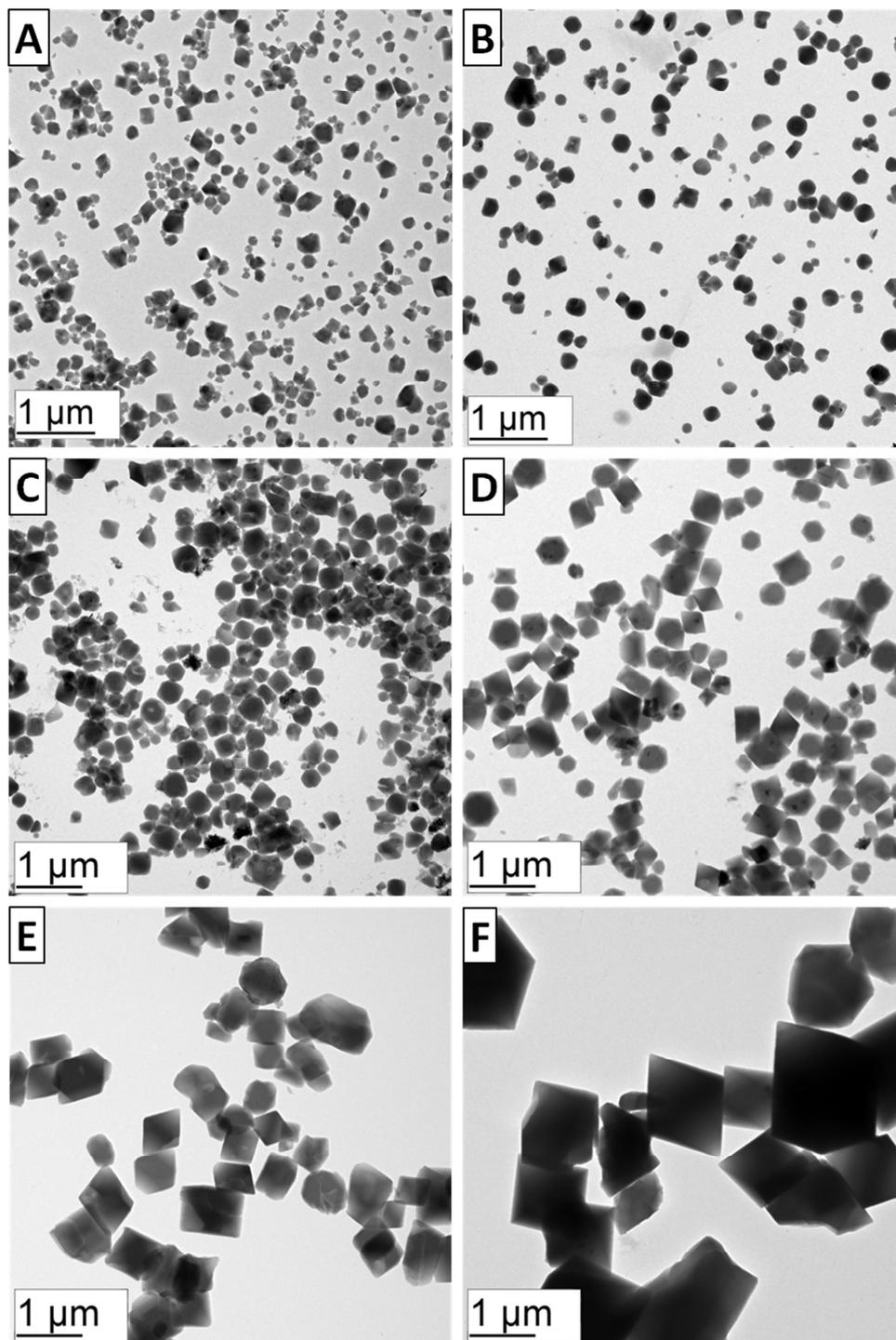
Figure S1: TEM analysis of MIL-101. A: S150, B: S180, C: S250, D: S400, E: S700, F: S1400. Crystallites are larger and have clearly defined edges for higher HF concentrations. Low HF concentrations result in roundly shaped small MIL-101 crystallites.
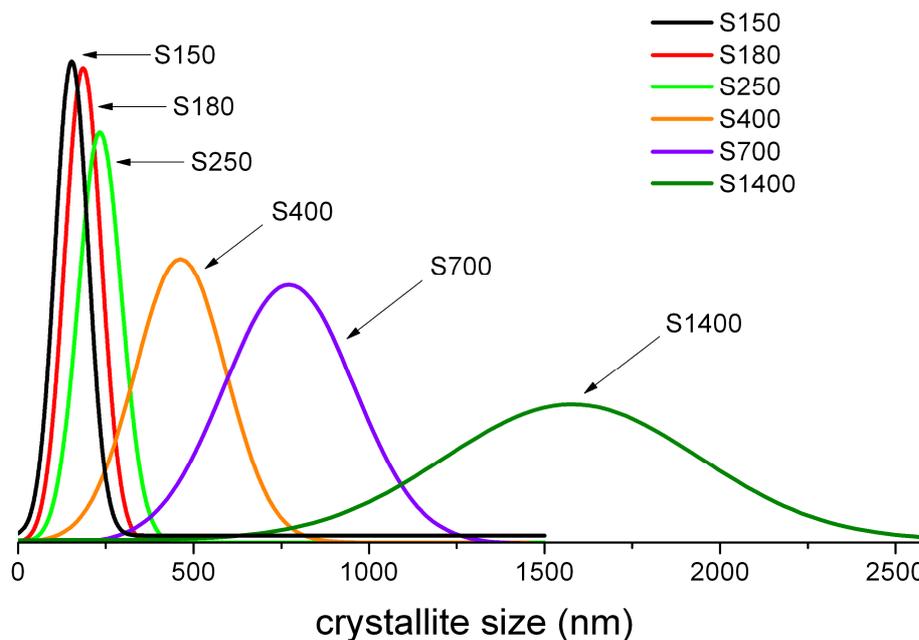
Figure S2: Crystallite size distribution of MIL-101 based on TEM analysis (Gaussian fit). A line broadening for increasing particle size is due to geometric problems caused by transfer into two-dimensional plane. As crystal shape varies, setting a uniform radius of gyration is difficult, hence leading to a broadening of crystallite size distribution. K1400 shows a comparatively broad distribution.
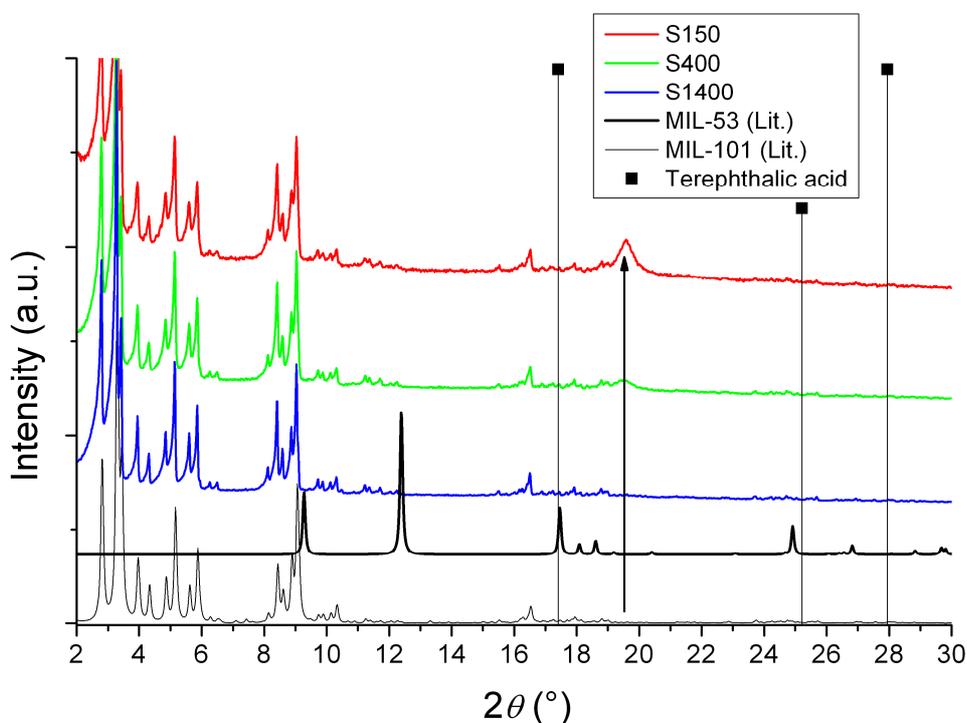
Figure S3: PXRD analysis of as-synthesized MIL-101 with different crystallite sizes (150 nm, 400 nm and 1400 nm). No formation of MIL-53 phase can be observed for different concentrations of HF. Terephthalic acid has been removed completely. An additional reflex at 19.5 2ϑ is observed for lower HF concentrations.
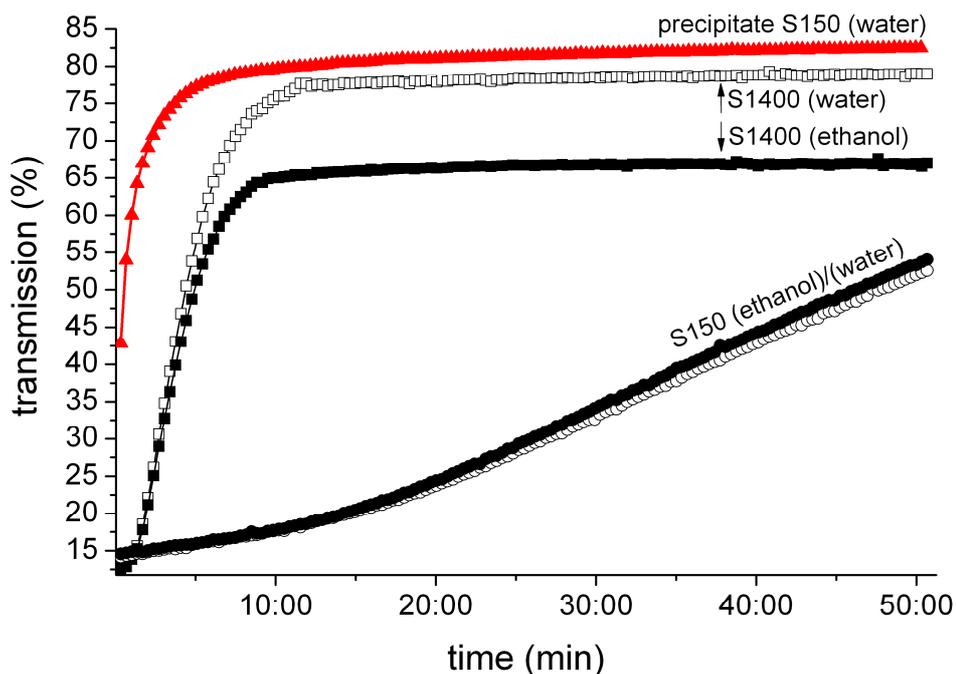
Figure S4: Stability of MIL-101 crystallites in EtOH and H_2O at 1800 rpm over 50 min. Small crystallites are quite stable in solution, whereas larger particles sediment almost quantitative after 10 min. Via repetitive differential centrifugation different sizes are accumulated. Red line shows deposition of precipitate of S150.
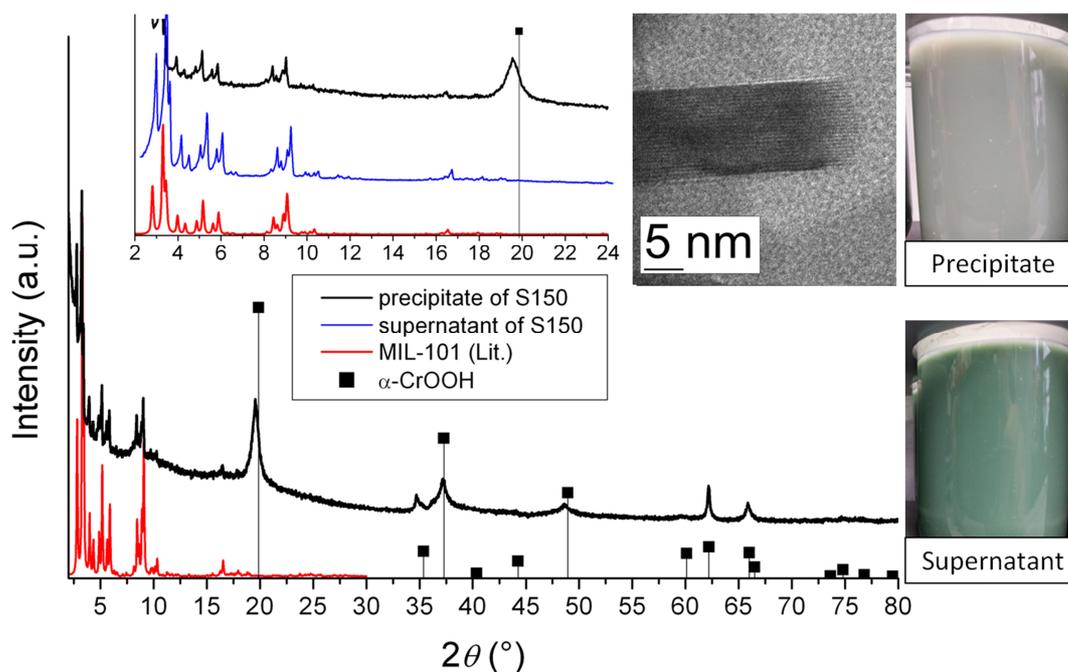
Figure S5: PXRD analysis of precipitate of S150 after repetitive differential centrifugation at 1800 rpm for 45 min. Inset shows TEM image with fringes of 0.46 nm of α-CrOOH corresponding to the additional reflection at 19.5 2ϑ. The typical green color of MIL-101 (lower right side) is found in the supernatant with phase pure MIL-101. The precipitate (α-CrOOH) (upper right side) has a grayish color after repetitive centrifugation.
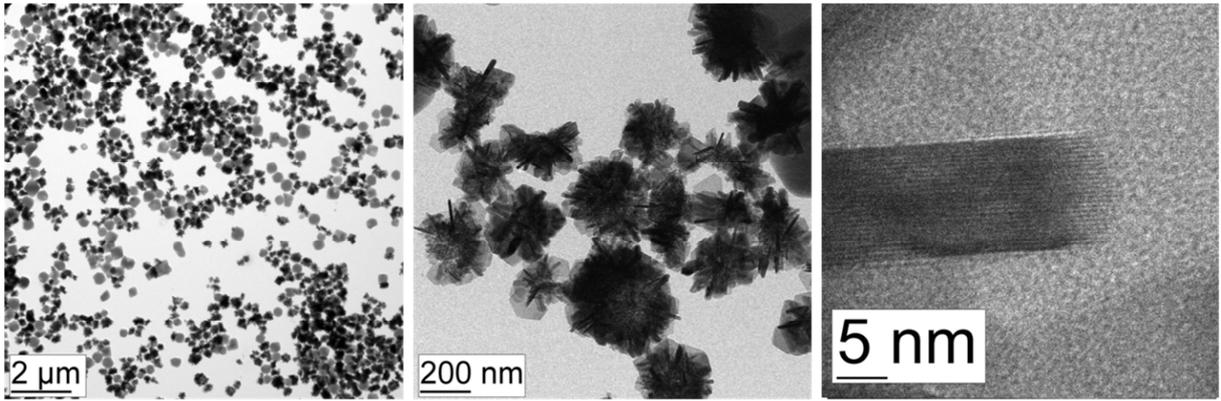
Figure S6: TEM images of precipitate of S150. The overview shows residues of MIL-101, giving an overall surface area of 300 m²/g. Higher resolution shows fringes of 0.46 nm corresponding to 19.5 2ϑ in PXRD analysis.
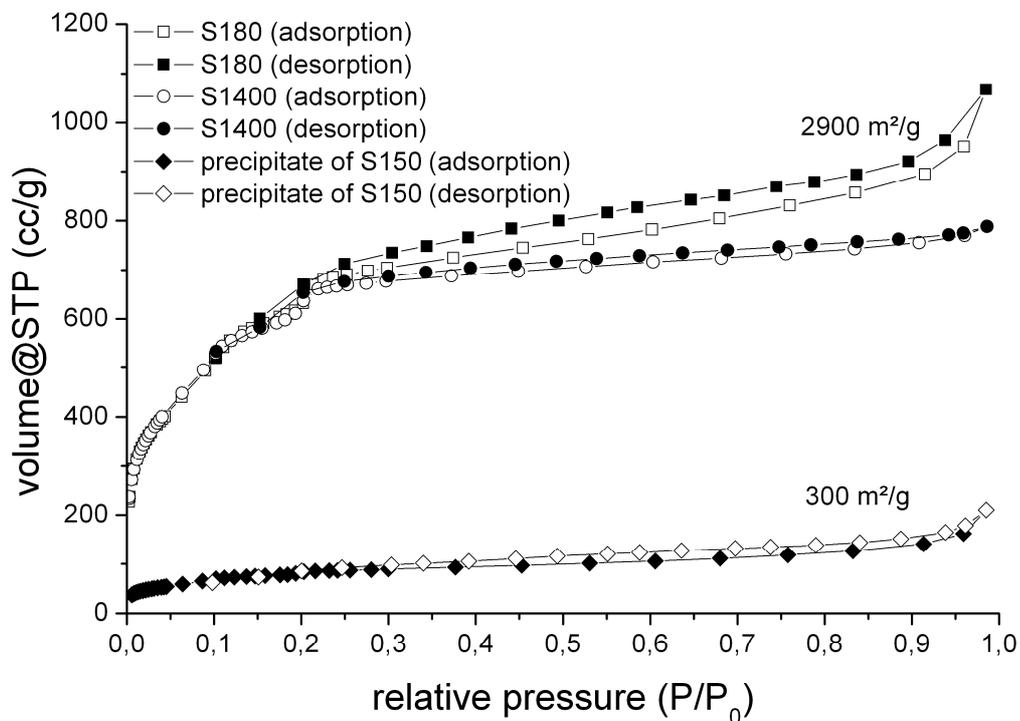
Figure S7: N$_2$-physisorption measurements of MIL-101. S180 = 180 nm, S1400 = 1400 nm average size. α-CrOOH is formed as by-product for low concentrations of HF during synthesis of MIL-101. A change in sorption behavior is observed. Larger crystallites show characteristic type for microporous systems. S180 shows additional hysteresis based on adsorption between MIL-101 crystallites. The increase at higher p/p$_0$ values is due to adsorption of higher external surface area. Surface area was calculated by BET method (0.02 - 0.22 P/P$_0$).
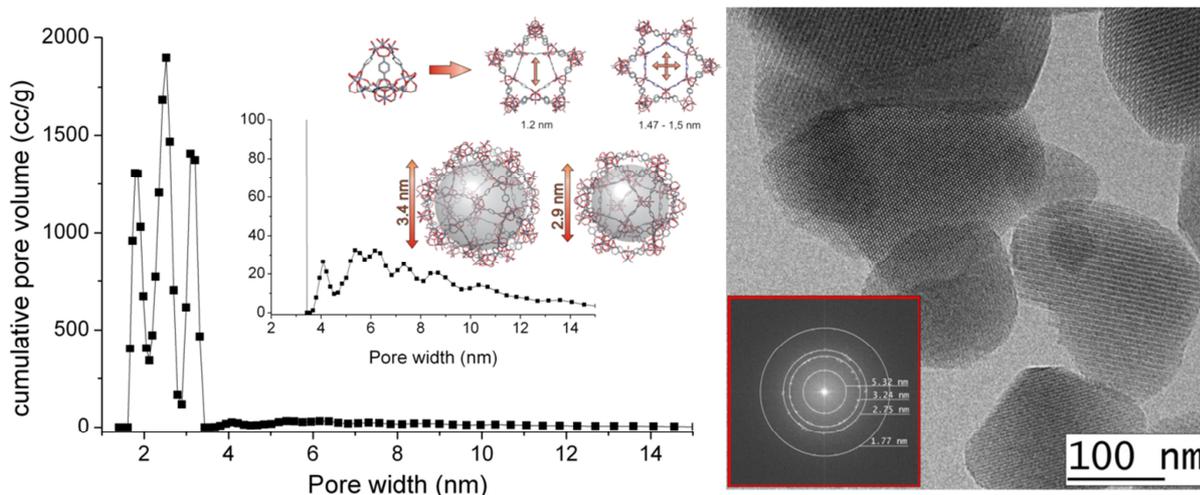
Figure S8: Left: N$_2$-physisorption measurements with MIL-101 (S180). The pore size distribution clearly shows cavity windows (1.7 nm) as well as small (2.9 nm) and big cavities (3.4 nm). Additional pores in the range of 4 - 15 nm are visible caused by macropores based on adsorption between MIL-101 crystallites. Right: TEM image of MIL-101 (S150 nm). FFT of overview TEM image shows typical sizes for cavity windows (1.8 nm), small cavities (2.8 nm), and big cavities (3.3 nm) of MIL-101. 2nd order of smaller cavities is visible too. Typical structure of MIL-101 is maintained at lower and higher HF concentrations.
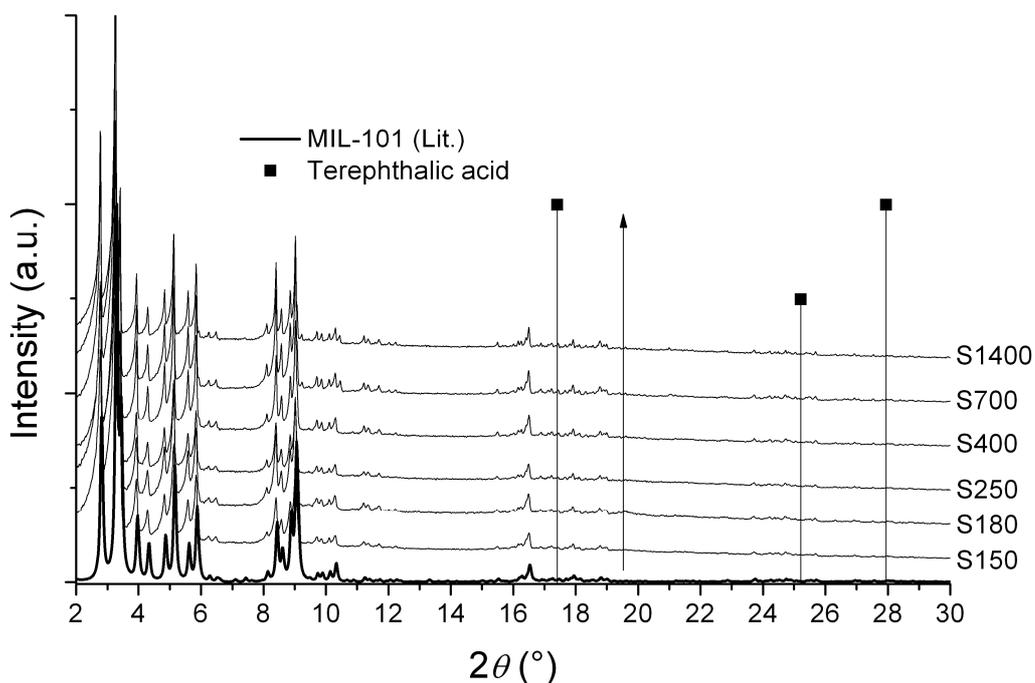
Figure S9: PXRD analysis of MIL-101 for different crystallite sizes. Terephthalic acid and α-CrOOH (arrow at 19.5 2ϑ) have been removed via repetitive centrifugation and washing. Different amounts of HF do not alter the MOF structure. Reflections for MIL-101 are sharper for bigger crystallites.
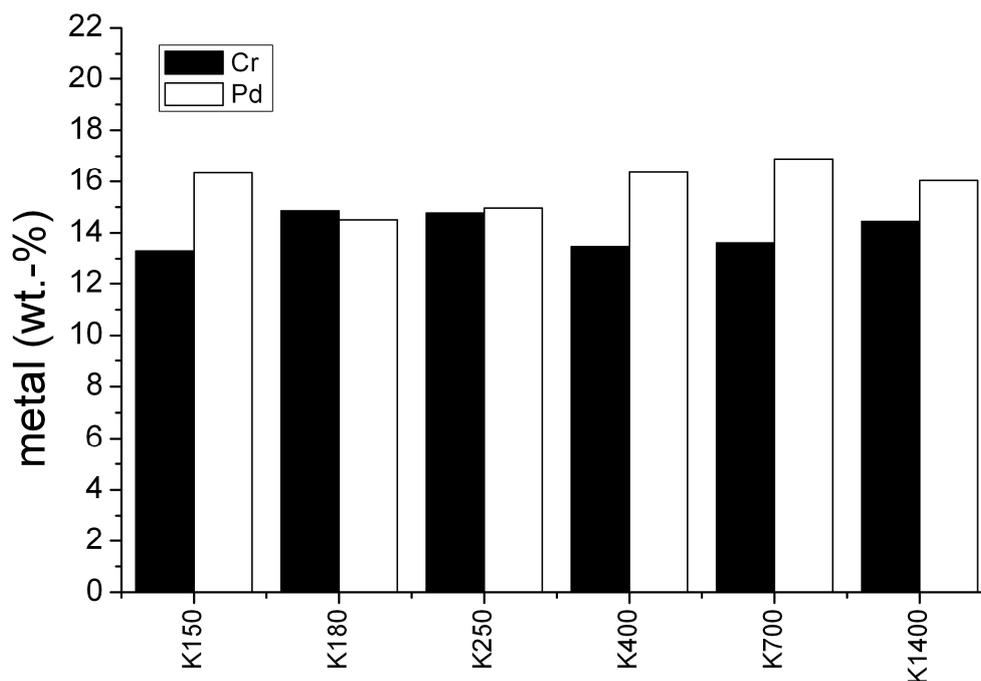
Figure S10: ICP-OES measurements for different Pd@MIL-101 systems. Loading of Pd is between 14.5 and 17 wt.-%. Cr-content varies between 13 to 14.5 wt.-%.
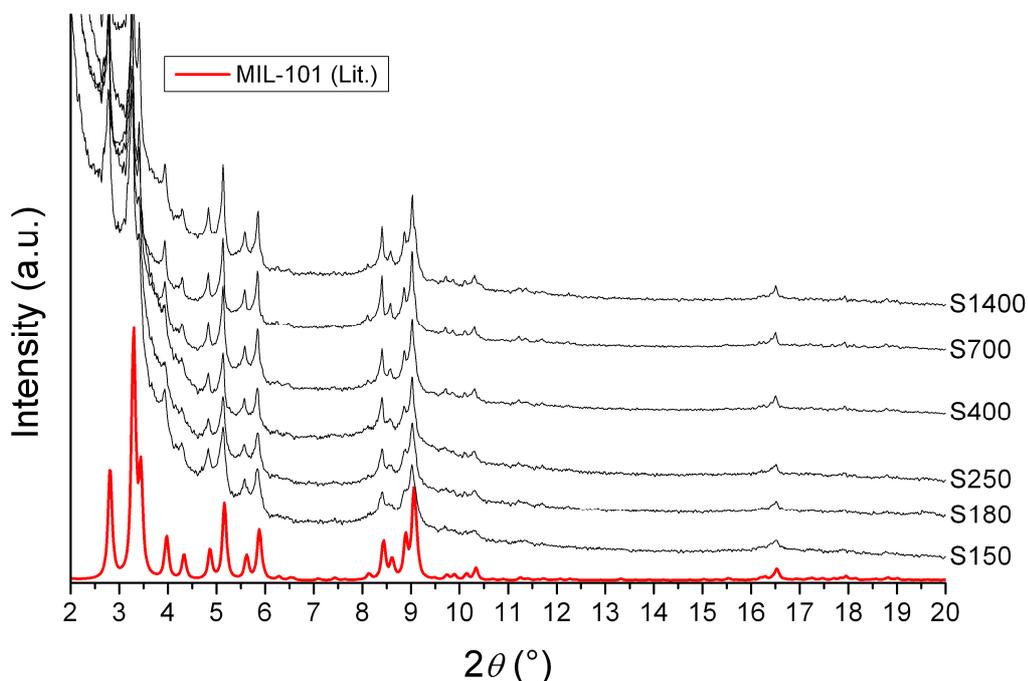
Figure S11: PXRD analysis of Pd@MIL-101 for different crystallite sizes. The reflections of MIL-101 of the metal loaded systems are stable under the chosen conditions (50 bar H_2, 70 °C). Broadening of MIL-101 reflections is due to metal infiltration. Different amounts of HF do not alter the MOF structure. Reflections for larger crystallites stay sharp even after loading with Pd.
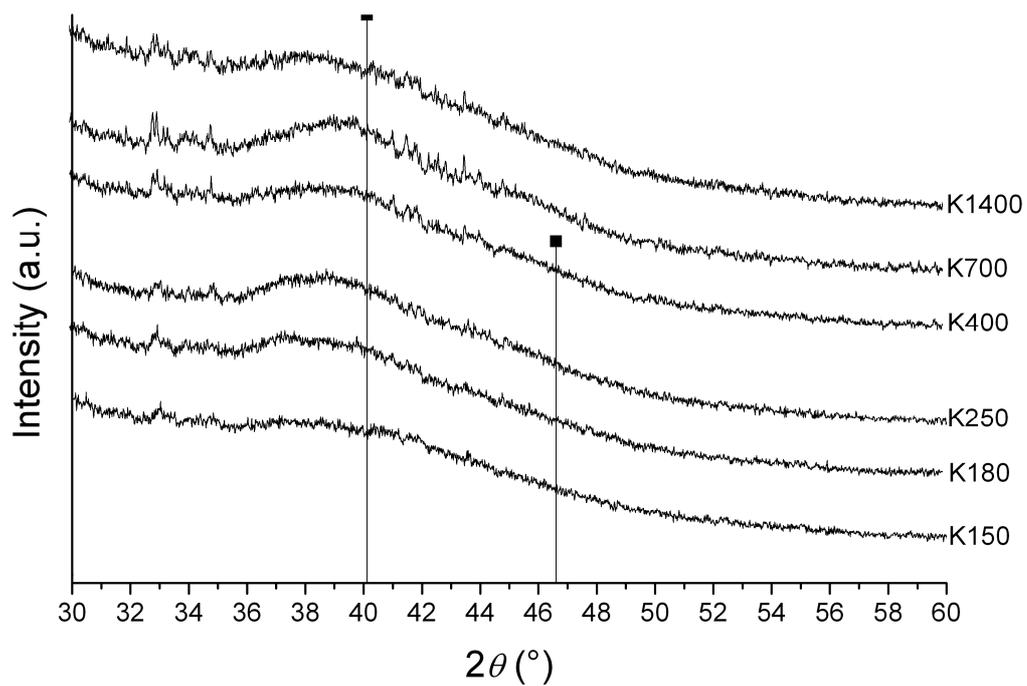
Figure S12: PXRD analysis of Pd@MIL-101 for different crystallite sizes. The downshift of Pd(111) reflection (in comparison to literature) is due to small particle size. Black squares represent bulk reflections for Pd fcc (111) and (200). Broad reflections indicate rather small particles/crystallites, which are shown in TEM analysis.
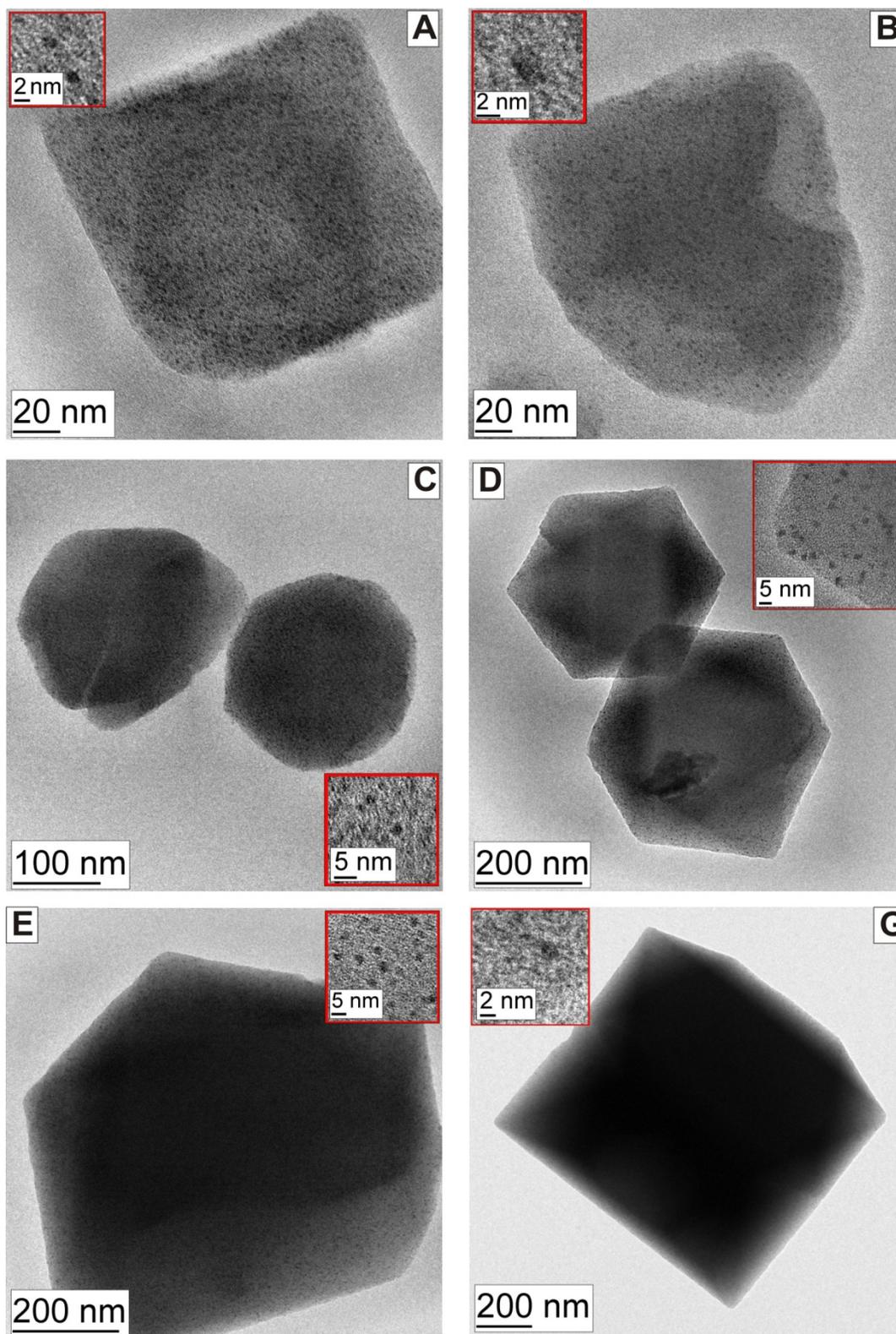
Figure S13: TEM analysis of Pd@MIL-101 for different crystallite sizes at low magnifications. The inset shows higher resolution of Pd-NP in the size regime of the cavities. A = 150 nm; B = 180 nm; C = 250 nm; D = 400 nm; E = 700 nm; F = 1400 nm. Particle size distribution shows MNP in size regime of cavities. Higher resolution for larger MIL-101 crystallites is difficult due to local damage by electron beam, which causes distortion and movement. K1400 was analysed at cryo conditions.
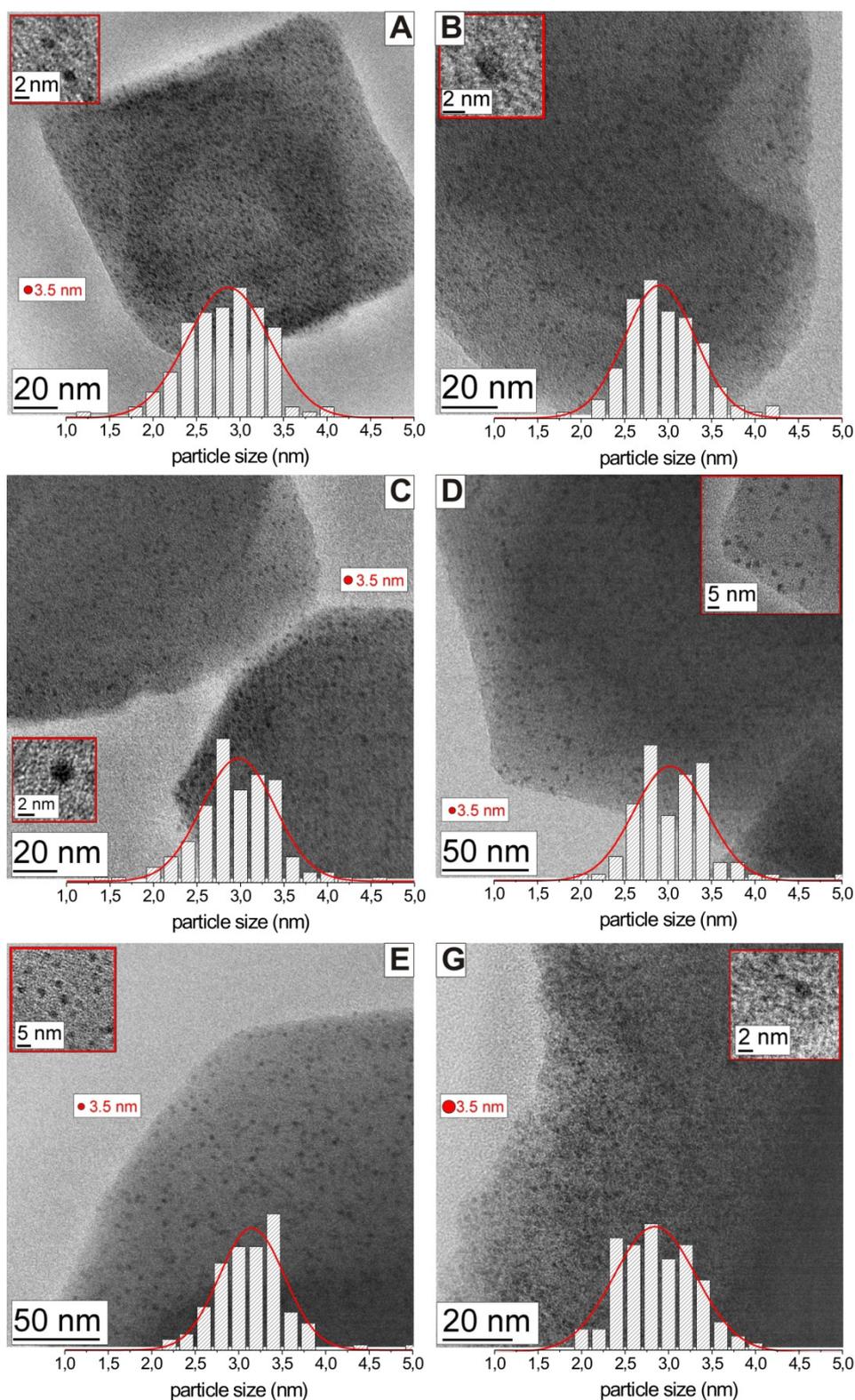
Figure S14: TEM analysis of Pd@MIL-101 at higher magnifications. The inset shows higher resolution of Pd-NP in the size regime of the cavities. A = 150 nm; B = 180 nm; C = 250 nm; D = 300 nm; E = 700 nm; F = 1400 nm. Particle size distribution shows MNP in size regime of cavities. Black/red spot indicates size of 3.5 nm, which is the maximum particle size available for cavity conform MNP. Higher resolution for larger MIL-101 crystallites is difficult due to local damage by electron beam, which causes distortion and movement. K1400 was analysed at cryo conditions.
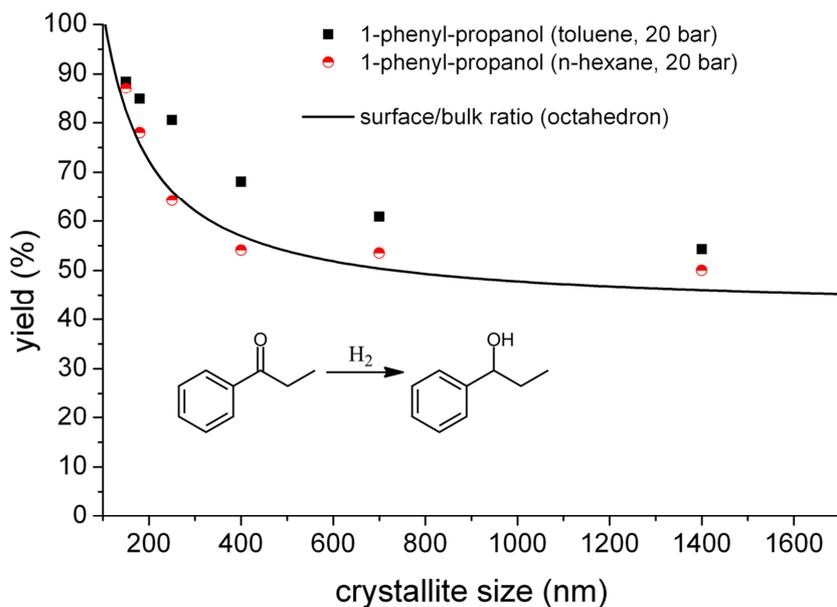
Figure S15: Reduction of propiophenone with Pd@MIL-101 (24 h, 20 bar, 800 rpm, 50 °C, 3 mg catalyst, 0.37 mL propiophenone dissolved in either 0.5 mL toluene or *n*-hexane; 0.16 mol-% Pd). A decrease in conversion is observed for larger crystallites. The effect is less obvious for solvents with lower hydrogen solubility like toluene.
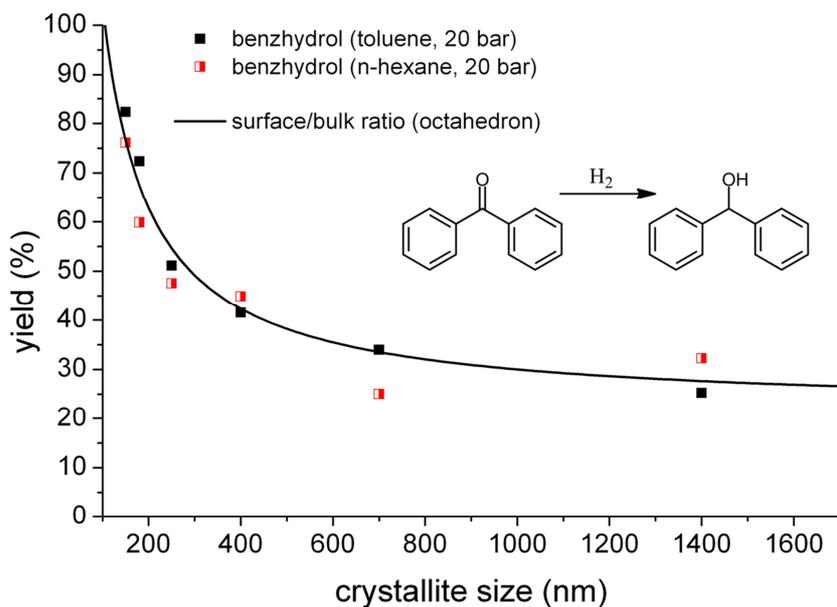
Figure S16: Reduction of benzophenone with Pd@MIL-101 (24 h, 20 bar, 800 rpm, 50 °C, 3 mg catalyst, 0.5 g benzophenone dissolved in either A: (0.61 mL *n*-hexane and 0.12 mL THF) or B: (0.73 mL toluene); 0.15 mol-% Pd). A decrease in conversion is observed for larger crystallites. Due to higher steric demands of benzophenone compared to propiophenone no influence of solvent is visible at 20 bar.
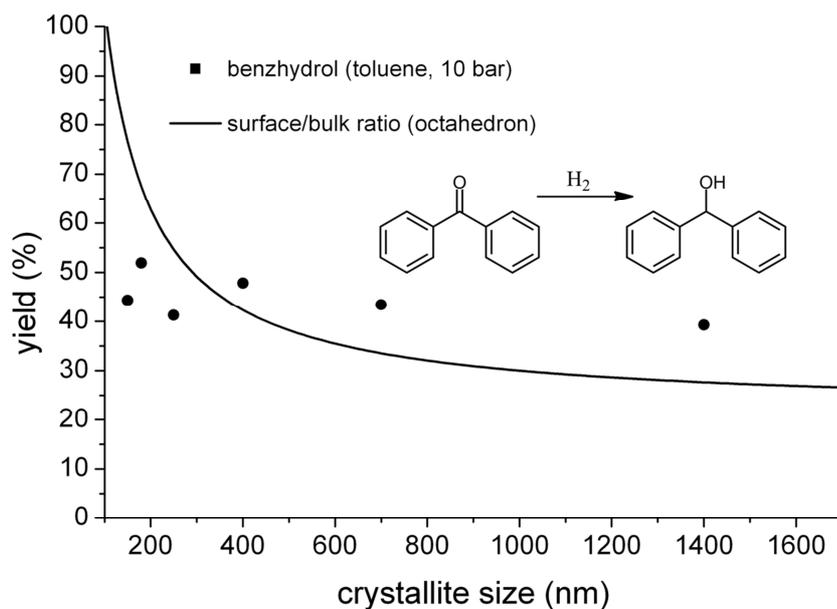
Figure S17: Reduction of benzophenone with Pd@MIL-101 (24 h, 10 bar, 800 rpm, 50 °C, 3 mg catalyst, 0.5 g benzophenone dissolved in 0.73 mL toluene; 0.15 mol-% Pd). No effect of crystallite size is detected. Lowering hydrogen pressure evens out conversion for different crystallite sizes.
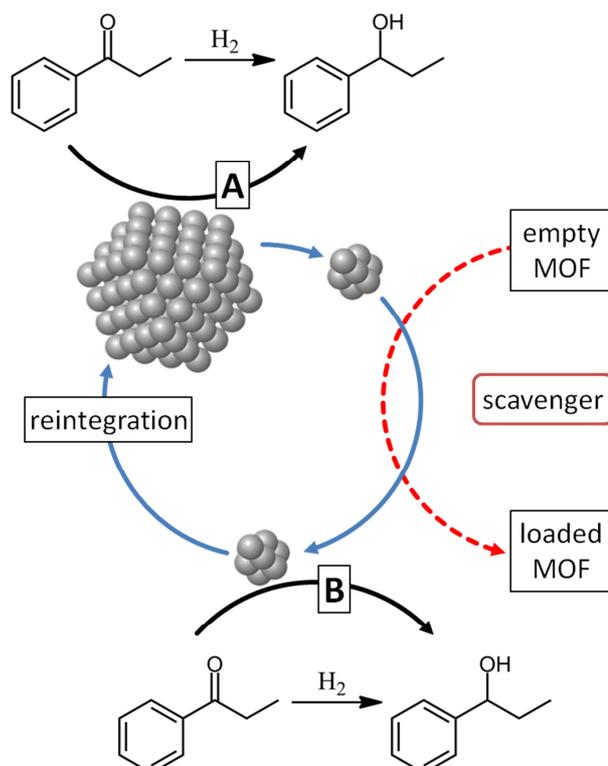
Figure S18: Possible reaction pathways for the reduction of aromatic ketones with Pd@MIL-101. A: reaction takes places at the surface of MNP. B: Reaction takes place at leached atoms or clusters, which may be reintegrated into the original MNP or may deposit as inactive Pd_{black}. Adding 'scavenger' MOFs with different crystallite size provides an easy way for observing possible leaching of atoms or clusters.
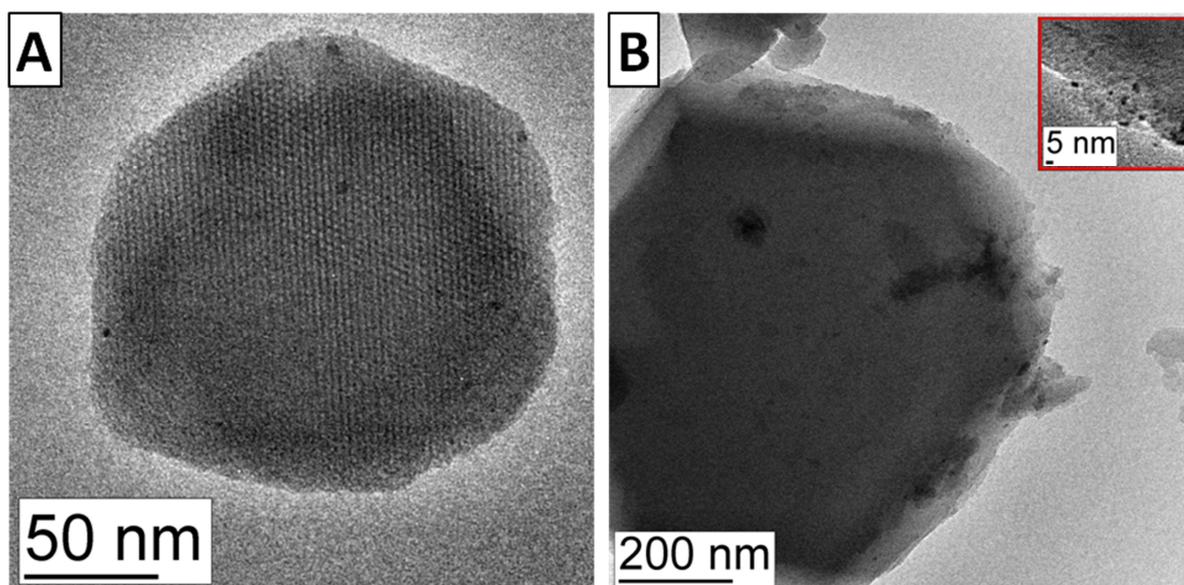
Figure S19: A: TEM Analysis of scavenger MIL-101 (S150) after catalysis (Pd@MIL-101 (K1400); 66 h, 50 °C, 20 bar H_2, 800 rpm); B: TEM Analysis of scavenger MIL-101 (S1400) after catalysis (Pd@MIL-101 (K150); 66 h, 50 °C, 20 bar H_2, 800 rpm). NPs are clearly visible in both scavengers. The almost empty MIL-101 crystallites are very unstable in the electron beam without the stabilizing effect of higher loadings of MNP within the pores. Whether MNPs are situated within the MOF structure or at the surface of the crystallite is unclear. Higher concentration of MNP at the surface of S1400 is observed, which suggests trapping of MNP in the outer sphere or at the surface of MIL-101.
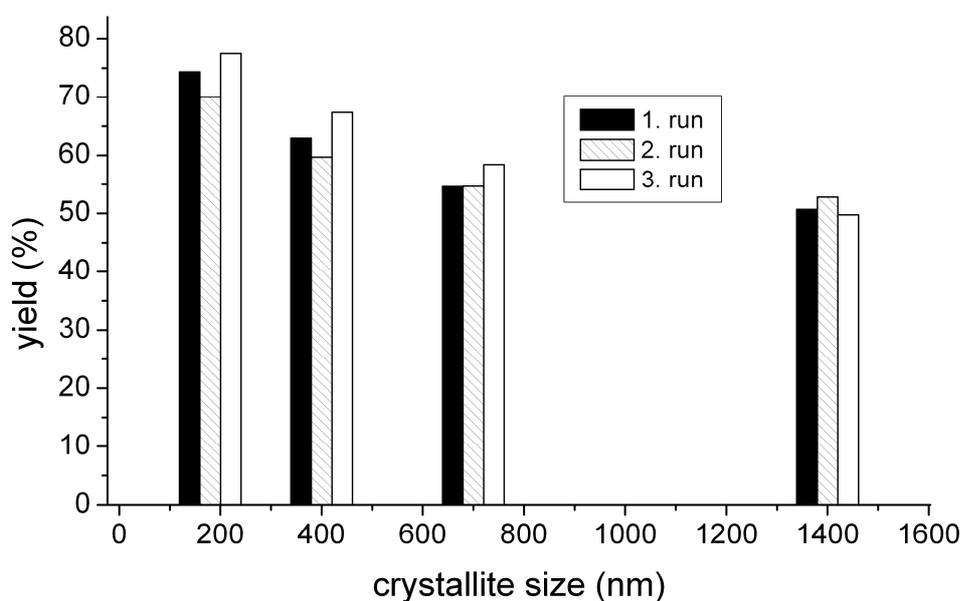
Figure S20: Reusability test with the catalyst systems K180, K400, K700, and K1400 in the reduction of Propiophenone. Reduction conditions: 66 h, 20 bar, 800 rpm, 50 °C, 5 mg catalyst, 1.85 mL propiophenone dissolved in 2.4 mL *n*-hexane; 0.05 mol-% Pd). No deactivation of the catalyst systems can be observed after 3x66 h of catalysis.
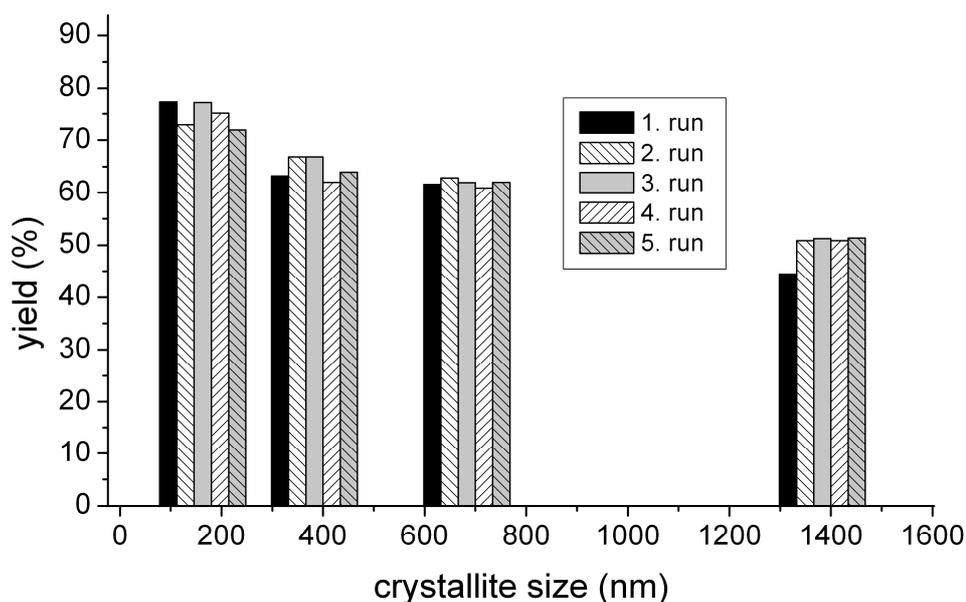
Figure S21: Reusability test with the catalyst systems K180, K400, K700, and K1400 in the reduction of Propiophenone. Reduction conditions: 24 h, 20 bar, 800 rpm, 50 °C, 12 mg catalyst, 2.0 mL propiophenone dissolved in 2.4 mL n-hexane; 0.11 mol-% Pd). No deactivation of the catalyst systems can be observed after 5x24 h of catalysis.

6.6 References

[1]   a) M. Meilikhov, K. Yusenko, D. Esken, S. Turner, G. Van Tendeloo, R. A. Fischer, *Eur. J. Inorg. Chem.* **2010**, 3701-3714; b) J. Juan-Alcañiz, J. Gascon, F. Kapteijn, *J. Mater. Chem.* **2012**, *22*, 10102-10118; c) J.-L. Wang, C. Wang, W. Lin, *ACS Catal.* **2012**, *2*, 2630–2640; d) A. Dhakshinamoorthy, H. Garcia, *Chem. Soc. Rev.* **2012**, *41*, 5262-5284; e) H. R. Moon, D.-W. Limb, M. P. Suh, *Chem. Soc. Rev.* **2013**, *42*, 1807-1824.

[2]   Nanoparticles and Catalysis, (Ed.: D. Astruc), Wiley-VCH, Weinheim, **2008**.

[3]   G. Ferey, C. Mellot-Draznieks, C. Serre, F. Millange, J. Dutour, S. Surble, I. Margiolaki, *Science* **2005**, *309*, 2040-2042.

[4]   a) Y. K. Hwang, D.-Y. Hong, J.-S. Chang, S. H. Jhung, Y.-K. Seo, J. Kim, A. Vimont, M. Daturi, C. Serre, G. Férey, *Angew. Chem. Int. Ed.* **2008**, *47*, 4144–414; b) A. Henschel, K. Gedrich, R. Kraehnert, S. Kaskel, *Chem. Commun.* **2008**, 4192-4194; c) B. Yuan, M. S. El-Shall, V. Abdelsayed, A. E. R. S. Khder, H. M. A. Hassan, H. M. El-Kaderi, T. E. Reich, *J. Mater.Chem.* **2009**, *19*, 7625–7631; d) Y. Pan, Y. Li, B. Yin, H. Jiang, *Angew. Chem. Int. Ed.* **2010**, *49*, 4054–4058; e) Y. Pan, B. Yuan, Y. Li, D. He, *Chem. Commun.* **2010**, *46*, 2280–2282; f) H. Liu, Y. Liu, Y. Li, Z. Tang, H. Jiang, *J.*

Phys. Chem. C **2010**, *114*, 13362–13369; g) Y. Huang, Z. Lin, R. Cao, *Chem.–Eur. J.* **2011**, *17*, 12706-12712; h) H. Liu, Y. Li, R. Luque, H. Jiang, *Adv. Synth. Catal.* **2011**, *353*, 3107-3113; i) H. Li, Z. Zhu, F. Zhang, S. Xie, H. Li, P. Li, X. Zhou, *ACS Catal.* **2011**, *1*, 1604-1612; j) X. Gu, Z.-H. Lu, H.-L. Jiang, T. Akita, Q. Xu, *J. Am. Chem. Soc.* **2011**, *133*, 11822–11825; k) A. Aijaz, A. Karkamkar, Y. J. Choi, N. Tsumori, E. Rönnebro, T. Autrey, H. Shioyama, Q. Xu, *J. Am. Chem. Soc.* **2012**, *134*, 13926–13929; l) F. G. Cirujano, F. X. Llabrés i Xamena, A. Corma, *Dalton Trans.* **2012**, *41*, 4249-4254; m) L. Bromberg, Y. Diao, H. Wu, S. A. Speakman, T. A. Hatton, *Chem. Mater.* **2012**, *24*, 1664–1675; n) E. V. Ramos-Fernandez, C. Pieters, B. v. d. Linden, J. Juan-Alcañiz, P. Serra-Crespo, M.W.G.M. Verhoeven, H. Niemantsverdriet, J. Gascon, F. Kapteijn, *J. Catal.* **2012**, *289*, 42-52; o) Y. Huang, S. Liu, Z. Lin, W. Li, X. Li, R. Cao, *J. Catal.* **2012**, *292*, 111-117; p) A. Aijaz, A. Karkamkar, Y. J. Choi, N. Tsumori, E. Rönnebro, T. Autrey, H. Shioyama, Q. Xu, *J. Am. Chem. Soc.* **2012**, *134*, 13926–13929; q) Z. Sun, G. Li, L. Liu, H. Liu, *Catal. Commun.* **2012**, *27*, 200-205; r) G. Chen, S. Wu, H. Liu, H. Jiang, Y. Li, *Green Chem.* **2013**, *15*, 230-235; s) M. Yadav, A. Aijaz, Q. Xu, *Funct. Mater. Lett.* **2012**, *05*, 1250039; t) J. Long, H. Liu, S. Wu, S. Liao, Y. Li, *ACS Catal.* **2013**, *3*, 647–654; u) M. Yadav, Q. Xu, *Chem. Commun.* **2013**, *49*, 3327-3329; v) A. Mariana Balu, C. S. K. Lin, H. Liu, Y. Li, C. Vargas, R. Luque, *Appl. Catal., A* **2013**, *455*, 261-266; w) C. M. Granadeiro, P. Silva, V. K. Saini, F. A. A. Paz, J. Pires, L. Cunha-Silva, S. S. Balula, *Catal. Today* **2013**, *doi.org/10.1016/j.cattod.2013.03.042*; x) F. Wu, L.-G. Qiu, F. Ke, X. Jiang, Inorg. *Chem. Commun.* **2013**, **32**, 5-8; y) Y. Huang, T. Ma, P. Huang, D. Wu, Z. Lin, R. Cao, *ChemCatChem.* **2013**, *5*, 1877–1883.

[5] a) S. Hermes, M.-K. Schröter, R. Schmid, L. Khodeir, M. Muhler, A. Tissler, R. W. Fischer, R. A. Fischer, *Angew. Chem. Int. Ed.* **2005**, *44*, 6237–6241; b) S. Hermes, F. Schröder, S. Amirjalayer, R. Schmid, R. A. Fischer, *J. Mater. Chem.* **2006**, *16*, 2464–2472; c) S. Hermes, D. Zacher, A. Baunemann, C. Wöll, R. A. Fischer, *Chem. Mater.* **2007**, *19*, 2168–2173; d) M. Müller, O. Lebedev, R. A. Fischer, *J. Mater. Chem.* **2008**, *18*, 5274–5281; e) M. Müller, S. Hermes, K. Kähler, M. W. E. van den Berg, M. Muhler, R. A. Fischer, *Chem. Mater.* **2008**, *20*, 4576–4587; f) S. Turner, O. I. Lebedev, F. Schröder, D. Esken, R. A. Fischer, G. Van Tendeloo, *Chem. Mater.* **2008**, *20*, 5622–5627; g) F. Schroeder, D. Esken, M. Cokoja, M. W. E. van den Berg, O. I. Lebedev, G. van Tendeloo, B. Walaszek, G. Buntkowsky, H. H. Limbach, B. Chaudret, R. A. Fischer, *J. Am. Chem. Soc.* **2008**, *130*, 6119–6130; h) D. Esken, X. Zhang, O. I. Lebedev, F. Schröder, R. A. Fischer, *J. Mater. Chem.* **2009**, *19*, 1314–1319; i) F. Schröder, S. Henke, X. Zhang, R. A. Fischer, *Eur. J. Inorg. Chem.* **2009**, 3131–3140; j) M. Meilikhov, K. Yusenko, D. Esken, S. Turner, G. V. Tendeloo, R. A. Fischer, *Eur. J. Inorg. Chem.* **2010**, 3701–3714; k) M. Meilikhov, K. Yusenko, R. A. Fischer, *Dalton Trans.* **2010**, *39*, 10990–10999; l) M. Meilikhov, K. Yusenko, A. Torrisi, B. Jee, C. Mellot-Draznieks, A. Pöppl, R. A. Fischer, *Angew. Chem. Int. Ed.* **2010**, *49*, 6212–6215; m) D. Esken, S.

Turner, O. I. Lebedev, G. Van Tendeloo, R. A. Fischer, *Chem. Mater.* **2010**, *22*, 6393–6401; n) M. Mueller, S. Turner, O. I. Lebedev, Y. Wang, G. van Tendeloo, R. A. Fischer, Eur. *J. Inorg. Chem.* **2011**, 1876–1887; o) D. Esken, H. Noei, Y. Wang, C. Wiktor, S. Turner, G. V. Tendeloo, R. A. Fischer, *J. Mater. Chem.* **2011**, *21*, 5907–5915; p) S. B. Kalidindi , K. Yusenko, R. A. Fischer, *Chem. Commun.* **2011**, *47*, 8506-8508; q) D. Esken, S. Turner, C. Wiktor, S. B. Kalidindi, G. V. Tendeloo, R. A. Fischer, *J. Am. Chem. Soc.* **2011**, *133*, 16370–16373; r) S. B. Kalidindi, H. Oh, M. Hirscher, D. Esken, C. Wiktor, S. Turner, G. V. Tendeloo, R. A. Fischer, *Chem. Eur. J.* **2012**, *18*, 10848–10856.

[6] a) S. Proch, J. Herrmannsdörfer, R. Kempe, C. Kern, A.Jess, L. Seyfarth, J. Senker, *Chem. Eur. J.* **2008**, *14*, 8204–821; b) J. Hermannsdörfer, R. Kempe, *Chem. Eur. J.* **2011**, *17*, 8071–8077; c) J. Hermannsdörfer, M. Friedrich, N. Miyajima, R. Q. Albuquerque, S. Kümmel, R. Kempe, *Angew. Chem. Int. Ed.* **2012**, *51*, 11473–11477.

[7] A. Carné, C. Carbonell, I. Imaz and D. Maspoch, *Chem. Soc. Rev.* **2011**, *40*, 291-305.

[8] W. J. Rieter, K. M. L. Taylor, H. An, W. Lin, W. Lin, *J. Am. Chem. Soc.* **2006**, *128*, 9024-9025.

[9] W. J. Rieter, K. M. Pott, K. M. L. Taylor, W. Lin, *J. Am. Chem. Soc.* **2008**, *130*, 11584-11585.

[10] a) T. Chalati, P. Horcajada, R. Gref, P. Couvreur, C. Serre, *J. Mater. Chem.* **2011**, *21*, 2220-2227; b) D. Liu, R. C. Huxford, W. Lin, *Angew. Chem. Int. Ed.* **2011**, *50*, 3696-3700.

[11] a) L. G. Qiu, Z. Q. Li, Y. Wu, W. Wang, T. Xu, X. Jiang, *Chem. Commun.* **2008**, 3642-3644; b) D. Tanaka, A. Henke, K. Albrecht, M. Moeller, K. Nakagawa, S. Kitagawa, J. Groll, *Nat. Chem.* **2010**, *2*, 410-416.

[12] a) K. M. L. Taylor, A. Jin, W. Lin, *Angew. Chem. Int. Ed.* **2008**, *47*, 7722-7725; b) D. Jiang, T. Mallat, F. Krumeich, A. Baiker, *Catal. Commun.* **2011**, *12*, 602-605; c) Y.-D. Chiang, M. Hu, Y. Kamachi, S. Ishihara, K. Takai, Y. Tsujimoto, K. Ariga, K. C.-W. Wu, Y. Yamauchi, *Eur. J. Inorg. Chem.* **2013**, 3141–3145.

[13] a) N. A. Khan, J. W. Jun, S. H. Jhung, *Eur. J. Inorg. Chem.* **2010**, 1043–1048; b) N. A. Khan, I. J. Kang, H. Y. Seok, S. H. Jhung, *Chem. Eng. J.* **2011**, *166*, 1152-1157.

[14] D. Jiang, A. D. Burrows, K. J. Edler, *Cryst. Eng. Comm.* **2011**, *13*, 6916-6919.

[15] S. Diring, S. Furukawa, Y. Takashima, T. Tsuruoka and S. Kitagawa, *Chem. Mater.* **2010**, *22*, 4531-4538.

[16] S. Hermes, T. Witte, T. Hikov, D. Zacher, S. Bahnmüller, G. Langstein, K. Huber, R. A. Fischer, *J. Am. Chem. Soc.* **2007**, *129*, 5324-5325.

[17] a) S. Kittaka, T. Morooka, K. Kitayama, *J. Solid State Chem.* **1985**, *58*, 187-193; b) M. E. Jones, K. E. S. Combs, S. E. Ziemniak, *J. Solution Chem.* **1998**, *27*, 33-66.

[18] Y. Tatsuno, T. Yoshida, S. Otsuka, N. Al-Salem, B. L. Shaw, in Inorganic Synthesis, Vol. 19 (Ed: D.F. Shriver), WILEY-VCH, Weinheim, **1979**, pp. 220-223.

7 List of Publications

1. Sebastian Proch, <u>Justus Herrmannsdörfer</u>, Rhett Kempe, Christoph Kern, Andreas Jess, Lena Seyfarth, Jürgen Senker, *Chem. Eur. J.* **2008**, *14*, 8204–8212.
   Pt@MOF-177: synthesis, room-temperature hydrogen storage and oxidation catalysis.

The following publications have been published during the work on this thesis:

2. <u>Justus Hermannsdörfer</u>, Rhett Kempe, *Chem. Eur. J.* **2011**, *17*, 8071–8077.

   <u>Justus Hermannsdörfer</u>, Prof. Dr. Rhett Kempe, *Chem. Eur. J.* **2011**, *17*, 7965.
   Selective Palladium-Loaded MIL-101 Catalysts.

3. <u>Justus Hermannsdörfer</u>, Martin Friedrich, Nobuyoshi Miyajima, Rodrigo Q. Albuquerque, Stephan Kümmel, Rhett Kempe, *Angew. Chem.* **2012**, *124*, 11640–11644.
   Ni/Pd@MIL-101: Synergetische Katalyse mit kavitätenkonformen Ni/Pd-Nanopartikel.

   <u>Justus Hermannsdörfer</u>, Martin Friedrich, Nobuyoshi Miyajima, Rodrigo Q. Albuquerque, Stephan Kümmel, Rhett Kempe, *Angew. Chem. Int. Ed.* **2012**, *51*, 11473–11477.
   Ni/Pd@MIL-101: Synergistic Catalysis with Cavity-Conform Ni/Pd Nanoparticles.

4. <u>Justus Hermannsdörfer</u>, Martin Friedrich, Rhett Kempe, *Chem. Eur. J.* **2013**, *19*, 13652–13657.
   Colloidal Size Effect and Metal Particle Migration in M@MOF/PCP Catalysis.

5. V. Perumal. Devarajan, Devaraj. Nataraj, Thangavelu Pazhanivel, Karuppanan Senthil, Minsu Seol, Kijung Yong, <u>Justus Hermannsdorfer</u>, Rhett Kempe, *J. Mater. Chem.* **2012**, *22*, 18454-18462.
   Molecular conformation dependent emission behaviour (blue, red and white light emissions) of all-trans-β-carotene–ZnS quantum dot hybrid nanostructure.

6. Muhammad Zaheer, Caroline D. Keenan, <u>Justus Hermannsdörfer</u>, Ernest Roessler, Günter Motz, Jürgen Senker, Rhett Kempe, *Chem. Mater.* **2012**, *24*, 3952–3963.
   Robust Microporous Monoliths with Integrated Catalytically Active Metal Sites Investigated by Hyperpolarized 129Xe NMR.

7. Muhammad Zaheer, <u>Justus Hermannsdoerfer</u>, Winfried P. Kretschmer, Guenter Motz, Rhett Kempe, *ChemCatChem*, **2013**, early view; doi: 10.1002/cctc.201300763.
Robust Heterogeneous Nickel Catalysts with Tailored Porosity for the Selective Hydrogenolysis of Aryl Ethers.

8 Acknowledgements

Saravana Pillai, Dr. Sadaf Qayyum, Stefan Schwarz, Emmanuel Sobgwi Tamne and Muhammad Zaheer, for the interesting discussions and helpful practical advice.

A special thanks goes to my parents and my two sisters, who always motivated me and whose support I could always rely on.

Most importantly, I would like to thank Julia for her enormous patience, constant moral support and her ability to bring me back to earth by reviving me to the true important things of life.

Danksagungen

9 Declaration/Erklärung

I hereby declare that I have written this work by myself and that no other sources than those mentioned in this work have been used.

This work has so far neither been submitted to the Faculty of Biology, Chemistry and Earth Science at the University of Bayreuth nor to any other scientific institution for the purpose of a doctoral thesis.

Date: 09-01-2014   Signature

Hiermit erkläre ich, dass die Dissertation von mir selbstständig angefertigt wurde und alle von mir genutzten Hilfsmittel angegeben wurden.

Ich erkläre, dass die wörtlichen oder dem Sinne nach anderen Veröffentlichungen entnommenen Stellen von mir kenntlich gemacht wurden.

Ich erkläre hiermit, dass ich mich bisher keiner weiteren Doktorprüfung unterzogen habe. Ich habe die Dissertation in der gegenwärtigen oder einer anderen Fassung an keiner anderen Fakultät eingereicht.

Datum: 09-01-2014   Unterschrift